FIELD PERFORMANCE OF EPOXY-COATED REINFORCING STEEL
IN VIRGINIA BRIDGE DECKS

Wioleta Agata Pyć

Dissertation submitted to the Faculty of the
Virginia Polytechnic Institute and State University
in partial fulfillment of the requirements for the degree of

Doctor of Philosophy

in

Civil Engineering

Richard E. Weyers, Chair

Thomas E. Cousins

John G. Dillard

John C. Duke

James P. Wightman

Michael M. Sprinkel

September 4, 1998

Blacksburg, Virginia

Keywords: epoxy-coated reinforcement (ECR), bridge decks, concrete, adhesion

FIELD PERFORMANCE OF EPOXY-COATED REINFORCING STEEL IN VIRGINIA BRIDGE DECKS

Wioleta A. Pyć

(**Abstract**)

The corrosion protection performance of epoxy-coated reinforcing steel (ECR) was evaluated in 18 concrete bridge decks in Virginia in 1997. The decks were 2 to 20 years old at the time of the investigation. The concrete bridge deck inspections included crack survey and cover depth determination in the right traffic lane. Maximum of 12 cores with the top reinforcement randomly located in the lowest 12th percentile cover depth and 3 cores with the truss bars were drilled from each bridge deck. The concrete core evaluation included visual examination and determination of carbonation depth, moisture content, absorption, percent saturation and chloride content at 13 mm depth. Rapid chloride permeability test was also performed for the surface and base concrete on samples obtained from cores containing truss bars. The ECR inspection consisted of visual examination and damage evaluation, coating thickness and adhesion determination. The condition of the steel underneath the epoxy coating was also evaluated.

Adhesion loss of the epoxy coating to the steel surface was detected for 4 years old bridge decks. The epoxy coating had debonded from the reinforcing bar before the chloride arrival. Visible signs of a possibility of a corrosion process underneath the coating suggest that ECR will not provide any or little additional service life for concrete bridge decks in comparison to black steel. Other systems, which will provide longer protection with a higher degree of reliability against chloride induced corrosion of steel in concrete, should be considered.

Acknowledgments

TABLE OF CONTENTS

LIST OF TABLES

LIST OF FIGURES

Chapter 1. INTRODUCTION

1.1 Protection Methods for Reinforcing Steel Against Chloride Induced Corrosion

The high pH environment of concrete, above 12, normally protects the reinforcing steel from corrosion. A passive film forms on the steel surface in the presence of water and oxygen in the alkaline environment produced by cement hydration [1]. Several factors, found to be responsible for the maintenance of steel passivity, are presented in Figure 1.
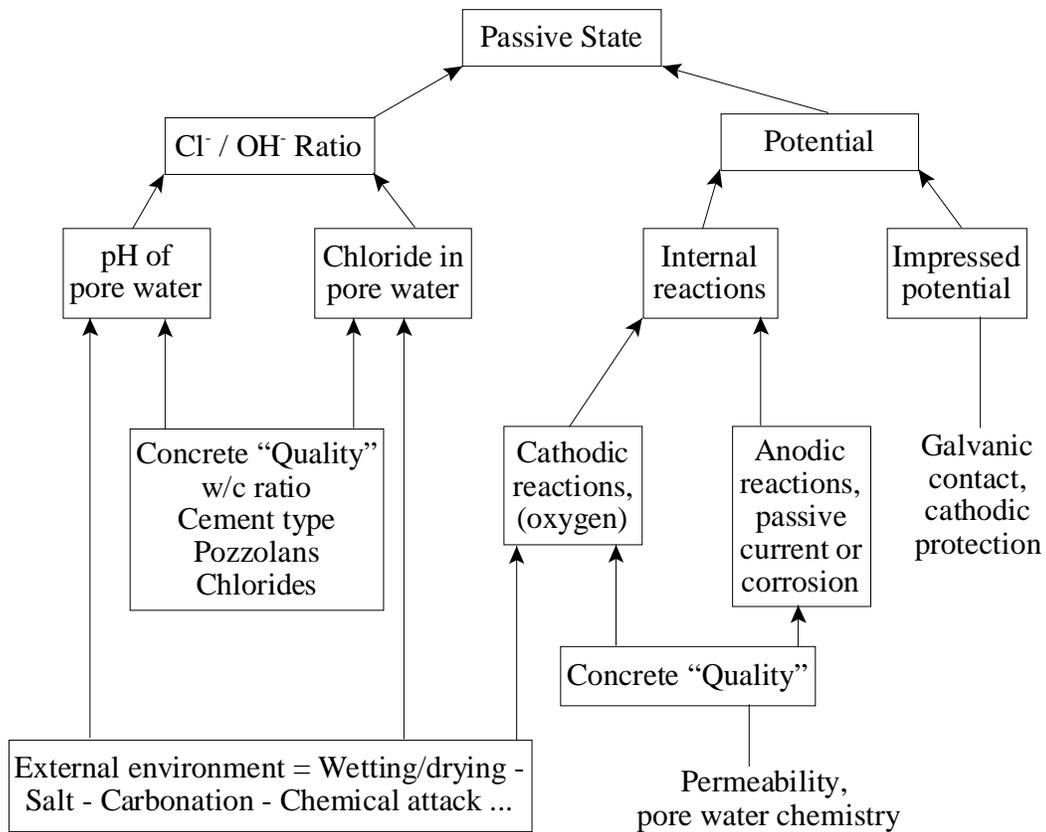
Figure 1. Factors Involved in the Maintenance of the Passive Layer of Steel in Concrete.

The correlation between chloride content and potential was emphasized in this model as the characteristic which should be considered in the corrosion of steel in concrete [2]. To sustain the

protective oxide film on a reinforcing steel surface a small passive current is required. The passive current density should be low enough to provide a lower potential and to protect the steel from chloride initiated attack by maintaining steel potential below the critical value.

Chloride concentration in concrete and concrete carbonation are the two main causes of the loss of passive layer on reinforcing steel. They are influenced by the external environment and the quality of the concrete. Chloride ions penetrate concrete through cracks and by diffusion and are present in the pore water. Once they reach the reinforcing steel surface, they penetrate the iron oxide film and react with iron to form a soluble iron chloride complex [3]. The iron chloride complex diffuses into the concrete to a more alkaline area with higher oxygen concentration and reacts with hydroxyl ions to form $Fe(OH)_2$. Chloride ions, that were bound with iron, become free and the corrosion process continues with an adequate supply of oxygen and water [4].

Concentration of chlorides in concrete varies due to concrete heterogeneity. Chloride distribution is not uniform along the reinforcing steel bar creating anodes and cathodes on individual bars and initiate the microcell corrosion. Chloride content is typically higher for the concrete surface and it decreases inside the concrete with depth. The existing variability in the chloride concentration of concrete at the top and bottom mat of reinforcing steel creates a difference in potential sets. The potential becomes more negative (anodic) for the top mat and more positive (cathodic) for the bottom steel and leads to galvanic corrosion, referred to as macrocell corrosion. In the case of either corrosion type, corrosion products will increase the volume of the original steel by three to six times causing cracks, delaminations, and spalling of the cover concrete.

A critical chloride threshold level in concrete at the reinforcing steel depth, at which corrosion initiates, is approximately 0.71 kg/m^3 [4]. The maximum allowable value of 0.4 % of Cl$^-$ per cement weight was also determined as well as the Cl$^-$/OH$^-$ ratio of 0.6 [4].

Since, the affect of the environment, to which concrete structures are exposed, cannot be controlled, concrete quality should be of main interest in the area of corrosion prevention. First,

low permeable concrete should be of primary interest. Low permeability will delay reinforcing steel corrosion by reducing the rate of chloride penetration into the concrete and extending the time to corrosion initiation. One way of decreasing the concrete permeability is to decrease the water-cement (w/c) ratio. For outdoor conditions, depending on the environment, w/c ratios should be between 0.55 and 0.4 [5]. Concrete permeability to chloride ions can be also decreased by an addition of mineral admixtures such as fly ash, granulated blast furnaces slag or microsilica (silica fume) as cement replacement in concrete mixtures. The cover thickness of concrete over the reinforcing steel will also postpone the corrosion initiation time and should be considered the most important structural parameter in the area of corrosion. Current bridge deck specifications in Virginia require a clear cover of 64 mm.

Corrosion of reinforcing steel in concrete can be further delayed by the use of corrosion inhibitors, which form a protective film on the steel surface. Corrosion inhibitors should reduce either anodic oxidation or cathodic reduction, or both reactions. Two corrosion inhibitor types have been used widely for corrosion protection of steel in concrete, nitrites (anodic inhibitor) and benzoates (cathodic inhibitor) [5].

Corrosion protection of reinforcing steel in concrete can also be provided by the application of protective coatings on the steel surface. Organic, epoxy coatings, serving as a barrier against the chloride ion attack and an electrical isolator against the flow of corrosion current, became the most popular method of protection in the United States, and their performance will be discussed in more details throughout this publication. Other types of protection metal coatings, which are sacrificed during the corrosion process, can be also used. Zinc coatings, applied as hot-dip galvanizing, are the most favored method for civil engineering applications [5]. In chloride free concrete subjected to extensive carbonation, galvanized coating delays the onset of corrosion induced cracking [6]. However, if concrete contains over 1 % of chloride by weight of cement intense corrosion of the zinc may occur [5]. Zinc coating should provide cathodic protection in areas with small defects, but can also produce localized corrosion of high rate if in contact with uncoated reinforcement.

3

Stainless steel, alloy steel reinforcement, represents another type of corrosion protection of steel in concrete. Previous research demonstrated a high corrosion resistance of austenitic stainless steel in concrete containing up to 3 % of Cl⁻ by weight of cement [5].

1.2 Epoxy Coating as the Most Used Protection Method

Bridge deterioration associated with the extensive use of deicing salts provided a background for the development of new methods of corrosion protection of reinforcing steel in concrete. In the early 1970s, the National Bureau of Standards, now the National Institute for Standards and Technology, conducted research on the applicability of various organic coatings for reinforcement protection [7,8,9]. Chemical resistance, physical durabilities and film integrity of liquid and powder coatings were evaluated as well as bond strength tests and electrochemical measurements. Four powder-epoxy coatings, recommended for future evaluation, demonstrated the best corrosion resistance performance, good bond strength, flexibility and creep characteristics, and provided a uniform and holiday free film. The optimum thickness for the epoxy coating was found to be between 127 and 229 μm [10].

Manufacturing process for coating small diameter pipes with an epoxy coating was adapted for ECR production [11]. Reinforcing bar is first cleaned to a near-white finish with grid or shot blasting. The purpose of this preparation process is to remove rust, contaminants and millscale from the steel surface. Then the bar is heated to approximately 230 °C and passed through an electrostatic spray, where the charged, and dry epoxy powder is applied. The epoxy powder melts, flows and cures on the bar surface before it goes through a water spray bath quenching process.

Since the early 1970s, when the epoxy-coating on reinforcing steel was first introduced into the market, until the Fall of 1977, the use of ECR became a standard construction procedure in 17 states and an experimental procedure in 9 states [12]. In 1987, approximately 41 states were using

4

ECR for concrete bridge decks built without overlays [13]. The widespread application of ECR was mostly related to minor adjustments that had to be made to incorporate ECR into the standard construction procedure: increase in the minimum radii for hooks; coated tie wire; use of nylon slings; plastic chairs; and padded bundling bands [11].

By 1989, there were 17 coating applicator firms in the United States and Canada, and the market was dominated by one product, Scotchkote 213, manufactured by 3M [11,14]. The advantage of the 3M product existed in its good flexibility, which allowed for a production line that could be operated at high speed [11].

Over the years, until the mid-1980s, bid prices for the supply and installation of ECR in comparison to bare steel dropped significantly. Estimated life-cycle costs for ECR, using 1986 prices and 50 years of service life, demonstrated that other protection systems including interlayer membrane, latex-modified concrete (LMC) overlay and low slump dense concrete (LSDC) overlay were more expensive than ECR, used for both top and bottom mats or top mat only [15]. Throughout the economical analysis, one corrosion protection system with a lower life-cycle cost than ECR was recognized, a reinforcement cover depth of 89 mm. Further comparison of cost effectiveness of ECR against additional corrosion protection systems of bare reinforcing steel including low permeable concrete and/or corrosion inhibitor is included in this report.

Objective of this research was to determine the field performance of epoxy-coated reinforcement (ECR) in concrete bridge decks in Virginia with the emphasis on the rate of loss of the bond strength of the epoxy coating to the steel after exposure to the concrete environment.

Chapter 2. BACKGROUND

2.1 ECR

"Bare road policy" was introduced by the majority of the state highway agencies in the United States in 1960s. As a result, a significant increase in the use of deicing salt was observed [10]. It also resulted in an accelerated chloride induced corrosion damage of bridge decks.

Epoxy-coated reinforcement was introduced into the market as the new corrosion protection method in the early 1970s. The first bridge with the epoxy-coated reinforcement (ECR) was constructed in West Conshohocken in Pennsylvania in 1973 [16]. By the early 1980s, the use of ECR in bridge structures, became a standard procedure. At the same time, a lack of fundamental or basic research that would examine protective mechanism(s) of epoxy coating against chloride induced corrosion in concrete environment existed in North America [10].

Countries outside of North America represented a slightly different approach relative to the incorporation of ECR into the market place [10]. Studies were initiated to evaluate protective properties of epoxy coating on reinforcing steel. This chapter presents the results of the laboratory and field performance investigation of ECR in and outside of North America.

2.1.1 Laboratory Performance

Extensive laboratory research on ECR began in the United States approximately 10 years after epoxy-coating of reinforcing steel was introduced as the new corrosion protection method. Before that time, production lines, transport and handling during the construction experiences, were the main research areas [10].

In 1980, the corrosion protection performance of ECR and calcium nitrite, a corrosion inhibiting

admixture, was investigated [17]. ECR assessed in this study was coated in 1977, stored outdoors for over two years, did not pass the bend test and had a high number of holidays, more than 82 per meter. Concrete slabs, a total of 32, containing ECR as top mat, top and bottom mat or a corrosion inhibitor, were prepared and evaluated throughout an accelerated outdoor test. Two parameters were used to accelerate the corrosion process: water to cement ratio of 0.53 and admixed chloride, 8.9 kg/m^3 . Results of testing indicated that ECR used as the top mat would require 12 times longer for the same amount of iron to be consumed in comparison to bare steel. If both mats were constructed with ECR, the time proportion changed to 46 to1.

A three year laboratory study, 1983-86, was performed on 124 small scale concrete slabs and 19 full scale slabs, constructed with ECR, prestressing strands, with various cover depths and w/c ratios [18]. Small scale and full scale slabs were exposed to wetting and drying cycles with salt water over a 48-week period or one year, respectively. No corrosion was developed on specimens containing ECR or prestressing strands, even when chloride ion concentration at the bar depth exceeded the corrosion threshold value in concrete 20 times. Premarked holiday areas had not experienced any corrosion either.

Between 1983 and 1988, a corrosion protection performance evaluation study of ECR and galvanized steel in comparison to black steel was conducted [19]. ECR and other reinforcement types embedded in concrete prisms, at various cover depths and chloride content, were evaluated visually and electrochemically, after five years of natural exposure. Results indicated that the corrosion process detected on the ECR was controlled cathodically and that the epoxy coating provided significant reduction in the rate of corrosion deterioration of reinforcing steel.

In 1988, Romano investigated coating disbondment for ECR on four epoxy-coated No. 10, 305 mm long, ECR specimens [20]. Artificial holidays were made on 6.5 % of the total bar area while holidays and handling marks in the coating were patched with an epoxy patching compound. Bar specimens were immersed half way in solutions simulating marine, fresh water and saline environments for a 30 day period. Detected coating disbondment was related to the galvanic

corrosion of the steel substrate.

In 1989, results of studies, analyzing the effects of fabrication and service conditions of the corrosion of ECR in concrete, were published [21,22]. Concrete specimens, containing ECR, were partially exposed, for 300 days, to a 5 % (w/w) sodium chloride solution, typical of Florida's substructure bridge elements. Open circuit potential, AC impedance measurements and visual observations were used to assess the performance of ECR, supplied by different coaters. Other variables included in this research consisted of bar bending and patching, and presence of cracks in the concrete. As a results of this study, corrosion was detected in areas of adhesion loss between the epoxy coating and steel surface due to fabrication bending. Corrosion of bent ECR had a rate of one magnitude lower than that of black steel.

Another studies on evaluation of performance of ECR in comparison to bare steel were conducted by Sohanghpurwala and Clear [23,24]. Small scale concrete slabs with ECR or black steel were prepared and tested through 47 and/or 70 accelerated Southern Exposure Cycles. The following variables were included in the study: bar fabrication and coating suppliers, coating thickness and patching of damaged areas, bend diameter, bending rate and temperature of steel during bending. The research demonstrated that ECR specimens performed better than black steel, their corrosion rates were about half of the values obtained for the bare steel specimens. However, measured electrical resistance suggested that the epoxy coating was deteriorating with time.

ECR coating disbondment was evaluated by exposure to calcium hydroxide, sodium chloride, and calcium hydroxide and sodium chloride solutions [25]. Mechanical coating damage, 0.25 % of bar surface area, was produced on 300 mm long specimens. Coating disbondment was observed for bars tested in the 3.5 % (w/w) sodium chloride solution.

Results of performance evaluation of straight and bent ECR in concrete, after 1.35 years testing with Southern Exposure Cycling, demonstrated corrosion damage for slabs with bare bars in contrast to minor corrosion on ECR specimens [26]. Straight ECR performed slightly better than

bent bars. Additional exposure of some concrete slabs to continuous tap water for 10.5 months and natural weathering for 9.5 months, revealed poor performance for ECR for five out of seven suppliers. The source of tested ECR was recognized as the only variable that had a significant influence on the epoxy coating effectiveness.

During a study performed by Sagues in 1991, eight commercial ECR types were examined [27]. Coatings on tested bars have exhibited surface damage due to fabrication, shipping, handling, exposure to salt water and uv light, assembly procedures, concrete placement and vibration. Variability in the amount of disbondment was observed among ECR from different manufacturers, however, surface damage was one of the main causes of the adhesion loss of the epoxy coating to the steel surface.

In 1992, results of a seven year research study on the performance evaluation of bare mild steel, ECR, galvanized steel, and stainless clad reinforcement were published [28]. An evaluation of the various types of reinforcing steel in chloride contaminated concrete, 2.37, 4.75 or 18.98 kg/m^3, demonstrated the best performance for stainless clad bars, which resisted corrosion at all chloride levels. ECR specimens exhibited corrosion protection at two low chloride concentrations and severe corrosion under the epoxy coating for the highest chloride level, coating breakdown and concrete cracking.

In 1995, results of NCHRP Project 10-37 were published summarizing the laboratory and field evaluation of ECR as a corrosion protection method [29]. Presented research was initiated based on the unsatisfactory corrosion performance of ECR in the Florida Keys bridges and dedicated to determine the reasons for ECR not providing the desired long term corrosion protection. Performance of ECR in highway bridges, located in the United States and Canada, and in a series of laboratory experiments was evaluated and recommendations were made to improve current practices and specifications. An attempt was also made to predict the long-term performance of ECR. Current practices for production, storage, handling and placement contributed to an inadequate quality of ECR being used in highway structures. Impedance measurements of the

epoxy coating , an accelerated hot water test, and solvent-extraction weight loss determinations were recommended as routine quality control tests that should be performed during ECR production. Presently used specifications, concerning the allowable damage on ECR, were not adequate to provide good quality coated bars. The findings demonstrated also that ECR, currently used in highway structures, will not provide long-term corrosion protection, over 50 years, in deicing salt and marine environments.

European and Asian countries were more cautious in introducing ECR into the market than the United States and Canada, with the beginning of performance evaluation studies in the late seventies. In 1976, outdoor exposure testing in London, UK, was conducted on 10 and 20 mm in diameter ECR specimens with a brush applied coating [30]. After one year of research, bare bars that served as a control, were covered with corrosion products, whereas the coated specimens were not affected. Concrete cubes, 70 mm, with 20 mm bars were prepared and exposed to 1 % (w/w) sodium chloride solution. A 1.5 V direct current was also applied to accelerate the corrosion process. Concrete cubes with bare steel cracked after few weeks, the ECR specimens were undamaged.

Between 1980 and 1983, a study on bare steel, ECR, and galvanized reinforcement was performed by Kobayashi and Takewaka [31]. Two types of epoxy coatings with various coating thicknesses, 100, 200 and 300 μm, embedded in small scale concrete specimens, 100 x 100 x 100 mm, and exposed to a marine splash zone, were evaluated. Findings demonstrated a significant influence of coating thickness on corrosion protective properties of ECR. No corrosion was observed for bars with coating thickness of 200 μm. Fatigue loading did not cause any damage to the coating. Surface preparation of the steel surface, prior to the coating procedure, was responsible for microscopic defects in the coating.

In 1981-93, ECR, galvanized steel, and bare reinforcement were evaluated in a Japanese laboratory study [32]. Concrete specimens with reinforcing steel at three different cover depths, 20, 40 or 70 mm, were first cracked, and a constant stress of 2000 kg/cm^2 was applied into the

reinforcement. The stressed specimens were exposed to a marine environment in the tidal zone of Kashima Harbor or a cycle of six hours immersion in sea water at 60 °C and six hours drying in the atmosphere, which served as an accelerated corrosion test. Evaluated ECR had three coating thicknesses: 100, 200 and 300 μm. The results of the accelerated corrosion test demonstrated that ,after 24 months of exposure, blisters developed in specimens with 100 μm coating thickness. However, ECR specimens with 200 and 300 μm coating thickness maintained all protective properties even for the 20 mm cover depth. For bare steel specimens, corrosion was observed in all specimens regardless of the cover depth.

In 1988, a study on one powder epoxy coating and three liquid epoxy paints, was conducted in Finland [33]. Concrete specimens were cracked initially and, in some cases, 4 % calcium chloride was added to the concrete mixture. After two years of exposure to tap and/or synthetic sea water, powder epoxy-coating and coal tar epoxy paint maintained good corrosion protection properties. However, it was also found that none of the tested coatings was totally impermeable.

In Australia, corrosion performance of ECR and hot-dip galvanized steel was evaluated in comparison to black steel [34]. The results demonstrated an excellent corrosion protection performance for undamaged epoxy coating. On the other hand, corrosion had developed on the cut ends of ECR, in spite of touch-ups, and progressed underneath the coating. Half-cell potential measurements were unreliable for the corrosion assessment of ECR.

Allowable coating damage that would ensure the long-term performance of ECR as a corrosion protection method was inspected during research conducted in Japan [35]. Field tests were performed to determine the damage in the epoxy coating formed during the construction of a highway bridge. Laboratory experiments were designed based on the results of the field investigation. Epoxy-coated bars used in the preparation of concrete specimens had a mechanical damage in the coating comparable with the defects obtained from the field. After a series of an accelerated corrosion testing, the ECR was extracted from concrete, the epoxy coating was removed, and the state of corrosion of the steel surface was examined. Based on the results, it

was determined that for the 20 and 40 mm cover depths allowable flaw size should not exceed 1 mm^2 with the acceptable total area of damage of 0.013 % for 20 mm concrete cover and 0.054 % for 40 mm concrete cover, respectively.

2.1.2 Field Performance

In addition to laboratory performance testing on ECR, field performance evaluations became an important part of evaluating the protective properties of epoxy coatings on reinforcing steel. The first investigation of bridge decks constructed with ECR was conducted in 1977 in Carol County, Virginia [36]. Performance of ECR was inspected in two bridge decks and compared with bare steel from two other bridge decks. Testing included chloride concentrations, resistivity, and corrosion potentials. The same four bridge decks were inspected again after 10 years and, in addition to previous evaluation methods, visual examination and a delamination survey were performed [37]. The findings demonstrated that, in spite of chloride content exceeding the corrosion threshold level of 0.71 kg/m^3 , there was no evidence of an active corrosion.

In Maryland, ECR performance in 11 bridge decks, constructed between 1975 and 1979, was investigated [38]. Resistance and corrosion potential measurements were determined as well as chloride content of the concrete. Epoxy coating was found to provide corrosion protection for reinforcing steel during the investigation period of five years. However, the author identified some concerns with the long-time performance of ECR.

Three bridge decks constructed with ECR, one seven and two four years old, were inspected in Minnesota [39]. Visual examination, delamination survey, reinforcement cover depth, chloride content and corrosion potential measurements, were included in the evaluation program. No corrosion deterioration was found except on one bridge deck where some corrosion activity, was detected.

In 1984 in Pennsylvania, the effectiveness of ECR in 11 bridge decks, was reported and compared to bare steel performance of 11 other bridge decks [40]. On all bridge decks, 6 to 10 year old, visual examination, delamination survey, reinforcement cover depths and chloride concentrations were determined. No visual signs of corrosion were detected for the bridge decks constructed with ECR. At the same time, about 40 % or four bridge decks with bare steel were experiencing the initial stage of corrosion-induced deterioration. Weyers and Cady suggested however, that all the decks should be re-inspected in five years [40].

Another study conducted in Pennsylvania included visual inspection of 148 bridge decks containing ECR, galvanized steel, waterproofing membranes, latex-modified concrete overlays or low-slump-dense concrete overlays [41,42]. Further examination was carried out on 21 bridge decks, four with ECR about eight years old. The examination included concrete permeability, chloride content and corrosion potential measurements. The epoxy coating was the most effective corrosion protection method since the majority of the tested ECR were in perfect condition despite the high chloride concentration, 1.96 to 6.94 kg/m^3. Additional findings of the research suggested that corrosion potential measurements are misleading and inadequate in the case of ECR, and should be discarded from methods used in performance evaluation of ECR.

In 1988, the first failure of ECR was detected in the Florida Keys in the Long Key Bridge in substructure elements, piers, columns and cross-ties, after only five to seven years of service [43]. In the next few years of the investigation, corrosion was also observed on four of five major Florida bridges, about 610 m long, constructed with ECR [44]. The fifth bridge from this group, Channel Five Crossing, developed corrosion damage in March 1993 [11].

Spalling and delaminations were detected in 1990 in a parking deck constructed with ECR in the northern United States, eight years after construction. Two of the four cores containing ECR examined in 1992 exhibited severe corrosion of the reinforcement. In addition, coating assessment showed cracked, embrittled, blistered, and disbonded coating [45]. Delaminations and spalling were also observed in 1990 in a bridge deck constructed with ECR in the mid 1970s in

13

the state of New York [46]. Further investigation of 14 bridges which were seven to twelve years old showed the presence of light rust at coating breaks on bars from 3 out of 54 tested cores [47]. In 1990, the corrosion of ECR was detected in panels of a noise barrier in Ontario, Canada, after 9 years of service life [46]. Two years later corrosion of ECR was detected in the concrete nosing in the Madawaska River Bridge in eastern Ontario and in the Ford Drive-QEW interchange in Toronto. Both structures were built in 1979 [11].

In 1992, the Minnesota Department of Transportation examined epoxy-coated reinforcing steel used in 10 bridge decks. Of the 10 cores containing ECR, one per structure, only one epoxy-coated bar showed slight corrosion [48]. In 1993, the North Carolina Department of Transportation evaluated ECR from the substructures in 3 coastal bridges built in 1985. Epoxy-coated bars were found in good condition despite chloride content exceeding the threshold value at the reinforcing steel depth [49]. The West Virginia Department of Transportation conducted a delamination survey of 12 bridge decks constructed with ECR built between 1974 and 1976. A delamination of 0.1 m^2 was detected in one deck only. Good condition was reported for the epoxy-coated reinforcing steel from the other 11 bridge decks [50].

In 1992, a field performance study of ECR in 12 bridges built between 1978 and 1992 took place in Ontario, Canada. All evaluated structures but one, which developed small spalls in a barrier wall, appeared to be in good condition. Other findings included the detection of adhesion loss of the epoxy to the reinforcing steel under service conditions and its relation to the structure age [11].

2.1.3 Previous ECR study in Virginia

A preliminary field investigation of the corrosion protection performance of ECR was completed in 1996 [51]. The evaluation included three bridge decks, SN1026, SN1029, and SN8003, and piles from three marine structures, SN1965, SN1812 and SN1008. Virginia uses a double protection system, ECR and two layers of an epoxy surface coating on the concrete pile. At the time of the

investigation, the bridge decks were seventeen years old and the piles were seven and eight years old. The research consisted of a field survey and a laboratory evaluation.

In the case of bridge decks, 12 cores, 102 mm in diameter, through a 16 mm ECR, were drilled. Random core locations were based on cover depth measurements, 40 sites per span. Cores were taken from the 12th percentile smallest cover depth readings. Powdered concrete samples were also determined at 13, 25, 38, and 51 mm in the vicinity of each core. In addition, a crack survey was performed on each bridge deck. Field inspection was limited to the right traffic lane only. Cores with ECR, 7 from SN1965, 11 from SN1812, and 12 from SN1008, 53 mm in diameter, were taken from the piles within the tidal zone.

All cores were examined visually in the laboratory to determine the quality of the concrete. The reinforcement cover depth and the AC impedance were also measured. Upon the removal of ECR specimens, carbonation depth was examined. ECR was inspected visually for coating defects (mashed areas, dents, scrapes, cracks and holes). The number of holidays and coating thickness were obtained, and a dry knife adhesion of the epoxy coating was measured. Concrete moisture content and absorption values, at the bar depth, were determined from the concrete cores. Powdered concrete samples, obtained from the bridge decks, were used to determine the background chloride content and calculate the chloride diffusion constants. The chloride concentration, at the bar depth, was also determined from concrete cores drilled from the bridge decks and the piles.

The results indicated that the epoxy coating will sustain its adhesive bond to the steel surface for about 15 years in bridge decks in Virginia and for 8 years or less in concrete piles in Virginia's marine environment. There is a high probability, that disbondment of the epoxy coating from steel will take place before chloride arrival at the bar depth. If epoxy coating stays intact when chlorides reach the reinforcement, ECR will provide additional service life for these structures, as demonstrated by the evaluation of the specimens obtained from SN8003. Coating disbondment progresses also at a faster rate for low quality concretes which have a high moisture content.

The corrosion mechanism observed in the evaluated ECR specimens, obtained from the piles and the bridge decks, indicated a similar process to one which was detected in Florida's investigation. The measured cover depths, on the evaluated bridge decks, met the cover depth specifications used currently in Virginia. They also provided the desired level of cover depth.

Epoxy coating on the concrete pile surface was well adhered and provide a protection against chloride ingress into the concrete for at least 8 years. However, the adhesive bond between the epoxy coating and the steel surface will be lost before chlorides reach the reinforcement.

Chapter 3. THEORY and PRACTICE: PROTECTION and EVALUATION METHODS

3.1 ECR

3.1.1 Protection Mechanism

Organic coatings are widely used by the industry as a protection method for metal structures against corrosion. Coating ability to provide corrosion protection depends on its properties, related to the polymeric network and flaws in this network, as well as the metal substrate, the surface pretreatment and the application procedure [52]. The composition of an organic coating, which consists primary of binder, fillers, additives, solvents and pigments, will also influence its protective properties.

Organic coatings on metal substrates serve either as a physical barrier between the metal surface and the aqueous corrosive environment, reducing the corrosion rate by an increase in the ionic resistance, or as a corrosion inhibitor through the pigments, or a combination of both. An active corrosion inhibition will retard the charge transfer between cathodic and anodic sites and slow the corrosion process. The corrosion rate will also be reduced by an increase in the electrical resistance, which is achieved through the formation of an oxide film on the metal surface.

An application of organic coatings in civil engineering was introduced in the early 1970s, when the epoxy coating on the reinforcing bars was proposed as the new method of corrosion prevention. ECR was to solve the problem of chloride ion induced corrosion in transportation structures which arose from an extensive use of deicing salts or the marine environment. The purpose of the epoxy coating on the reinforcing steel surface was to provide a physical and an electrochemical barrier. The physical barrier provided protection against water and chloride ions reaching the steel surface and initiating the corrosion process. The electrochemical barrier is due to the high resistance of the coating, which reduces macro cell corrosion through an increase in the electrical resistance at the cathodic reaction locations.

3.1.2 Failure Mechanism

Corrosion protection of metals by organic coatings, serving as a physical barrier between the metal surface and the corrosive environment, has its limitations. All organic coatings, including epoxy coatings, are permeable to water, oxygen and various ions. The results of a study on the permeability of oxygen and water in coatings, obtained from free films cast on glass, are presented in Table 1. Another study by Leidheiser, Jr., concentrated on testing the diffusion of water, Na^+ and Cl^- ions through an alkyd coating, 28 to 51 μm thick, on a steel substrate exposed to 0.05 M NaCl, see Table 2. The findings demonstrated diffusion coefficients of the same order of magnitude for the evaluated ions and water [53].

Table 1.   Permeability of Oxygen and Water Vapor in Resin and Coating Films [52].

Polymer Type	Permeability[a]	
	Oxygen, $[cm^3\ 100\ \mu m\ (m^2\ d\ atm)^{-1}]$ at 23°C and 85 % RH	Water Vapor, $[g\ 10\ \mu m\ (m^2\ d)^{-1}]$ at 23°C and 85 % RH
Resin films:		
epoxy/polyamide	130 ± 33	155 ± 20
chlorinated rubber, plasticized	183 ± 7	95 ± 5
styrene acrylic latex	1464 ± 54	2300
Coating films:		
chlorinated rubber unmodified	30 ± 7	50 ± 8
aluminum epoxy mastic	110 ± 37	105 ± 15
coal tar epoxy	213 ± 28	75 ± 3
acrylic water-borne primer	500	1800 ± 92
TiO_2 pigmented alkyd	595 ± 49	645 ± 15
red lead oil based primer	734 ± 42	535 ± 8

[a] The permeability of oxygen is given as the number of "cm^3 gas of 1 atm" permeating through a coating of 100 μm thickness per m^2 per day.

Table 2. Average Diffusion Coefficient for Water, Na^+, Cl^-, Through an Alkyd Coating on Steel Immersed in 0.5 M NaCl [53].

			Diffusion Coefficients (cm^2 / hr) x 10^8			
			Water		Na^+	Cl^-
Sample Designation	Coating Thickness (μm)	No. of Samples	First 3 Hours	Steady State	Steady State	Steady State
1.10	28	2	167	1.26	-	1.18
1.15	29	2	-	-	3.44	1.25
1.25	32	2	-	-	3.97	2.27
1.30	33	2	272	2.59	3.35	1.46
1.40	36	1	260	2.49	-	1.39
1.45	37	2	-	-	1.00	3.99
1.50	38	1	310	2.49	-	5.40
1.58	40	2	-	-	2.92	1.52
1.60	41	2	329	4.18	2.56	5.55
1.78	45	2	-	-	4.12	3.19
1.80	46	2	541	9.97	4.31	2.75
2.00	51	4	-	-	3.23	3.78

While used as a protective barrier against corrosion of metals, an organic coating is saturated with water for half of the time. Water, present in the coating, represents in its quantity an atmosphere of a high humidity [52]. Water transfer through the coating is about 10 to 100 times larger than the quantity of water consumed during the bare metal corrosion. The presence of water in the coating and its migration to the steel surface, combined with the oxygen diffusion, creates a corrosion prone environment underneath the coating.

Understanding the mechanical properties of organic coatings, including the glass transition temperature and other related characteristics of polymers, will help to determine the sensitivity of the coating to an external damage. Damage in the organic coatings can be a result of a mechanical or thermal load. The corrosion process can develop at damaged sites and in the neighboring areas underneath the coating. However, it should be emphasized that the protective properties of an organic coating can be satisfactory only, if the coating remains well adhered to the metal surface [52].

Water disbondment was the main mechanism of adhesion loss of organic coatings bonded to metal surfaces. The disbondment is a result of an exposure of the coating-metal system to a liquid phase or a high relative humidity. ECR embedded in concrete are subjected to such an environment, since, in Virginia bridge decks, the relative humidity of the concrete at the bar depth was greater than 80 % [51]. Another factor that can accelerate the adhesion loss is an increase in temperature. Coating disbondment progresses more rapidly at higher temperatures. However, to understand the water disbondment phenomenon, the adhesion of the coating to a steel surface should be explained in more details.

First, the nature of a metal surface, to which the coating bonds, should be defined. As was stated by Leidheiser and Funke, steel that was subjected to a chemical or mechanical cleaning process and than exposed to the atmosphere, becomes instantly covered with a 1 to 3 nm thick oxide layer [54]. Most of the surface iron (III) ions contain surface hydroxyl groups, which interact with cations in acid base reactions when exposed to an aqueous environment. Different impurities like carbonaceous material, compounds of calcium, fluorine, silicone, sulphur, manganese, and chlorine, can also be found on the steel surface. Due to such impurities, the coating-steel interface will contain non-bonded areas, where water can accumulate.

Water molecules migrate through the coating as a result of a diffusion through the open spaces in the polymer network that form during thermal motions of polymer segments. Water travels also through channels, capillaries and pores in the coating. Pores in the coating are caused by

improper solvent evaporation, impurities, poor curing, undesirable interactions between binder and additives, or air entrapped during coating application. Water diffusion through the coating is induced by an osmotic pressure or thermal gradient. A multilayer water film forms on the steel surface, underneath the coating, and grows along the metal-polymer interface, causing coating disbondment. In some areas a localized adhesion loss takes place and blisters are formed in the coating, as a result of differences in coating thickness and coating heterogeneities. Two proposed mechanisms of water disbondment are presented schematically in Figure 2 [54]. One mechanism, chemical disbondment, is the adhesion loss related to chemical interactions between water molecules and covalent, hydrogen or polar bonds existing in the coating-metal surface system. The other mechanism suggests an adhesion loss due to forces generated by water accumulation and osmotic pressures, mechanical or hydrodynamic disbondment.
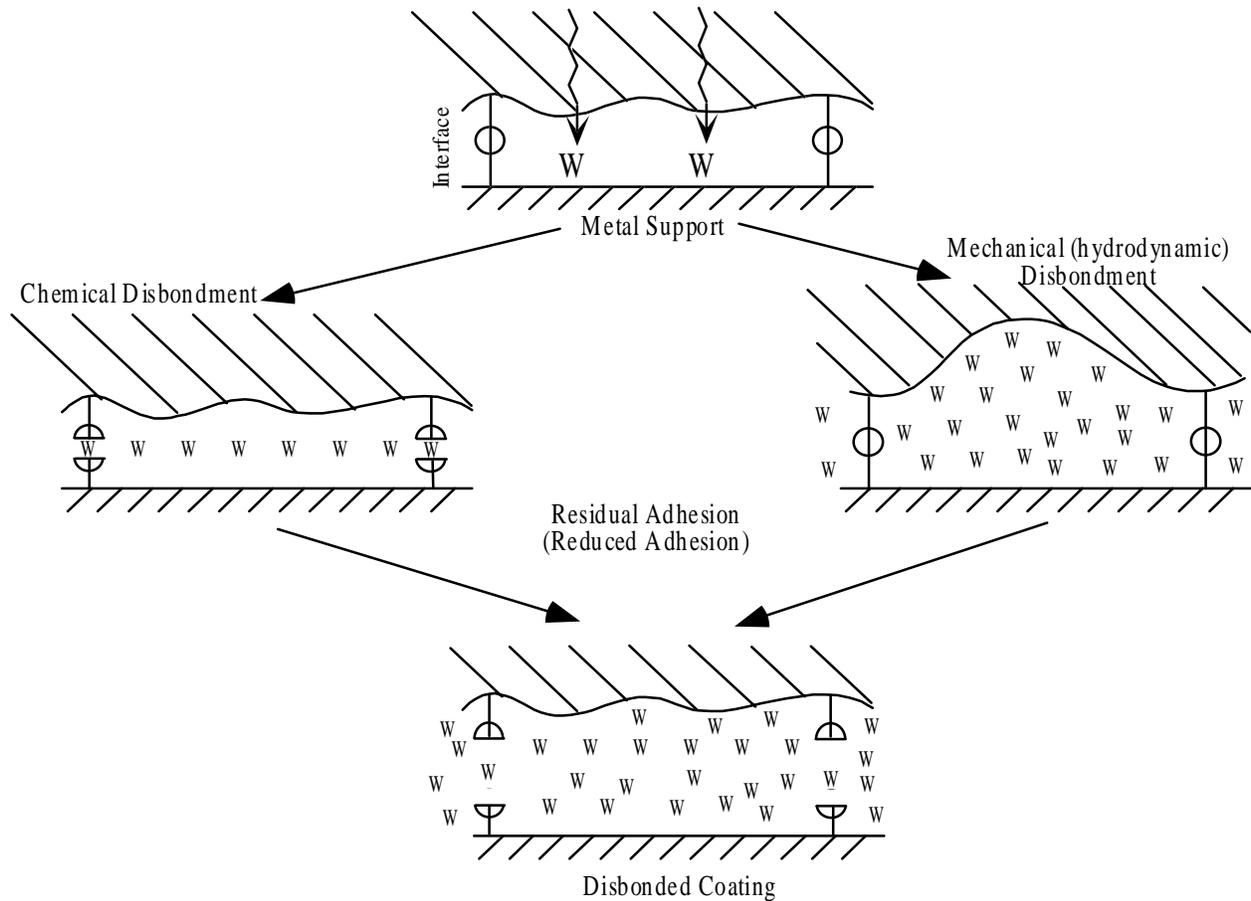

Figure 2.   Schematic Representation of the Mechanisms of Adhesion Reduction and Water Disbondment [54].

The existence of a potential for water disbondment of the epoxy coating from the reinforcing steel surface was presented by Weyers et al. [51]. Based on the results of an experiment performed by Gledhill and Kinlock in 1974, two observations were made. First of all, the change in the sign of the measured work of adhesion of the epoxy-ferric oxide interface from 291 to -255 mJ/m^2, for dry and wet environments, suggests the possibility of a displacement of an epoxy coating from the steel surface in an aqueous medium. The second finding supporting the disbondment of the epoxy coating by water refers to the activation energy for this process equal to 32 kJ/mole, below $T_g = 85°C$, which was greater than the secondary bond energy of 10 to 26 kJ/mole, characteristic of an adhesion bond between the two surfaces.

Water and iron accumulation at the coating-metal interface at sites of poor adhesion may lead to a corrosion reaction in the presence of an adequate oxygen content. The anodic and cathodic sites are randomly distributed over the metal surface at that stage of the corrosion process, Figure 3A. An electrochemical corrosion cell is created, iron ions are dissolved at the anode,

$$Fe \rightarrow Fe^{2+} + 2e^- \tag{1}$$

and oxygen is reduced at the cathode,

$$H_2O + \tfrac{1}{2} O_2 + 2e^- \rightarrow 2OH^- \tag{2}$$

The concentration of hydroxide ions increases with time and results in a pH increase. The corrosion reaction, that takes place, leads to blister formation due to the hydrodynamic pressure generated at the interface, and cathodic delamination or anodic undermining.
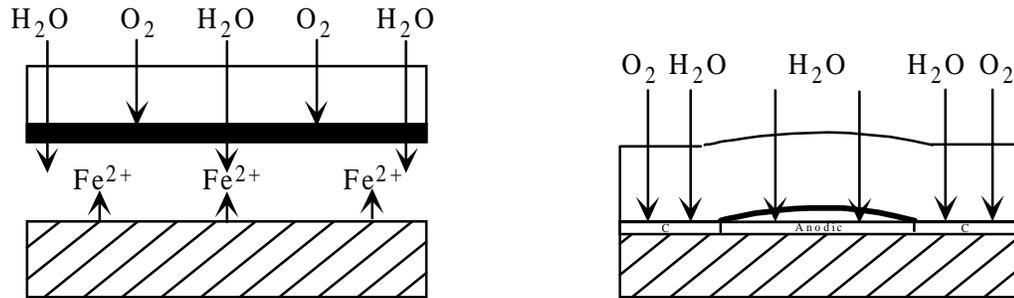
Cathodic delamination is caused by oxygen reduction,

$$O_2 + 2H_2O + 4e^- \rightarrow 4OH^- \tag{3}$$

or hydrogen production,

$$2H_2O + 2e^- \rightarrow H_2 + 2OH^- \tag{4}$$
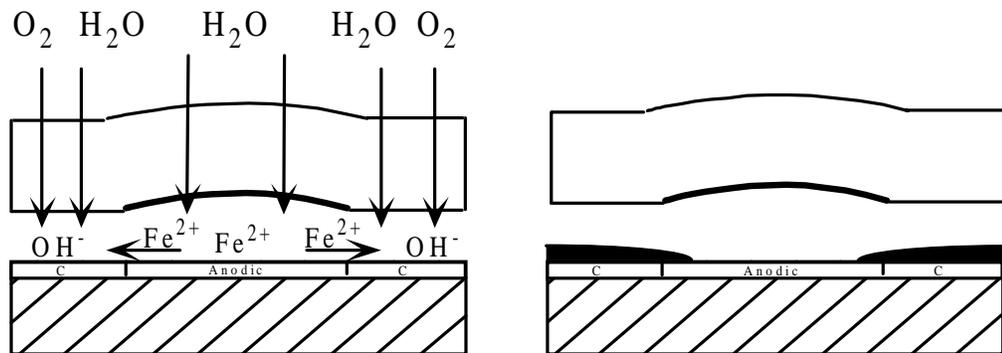
A.

B.

Figure 3.   Blister Initiation and Propagation Due to Cathodic Delamination under an
            Undamaged Organic Coating [52]:
            A.   separation of Anode and Cathode
            B.   cathodic Delamination.

and cathodic reactions which may take place at the metal-coating interface. The reactions result
in an increase in the pH followed by coating delamination and blister formation, due to the
evolution of hydrogen gas. In the case of an undamaged coating, corrosion initiates at poor
adhesion sites. A complex iron oxide forms from the reaction of Fe^{2+} and OH^-, in presence of
oxygen, and acts as water permeable and oxygen impermeable membrane, if participating
separation of cathodic and anodic sites under the coating takes place, Figure 3B. The space under
the blister is covered by a large anodic area, while a small cathodic area moves to the edge of the
blister. The pH value at the cathode increases, causing delamination and blister growth.

A similar mechanism of blister formation was observed for corrosion under a defective coating, Figure 4. Oxygen and water reach the exposed metal through the defect in the coating, corrosion takes place and corrosion products accumulate. Corrosion propagation and blister growth occur in the same manner as in the case of an undamaged coating.

Anodic undermining takes place mainly on the metal surface underneath the coating in corrosion prone areas, sites of mechanical damage or sites with a residue of a cleaning process [52]. However, it can also initiate at damaged areas in the coating. In the case of anodic undermining, the anodic areas are located at the edges of a blister and are fully separated from the cathodic sites due to the corrosion product accumulation or as a large number of small blisters around the anode. Blister growth is associated with anodic crevice corrosion taking place at blister edges.

Sagues and Powers reported that both types of disbondment, cathodic and anodic, were characteristic of ECR [25,27]. Anodic disbondment was observed for the specimens exposed to $Ca(OH)_2$ and NaCl solutions. Cathodic disbondment occurred for specimens tested in 3.5 % NaCl solution.

The other corrosion mechanism of the steel underneath the epoxy coating was observed and proposed by Sagues [55] and validated by Pyc, Weyers, and Sprinkel [56] in the pore water solution studies. First, pore solution penetrates the coating and causes the coating to disbond in weak adhesion areas. The blister forms and the pH of the solution inside the blister changes to around 12. Next, chloride ions arrive at the clean steel surface at the sufficient concentration to initiate corrosion, and the pH decreases to 5 as the corrosion process proceeds. Corrosion products accumulate underneath the coating, and their expansion causes the coating to crack. Pore solution mixes with the solution inside the blister, and the pH under the coating increases to the previous value of about 12 as more pore solution enters the blister.
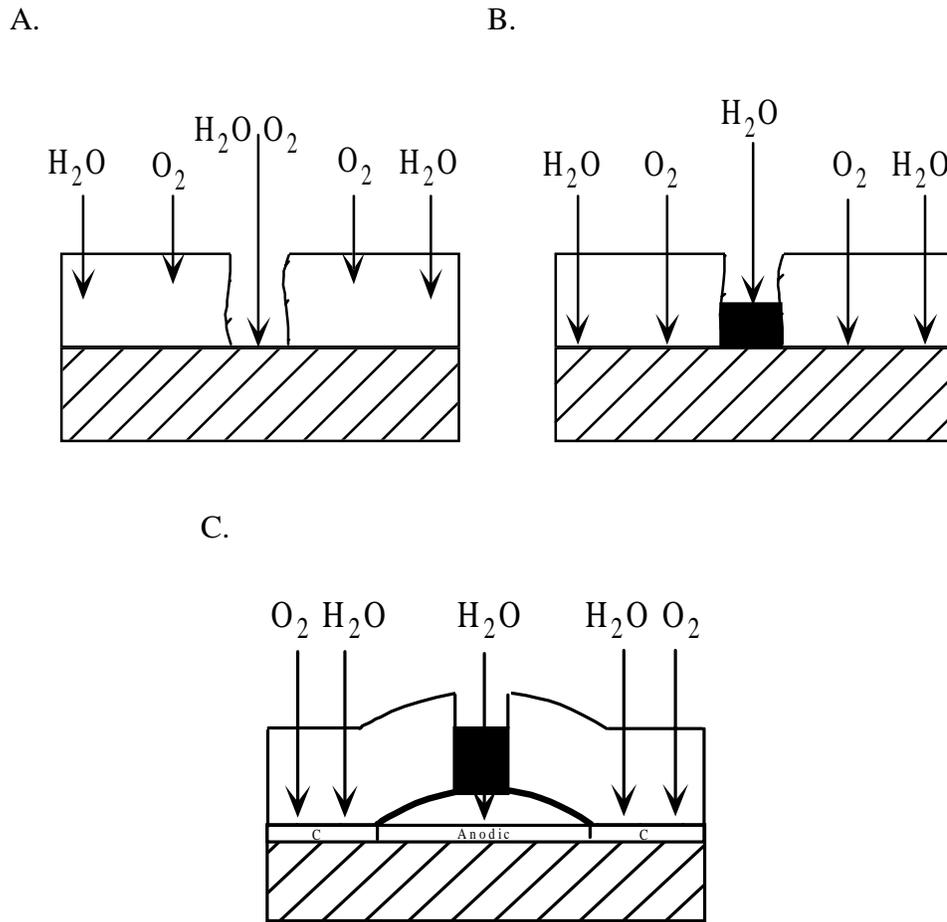
A.   B.

C.

Figure 4.   Blister Initiation and Propagation Due to Cathodic Delamination under a Break in an Organic Coating [52]:
A.   corrosion Initiation
B.   blocking of a Coating Defect
C.   cathodic Delamination.

3.1.3 Evaluation Methods

3.1.3.1   Material Acceptance

The first ASTM specification, A 775/A 775 M, concerning ECR was published in 1981.
Requirements proposed by the specification dealt with steel reinforcing bars, coating and patching
materials, material section, surface preparation, coating application, and coated bars. Criterion
were specified for coating thickness, 0.13 to 0.30 mm, coating continuity, 2 holidays per 0.3 m,
and coating damage, 2 % of the surface area of the bar. Prescription tests were also
recommended to evaluate coating characteristics:

− adhesion of coating: bending coated bars 120° around a mandrel of a specified size at a
   uniform rate in about 90 seconds;

− chemical resistance: the immersion of intact and mechanically damaged ECR specimens in
   distilled water, a 3 M aqueous solution of $CaCl_2$, a 3 M aqueous solution of NaOH, and a
   solution saturated with $Ca(OH)_2$, at 24 ± 2 °C for 45 days;

− resistance to applied voltage (accelerated corrosion test): ECR specimens tested as the
   cathode and anode in a 7 % aqueous NaCl solution under a 2 V potential;

− chloride permeability: the method outlined in FHWA-RD-74-18 performed at 24 ± 2 °C
   for 45 days;

− bond strength to concrete: the method outlined in FHWA-RD-74-18;

− abrasion resistance: the inspection of the ECR abrasion resistance tested using a Taber
   abraser or its equivalent;

− impact test: the evaluation of the ECR resistance to a mechanical damage with an impact
   of 9 Nm;

− hardness test: the coating hardness determination using a 0.01 kg weight.

The specifications on the inspection of ECR remained unchanged until 1989, when the new
requirement of 1 % of the surface area of the allowable coating damage per 0.3 m was submitted.
The proposal was incorporated into the A 775/A 775 M specification in 1992, with the suggestion

of the new coating thickness of 0.18 to 0.30 mm and the rejection of the ECR with the coating thickness below 0.13 mm or above 0.33 mm. The new coating thickness and continuity specifications were adopted in 1995. The coating thickness range is 175 to 300 μm with rejection of coated bars with the thickness below 125 μm. The previously suggested number of 2 holidays in the coating per 0.3 m was replaced by 3 holidays per 1 m.

Several test methods are used in the performance evaluation of ECR. An overview of currently used laboratory and field evaluation techniques was given by Weyers [44]. In general, test methods are divided into laboratory and field assessment practices. Laboratory test methods include an evaluation of the structural behavior of ECR, mainly the bond strength between the ECR and concrete (pullout test, flexural bending, bending fatigue) as well as bar flexibility and creep. However, since the application of the epoxy coating on the reinforcing bar is a corrosion protection method, tests which measure the corrosion protection performance of ECR should be of the primary concern. Tests that propose to address this issue can be classified into three major groups: tests on the coating, tests on the coated bar, and tests on coated bar in concrete.

Chemical resistance, an examination of the coating resistance to the concrete pore water solution, and degree of polymerization, an inspection of the film's resistance to form conductive paths, can be found among the techniques used for the corrosion performance assessment of organic coatings. The performance testing of coated bars includes an evaluation of physical, chemical, electrical and electrochemical parameters. The physical parameters controlling the corrosion protection performance of the coating are evaluated through the following tests: coating thickness and evenness, coating integrity, hardness, impact resistance, and coating adhesion. An examination of the ECR resistance to concrete pore water solution belongs to the inspection of chemical parameters influencing the corrosion performance of coated bars. Testing of electrical parameters, number of holidays and electrical resistance, determines the film integrity. Measuring corrosion potential and electrochemical impedance spectroscopy (EIS), as well as the determination of the degree of coating disbondment allows for an identification of electrochemical parameters of ECR.

27

3.1.3.2 Performance Methods

Performance evaluation of ECR as the corrosion protection method in concrete consists of the inspection of the concrete-coated bar system. Among those tests are cracking and delamination survey; carbonation depth, chloride content and pH of concrete at bar location; corrosion current density and electrical resistance measurements. Concrete temperature and a visual corrosion assessment of coated bars extracted from concrete are also of the primary interest. Two electrochemical methods used for the determination of the corrosion activity of ECR in concrete, linear polarization (LP) and EIS, became the most popular in the evaluation of the corrosion protection performance of coated bars. These techniques were incorporated into the present studies and the results determined using LP and EIS are presented.

The LP technique is a simple DC method used to obtained a rapid estimate of the corrosion rate of a metal in an electrolyte. Measurements are recorded during a very short, slow potential sweep. The sweep ranges typically between -20 and +20 mV, for which the current vs. voltage curve becomes almost linear. An estimate of the polarization resistance, R_p, is obtained and used to calculate corrosion current, I_{corr}, or corrosion current density, i_{corr}.

Polarization resistance, R_p , may be calculated by subtracting the solution resistance, R_Ω, measured at high frequency, from the sum of $R_p + R_\Omega$ measured at a low frequency. Polarization resistance, R_p , is also inversely proportional to the corrosion current [57]:

$$I_{corr} = [\beta_a\beta_c / 2.303 (\beta_a + \beta_c)] \times (1 / R_p), \qquad\qquad (5)$$

where I_{corr} - corrosion current in amps

β_a - anodic Beta coefficient in volts/decade, Tafel constant

β_c - cathodic Beta coefficient in volts/decade, Tafel constant

R_p - polarization resistance.

28

The corrosion current density is calculated by dividing the corrosion current by the polarized surface area.

In the previous study performed on ECR in solutions the linear polarization measurements could be determined only for resistance values up to 10^6 ohms [58]. As a result, the corrosion resistance of ECR with poor coating performance was evaluated. Measured values were close to the "total" impedance measured at 0.001 Hz using Electrochemical Impedance Spectroscopy (EIS).

EIS (AC impedance) is a technique used to determine the electrical impedance of the metal-electrolyte interface at various AC excitation frequencies. EIS measurements allow for the prediction of corrosion rates and the performance evaluation of chemical corrosion inhibitors and protective coatings. The range frequency of 10^{-3} to 10^5 Hz is usually used in EIS experiments.

Impedance, $Z(\omega)$, may be expressed as

$$Z(\omega) = ReZ - j(ImZ) \tag{6}$$

where ReZ and ImZ represent the real and imaginary parts of the impedance, and $j = (-1)^{\frac{1}{2}}$ [59]. A small excitation signal, a sine-wave voltage, is used in EIS to produce the pseudo-linear response of the cell, the sine-wave current.

$$E = \Delta E \sin(\omega t) \tag{7}$$

 and

$$i = \Delta i \sin(\omega t + \varphi) \tag{8}$$

where ΔE and Δi are the amplitudes of the voltage and current waves, and φ is the phase shift between the applied sine-wave and the resulting sine-wave current. $Z(\omega)$ can be presented as a

vector in the complex plane, with X-axis and Y-axis representing ReZ and ImZ, respectively, see Figure 5.
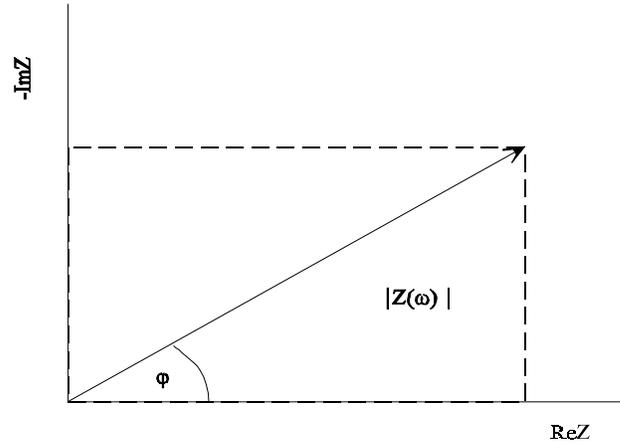

Figure 5.   Vector Representation of the Impedance Z(ω) in the Complex Plane [59].

The impedance is usually presented as Nyquist or Bode plot. In the Nyquist plot the imaginary part, ImZ, is expressed as a function of the real part, ReZ. In Bode plots log $|Z|$ and log φ are presented as the log of the frequency, ω. Nyquist and Bode plots for a simple parallel-connected resistance-capacitance circuit representing a simple corroding surface under activation control are presented in Figure 6. For the Nyquist plot, in a semicircle form, the frequency is increasing in a counterclockwise direction. At very low and very high frequency, the imaginary part, ImZ, disappears, resulting in the sum of the solution resistance, R_Ω, and polarization resistance, R_p , at a low frequency, and only the solution resistance, R_Ω, at a high frequency. For the Bode plot, a linear part with a slope of -1 and maximum phase angle, φ, are typical for the capacitance [57].
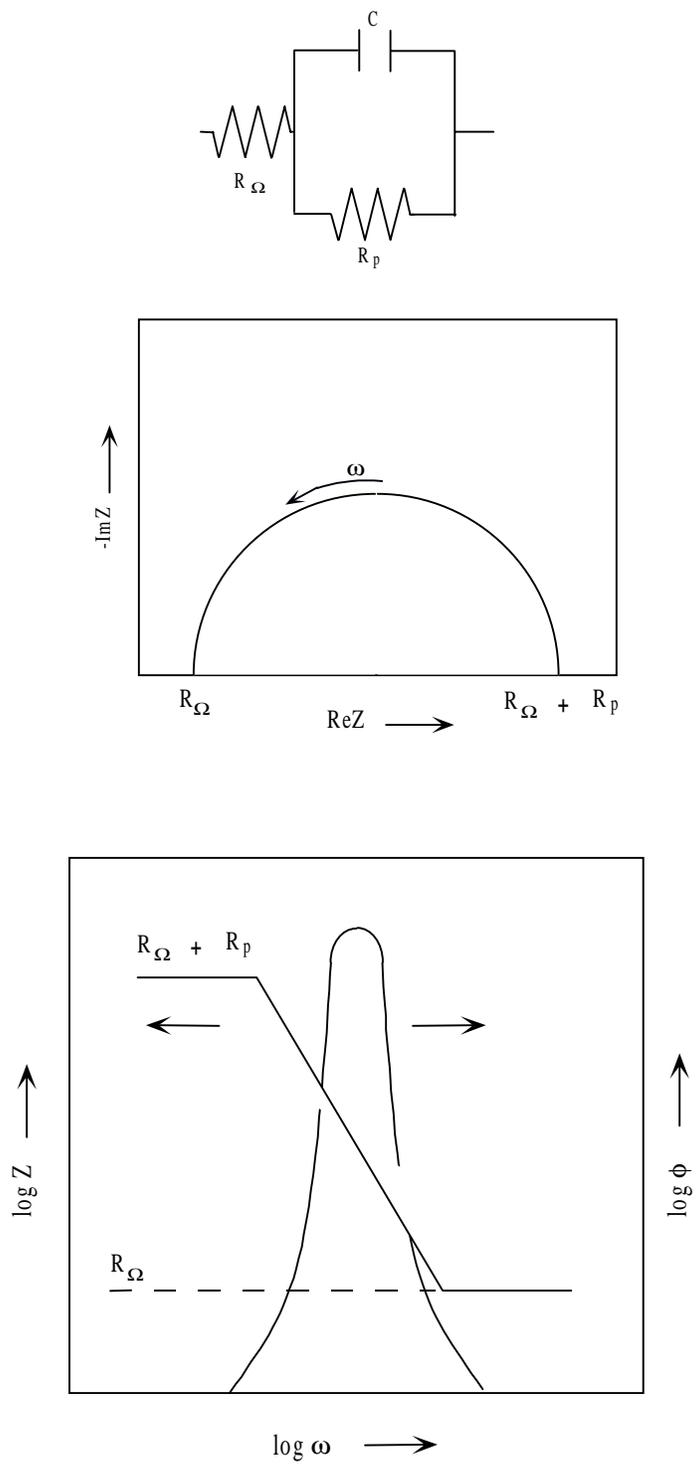
Figure 6.   Data Display for Eis for a Corroding Electrode Simulated by Parallel-Connected Resistance R_p and Capacitance C: (A) Nyquist Plot; (B) Bode Plot [57].

31

A typical equivalent circuit for aqueous corrosion of coated metal is presented in Figure 7. In this model, R_Ω represents the uncompensated resistance between the working electrode and the reference electrode. R_{cp} is the coating pore resistance representing the resistance of areas on the coating with more rapid solution uptake and R_{ct} is the charge transfer resistance representing the corrosion resistance of the metal. C_d represents the double layer capacitance at the coating-metal interface and C_c is the coating capacitance of areas where the coating remains intact during immersion. Z_w is called Warburg impedance and represents the diffusion process of corrosive elements [58].
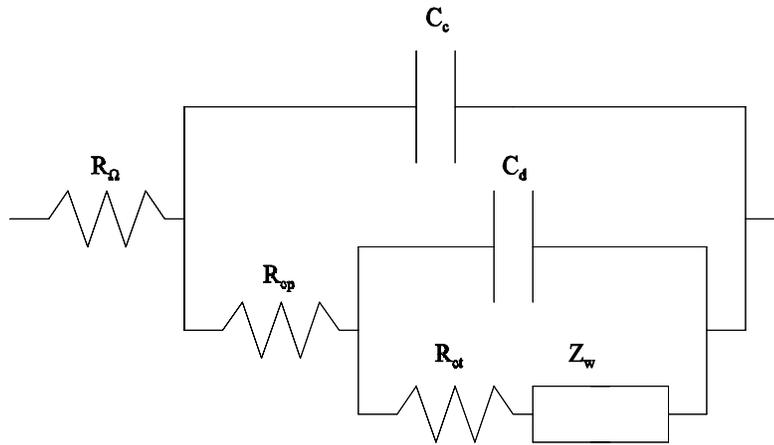
Figure 7.   The Equivalent Electrical Circuit for Coated Metal-Solution Interface [58].

Ignoring the Warburg impedance in the above model, the Nyquist and Bode plots would have the form presented in Figure 8. However, for real coated metal systems two semicircles in the Nyquist plot can be distinguished only when their time constant values are not too close and their diameters have close values. The following criteria have to be followed to construct the desired graphs shown in Figure 8: $0.2 \leq R_{ct} / R_{cp} \leq 5$ and $\tau_{ct} / \tau_{cp} \geq 20$ or $\tau_{ct} / \tau_{cp} \leq 0.05$, where $\tau_{ct} = R_{ct} C_d$ and $\tau_{cp} = R_{cp} C_c$. If the Warburg diffusion impedance, Z_w, is included, the curve shape depends on

32

the two competitive controlling mechanisms of corrosion rate: charge transfer and diffusion, see Figure 9.
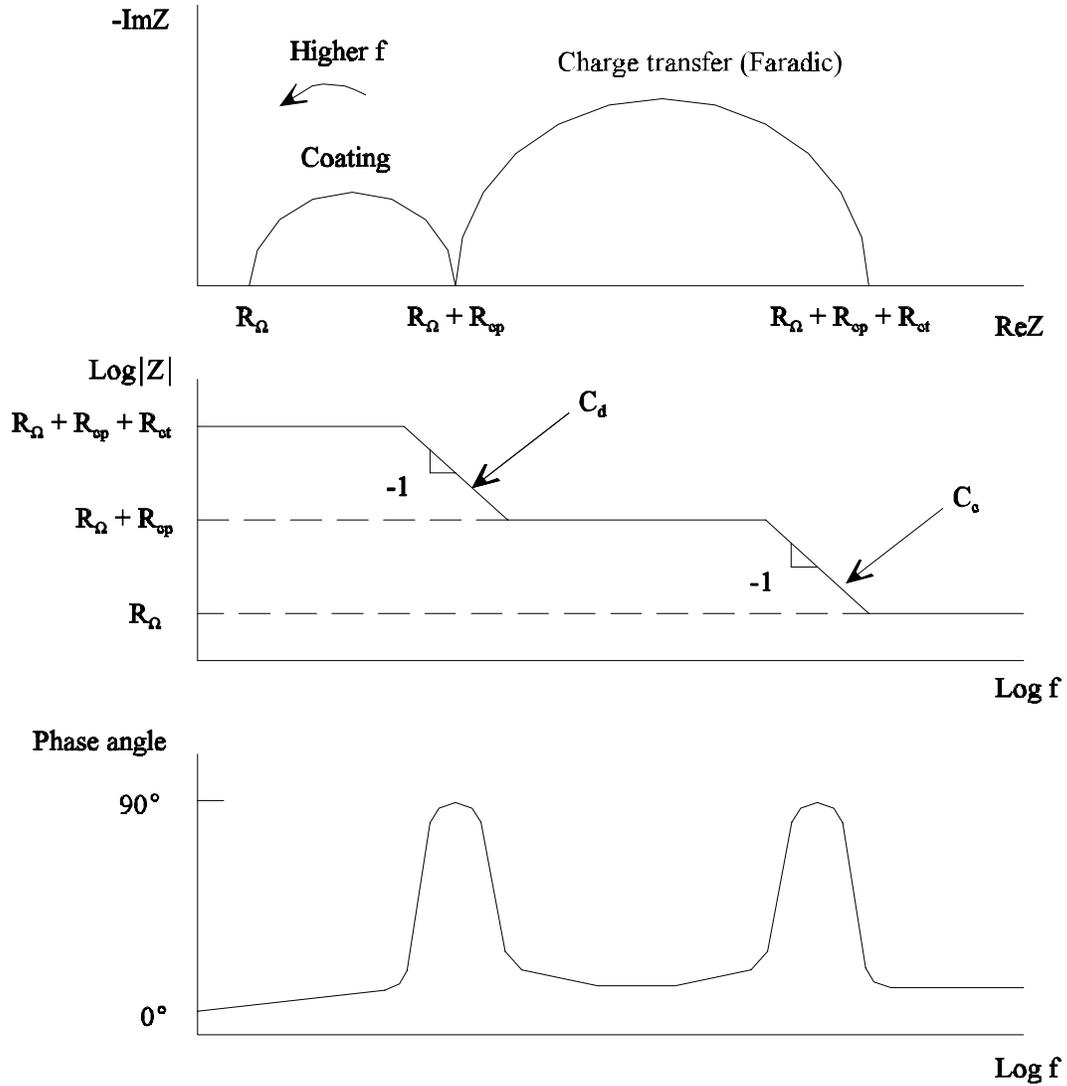

Figure 8.   Theoretical Nyquist Plot and Corresponding Bode Magnitude and Phase Angle Diagrams for the Equivalent Circuit Model in Figure 7, with the Diffusion Impedance, Z_w, Neglected [58].
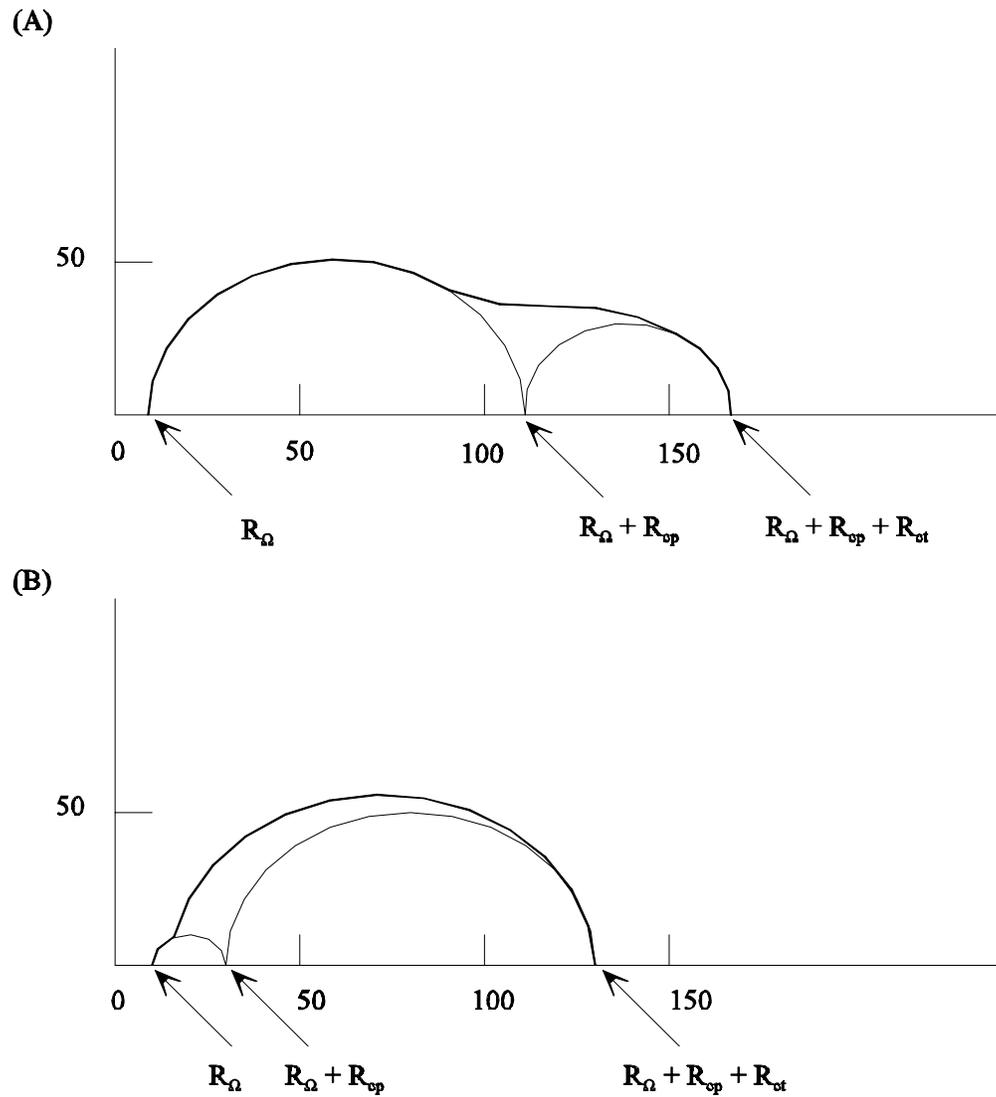
Figure 9.   Nyquist Plots for the Equivalent Circuit in Figure 7 [58]:
(A)   clear Separation of Two Semi-Circles; R_{ct}/r_{cp}=0.5, T_{ct}/τ_{cp}=20 (R_{cp}=100, R_{ct}=50);
(B)   indistinct Separation of Two Semi-Circles: R_{ct}/r_{cp}=5, T_{ct}/τ_{cp}=10 (R_{cp}=20, R_{ct}=100).
Resistance Values in Kilo-Ohms.

From the previous research it is known that the impedance response of a coated metal system is in reality more complicated than that of the theoretical systems presented above. A Nyquist plot, for example, will not have a form of an ideal semicircle, if the Warburg diffusion impedance, Z_w, is included in the model, Figure 10. Therefore, both diagrams, Bode and Nyquist, will be constructed when collecting typical data for a tested system. Their interpretation should be also done carefully.
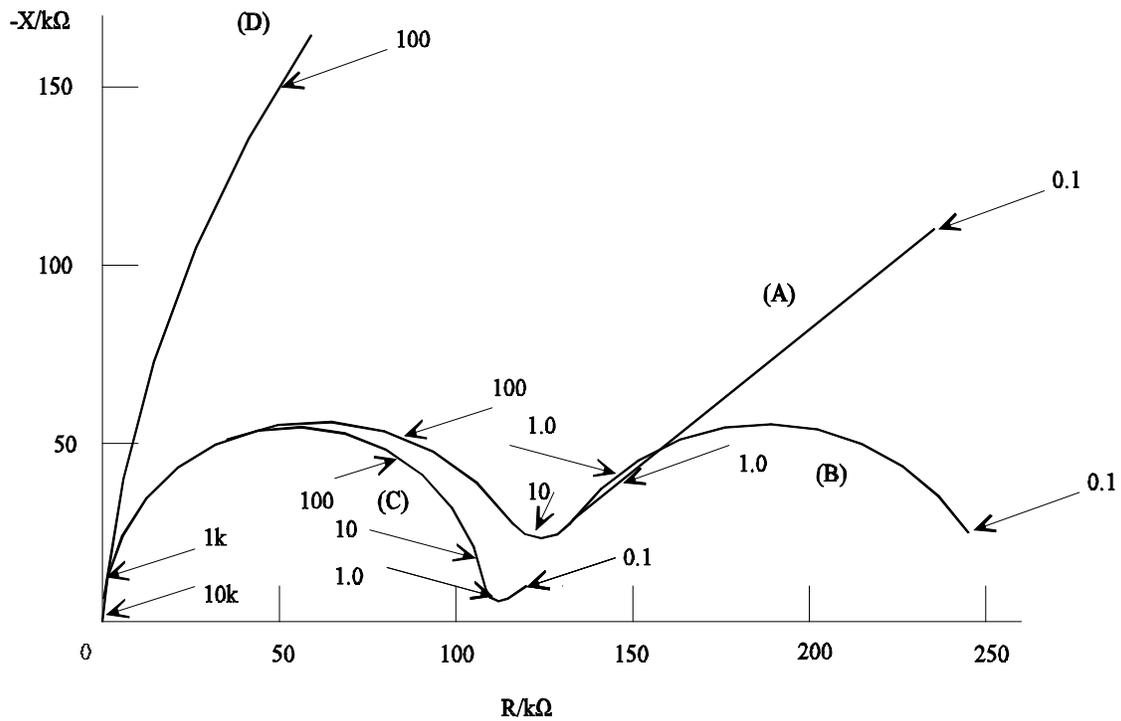

Figure 10.   Nyquist Plot for the Equivalent Circuit in Figure 7 Showing Influence of Diffusion on Charge Transfer Semi-Circle [58]:
(A)   combined Charge Transfer and Diffusion Rate Control:
(B)   as (A) with Different Diffusion Coefficient:
(C)   charge Transfer Rate Control;
(D)   diffusion Rate Control.
Rcp = 1 E4 Ohm, Rct = 1 E5 Ohm.
Numbers on Curve Indicate Frequency in Hz.

35

The EIS testing of epoxy-coated reinforcing steel has shown that for the perfect epoxy coating, the measured impedance values are greater than 10^8 Ω/cm^2, intermediate corrosion protection was found for impedance values between 10^6 and 10^8 Ω/cm^2, and poor corrosion performance was observed for impedance values below 10^6 Ω/cm^2 [60]

3.2 Corrosion Inhibitors

Corrosion inhibitors can be divided into three basic types: anodic, cathodic, and mixed. Anodic inhibitors react with existing corrosion products and form a highly insoluble film on the metal surface stopping the corrosive reaction at the anode. Cathodic inhibitors reduce the cathodic reaction. However, a mixed corrosion inhibitors seem to be the most suitable in the area of the corrosion prevention of the reinforcing steel in concrete because of the possibility of a microcell corrosion. Various inorganic and organic corrosion inhibitors are recommended for the protection of steel in concrete. Among them stannous chloride, zinc and lead chromates, potassium dichromate, calcium hypophosphite, sodium nitrite, and calcium nitrite, which belong to the group of inorganic inhibitors, and sodium benzoate, ethyl aniline, and mercaptobenzothiazole, members of the organic inhibitor category [4]. Two inhibitors were the most promising in the corrosion prevention of steel in reinforced concrete structures, calcium nitrite, in the United States, and sodium nitrite, in Europe. However, the use of sodium nitrite became questionable because of negative effects of this inhibitor on concrete durability, low strength, erratic setting times, efflorescence, and a high probability of an alkali-aggregate reaction.

Calcium nitrite represents an anodic type corrosion inhibitor. It reacts with Fe^{2+} ions that form in concrete, according to the following reaction:

$$2Fe^{2+} + 2OH^- + 2NO_2^- \rightarrow 2NO\uparrow + Fe_2O_3 + H_2O \tag{9}$$

changing ferrous ions into a stable passive layer. Since nitrite ions compete for ferrous ions with

chloride ions their concentration in concrete influences the protection mechanism. Through a series of tests, it was determined that if the Cl^- / NO_2^- ratio was below 1.5 or 2, corrosion could be controlled [61]. Other important information on the corrosion protection of reinforcement in concrete suggested that in the case of a concrete with a calcium nitrite concentration of 20 l/m^3 corrosion will not initiate until the chloride ion concentration reaches 7.6 kg/m^3 of concrete in comparison to 0.59 to 1.2 kg/m^3 for an unprotected concrete [61]. Estimated values of the calcium nitrite needed to protect reinforcing steel in concrete given the expected amount of chlorides reaching the bar depth are presented in Table 3.

Table 3.   Calcium nitrite dosage rate vs. chloride [61].

Calcium Nitrite, l/m^3	Chlorides, kg/m^3
10	3.6
15	5.9
20	7.7
25	8.9
30	9.5

The performance of calcium nitrite and two other corrosion inhibitors recommended for use in concrete, one being an aqueous mixture of amines and esters, and the other based on a mixture of alcohol and amine, was evaluated in solutions simulating concrete pore water [62]. Results of an accelerated testing demonstrated that only calcium nitrite inhibited the corrosion of reinforcing steel in chloride contaminated solutions up to the 5.86 kg/m^3 chloride concentration in concrete. The two other corrosion inhibitors demonstrated similar behavior as the specimens tested in solutions with no corrosion inhibiting admixtures.

3.3 Low Permeable Concrete

Addition of chemical and/or mineral admixtures can influence concrete properties including strength, permeability, freeze-thaw durability, alkali-silica reactivity, and resistance to chloride induced corrosion. Pozzolanic materials, fly ash and silica fume, and ground-granulated blast furnace slag, used as cement replacement have been successfully introduced into concrete mixtures to improve quality and performance.

Resistance to chloride ion penetration of concrete containing fly ash, silica fume (microsilica) or slag was investigated by Ozyildirim and Halstead [63]. Concrete with fly ash or slag demonstrated lower early strength but higher ultimate strength in comparison to the controls. Concrete with silica fume developed similar strengths or slightly higher. An addition of pozzolans or slag influenced rapid permeability test results. The obtained Coulomb values were lower for concrete with mineral admixtures or slag than for controls. A decrease in chloride intrusion into concrete was also detected for specimens with fly ash, microsilica or slag.

Berke also found that silica fume improves the compressive strength and reduces resistivity and chloride ingress of concrete mixtures [64]. A series of test performed on concrete containing microsilica and an air-entraining agent demonstrated an excellent resistance to freeze-thaw damage according to ASTM C 666.

Ozyildirim and Halstead investigated the influence of combining silica fume and fly ash on concrete quality [65]. Satisfactory strength and very low permeability were observed when small quantities of silica fume were added to the concrete with fly ash and water to cement ratio of 0.40 to 0.45. The authors recommended the use of concrete mixtures containing fly ash and silica fume as a possible protection method against corrosion of reinforcing steel for pavements and bridge structures exposed to deicing salts or marine environments.

Improved characteristics of concrete with silica fume relative to protection against chloride

induced corrosion were investigated by Gjørv [66]. Silica fume decreased the chloride diffusivity of concrete. Chloride diffusion rate was reduced by a factor of about five for a 9 percent cement replacement with silica fume in high-grade concrete. Concrete with silica fume demonstrated also an increase in electrical resistivity. At the same time, the pH value of about 12.5 was determined for a silica fume concrete with a 20 percent cement replacement. The obtained pH of 12.5 was higher than 11.5 considered as a threshold limit for maintaining the passivity of reinforcing steel.

3.4 Combined Systems

Calcium nitrite as a corrosion inhibitor admixture was found to meet the requirements of ASTM C494 on compressive strength and setting time and to perform well in the presence of cracks in concrete. Previous research demonstrated that the corrosion protection performance of calcium nitrite improves when used in combination with the high quality, low permeable, concrete. Low water to cement ratio and an adequate reinforcing steel cover depth were mentioned as two characteristics important in concrete quality assurance programs which will influence the protective action of calcium nitrite. The use of an air entraining agent and a high-range water reducer with calcium nitrite improves the resistance to freezing and thawing damage. The compatibility of calcium nitrite with low permeable concrete containing microsilica or fly ash was also demonstrated [61].

Chapter 4. PURPOSE AND SCOPE

The objective of this research is to determine the performance of epoxy-coated reinforcement (ECR) in concrete bridge decks. Parameters influencing the service life of ECR in the field, coating damage and thickness, bond strength between the coating and steel surface, and surrounding concrete properties, were also examined. The cost effectiveness of ECR was estimated , initial and life cycle cost, and compared to other systems typical for concrete bridge decks.

All analysis was based on the data obtained from ECR used in bridge decks in Virginia. Construction costs of concrete bridge decks with ECR or black steel were estimated with current reinforcement, concrete and corrosion inhibitor bid prices.

The research presented here provides field performance characteristics of epoxy coating on reinforcing steel used as the main protection method against chloride ion induced corrosion. The fundamental quality determined in this study was the approximate time for the epoxy-coating to sustain its protective properties, time after which the adhesion between the coating and the steel bar was lost. Other characteristics, influence of the cover depth, concrete properties, and the presence of chloride ions on the performance of the epoxy-coated reinforcing steel were also examined.

Chapter 5. METHODS AND MATERIALS

ECR specimens obtained from existing bridge decks built in Virginia were evaluated in this study.
Eighteen bridge decks built between 1977 and 1995 with the epoxy-coated reinforcing steel, used
as the top and in most cases the bottom reinforcement, were randomly selected, with two decks
being in each of the nine Engineering Districts. Cores, 102 mm in diameter, were drilled through
top ECR and bottom ECR (truss bars). Table 4 presents the bridge structure number, year built,
age at coring, and number of cores taken. In addition, the results of the analysis of three bridges,
sampled in Phase I of this study, are included [51].

Table 4.   Bridge Deck List - ECR Phase II.

District	Structure Number	Year Built	Bridge Age, years	Number of Cores	
				top mat	bottom mat
1 - Bristol	1136	1995	2	12	3
1 - Bristol	6243	1995	2	12	2
2 - Salem	6161	1987	10	12	3
2 - Salem	1015	1987	10	10	3
3 - Lynchburg	1020	1983	14	9	2
3 - Lynchburg	1004	1983	14	12	3
4 - Richmond	2022	1989	9	10	3
4 - Richmond	6005	1989	9	12	3
5 - Suffolk	2021	1981	16	12	3
5 - Suffolk	1032	1980	17	12	3
6 - Fredericksburg	1006	1993	4	12	3
6 - Fredericksburg	1004	1993	4	12	3
7 - Culpeper	1001	1992	5	12	3

Table 4.   Bridge Deck List - ECR Phase II (cont.).

7 - Culpeper	1019	1990	7	9	2
8 - Staunton	2068	1978	19	12	3
8 - Staunton	1056	1977	20	12	2
9 - Northern Virginia	2262	1985	12	12	3
9 - Northern Virginia	1029	1986	11	12	3
Total				206	50

The research consisted of two main tasks: field investigation and the laboratory testing. Life cycle cost analysis for bridge decks built with ECR and other corrosion protection systems are included in the study.

5.1 Field Survey

Visual examination of each bridge deck was performed. Structure dimensions, the deck configuration and the superstructure type were determined as well as general condition of the bridge deck. Based on the general observation that the right traffic lane deteriorates first, the field survey was limited to this lane [44].

For each bridge deck chosen for the evaluation a maximum of 12 cores with the top ECR and 3 cores with the bottom ECR were obtained. Statistically, twelve samples is a sufficient number of samples for the observations being evaluated for a bridge [44].   All cores were 102 mm in diameter. Core locations were determined based on the lowest 12 % cover depth calculated from cover depth measurements for each bridge deck. Total of 40 random cover depth measurements were obtained for each bridge span or 1/3 section using the rebar locator, Profometer 3, produced by Proseq SA, Switzerland.

Drilled cores were tested first for depth carbonation and allowed to surface dry, then numbered, wrapped in the clear polyethylene wrap, aluminum foil, and duct tape to maintain the in-place moisture content. The cores were transported to the laboratory and stored in plastic-covered containers until testing.

5.2 Laboratory Testing

A visual examination was performed on each concrete core immediately after unwrapping. Cover depth was measured and compared to cover depth values obtained in the field. Electrochemical Impedance Spectroscopy (EIS) and Linear Polarization (LP) measurements were collected from 3 ECR top mat specimens from each bridge deck. EIS is a technique used in the evaluation of coatings and the interface between a metal and a conductive solution. Direct current (DC) potential and a small superimposed alternating current (AC) excitation are applied to a metal sample immersed in solution using a potentiostat. AC current and AC potential are measured and converted into a complex impedance. LP, a direct current technique, permits the rapid determination of the instantaneous corrosion current density (corrosion rate). LP is capable of measuring very low corrosion rates (less than 0.1 mpy). Linear-polarization analysis is based on the observation that for more noble or more active potentials than the corrosion potential, within 10 mV, the applied current density is a linear function of the electrode potential [45].

Small disks containing the ECR were cut from each core using a water-cooled diamond saw to allow for the easy removal of bar samples from concrete. Rapid chloride permeability testing (ASTM C 1202 "Electrical Indication of Concrete's Ability to Resist Chloride Ion Penetration") was performed on 2 to 3 cores from each bridge deck at Virginia Transportation Research Council. The test is based on the evaluation of the electrical conductance of concrete samples and its relation to concrete resistance to chloride ion penetration. Electrical current is passed through 51 mm thick concrete disk, 102 mm in diameter, for a 6 hour period. One end of the specimen is immersed in a 0.3 N sodium hydroxide solution and the other in a 3 % by mass sodium chloride

solution. A potential difference of 60 V dc is applied to the specimen and the total charge passed, in Coulombs, is recorded. Resistance to chloride ion penetration is based on the measured total charge transfer, see Table 5.

Table 5.   Chloride Ion Permeability Based on Charge Passed [67].

Charge Passed (Coulombs)	Chloride Ion Penetration
> 4,000	High
2,000 - 4,000	Moderate
1,000 - 2,000	Low
100 - 1,000	Very Low
< 100	Negligible

Moisture content and absorption of concrete at top and bottom bar depths was determined in accordance with ASTM C 642 "Specific Gravity, Absorption, and Voids in Hardened Concrete". Two individual portions from each concrete core were obtained. The following weights were determined for each test sample: initial weight, oven-dry weight, and saturated weight after immersion. Moisture content, absorption and saturation were calculated from the obtained weights.

Powdered concrete samples at 13 mm depth were collected from each core and tested for the chloride content according to ASTM C 114 "Chemical Analysis of Hydraulic Cement", Section 19. Chloride. The test procedure is based on a potentiometric titration of 10 g concrete samples with 0.05 N silver nitrate solution. The percent chloride was calculated along with the chloride equivalent in kilogram per meter cubed of concrete.

Damage evaluation was performed for each ECR specimen extracted from the concrete core. The Tinker & Rasor Model M/1 Holiday detector was used according to ASTM G 62 "Holiday

44

Detection in Pipeline Coatings" to locate any flaws (holidays) in the coating not visible with the unaided eye. Coating thickness was measured according to ASTM G 12 "Nondestructive Measurement of Thickness of Pipeline Coatings on Steel" using the coating thickness gauge Minitest 500 produced by Elektro-Phisik, Germany.

Adhesion of the epoxy coating was tested using MTO - Draft 93 10 27 "Hot Water Test for Epoxy-Coated Reinforcing Bars." An "x" cut was made in the coating between bar deformations and an area exposed by inserting the blade of an ex-acto knife underneath the coating. An adhesion number between 1 and 5 is assigned to each test, see Table 6 . A total of 6 adhesion tests were performed on each ECR specimen and the average adhesion was calculated for each specimen.

Table 6.   Adhesion Rating.

Adhesion Number	Description of Tested Area
1	unable to insert blade tip under the coating
2	total area of exposed steel < 2 mm^2
3	2 mm$^2 <$ total area of exposed steel < 4 mm^2
4	total area of exposed steel > 4 mm^2
5	blade tip slides easily under the coating, levering action removes the entire section of the coating

Visual examination and the Scanning Electron Microscope (SEM) were used to examine the steel surface under the coating. Energy Disparsion Analysis of X-rays (EDAX) and X-ray Photoelectron Spectroscopy (XPS) were used to evaluate the chemical composition of the exposed steel. The visually observed color of the steel surface color under the coating was compared later with determined adhesion values. SEM, XPS, and EDAX measurements were

performed on 5 selected specimens, which represented the range of the visually observed steel surface colors.

5.3 Life Cycle Costs

Service life extension of bridge decks with ECR in comparison to other corrosion protection systems presently used in the United States was estimated. Initial costs for bridge decks with ECR, black steel (BS), low permeable A4 concrete, corrosion inhibitors and their combinations were calculated. The present value of the life-cycle cost using a 5% interest rate for 75 year design life was determined for the following systems:

- ECR with A4 concrete
- ECR with low permeable A4 concrete
- BS with A4 concrete
- BS with low permeable A4 concrete
- BS with A4 concrete and corrosion inhibitor, DCI-S 10 l/m^3 of concrete
- BS with low permeable A4 concrete and corrosion inhibitor, DCI-S 10 l/m^3 of concrete.

The results of the analysis were then compared and the most cost effective method was selected.

Data used for the life-cycle cost determination included the following parameters: cost, inflation, interest rate, and service life. Costs were estimated for a one square foot of bridge deck surface area. The bridge deck was assumed to be 8 in. thick with two layers of reinforcing steel, top and bottom: #5 bars with 8 in. spacing and #4 bars with 12 in. spacing. Concrete and reinforcing steel costs were calculated based on bid information provided by VDOT.

The inflation rate for the evaluated systems, with the exception of low permeable concrete, was assumed to be equal to the actual price change. Based on a deflation in price expected for low permeable concrete the 1997 and 1996 prices of this product were anticipated to be equal. The

true interest rate should be considered to be about 4 to 6 % [68]. Thus an interest rate of 5 % was used in the presented life-cycle cost analysis.

A design service life of 75 years was selected as the comparison period for the evaluated systems. Service life estimates were calculated based on the time-to-initiated corrosion and time-to-spalling estimated in previous field and laboratory studies [68,69].

Chapter 6.   RESULTS

6.1 Field Survey

During the field survey, prior to drilling the cores with ECR specimens, all span lengths were measured, and number of coring locations per each span was determined. Skew angle was also calculated to indicate the direction of the main reinforcement. According to the present practice in Virginia, the transverse reinforcement should be parallel to the end of the slab on bridges having skews of less than 20°, and perpendicular to the beams on bridges having skews of more than 20°. Direction of the reinforcement in the deck, cover depth measurements, and the calculation of the lowest 12th percentile cover depth for each span of the bridge were the main steps necessary in selecting the core locations.

Cores were drilled through the main reinforcement only, in a certain distance from the beams to avoid cutting through the additional bars. Precautions were also taken while drilling the "deep" cores containing truss bar specimens. Knowing the approximate deck thickness and the use of stay-in-place forms during the bridge construction, the VDOT drilling crews were instructed to avoid drilling through the full depth of the deck.

Last stage of the bridge deck evaluation included delamination inspection. A heavy metal rod was used to detect delaminations around top reinforcing bar core locations.

6.1.1 Cover Depths

Cover depth measurements for the 21 bridge decks (Phase I and Phase II) were normally distributed with the mean of 65 mm and the standard deviation equal to 9.1 mm, see Figure 11. As shown in Figure 12, 8 bridge decks had an average cover depth between 50 and 65 mm, 9 decks between 66 and 74 mm, and the cover depth for one deck was greater than 75 mm.
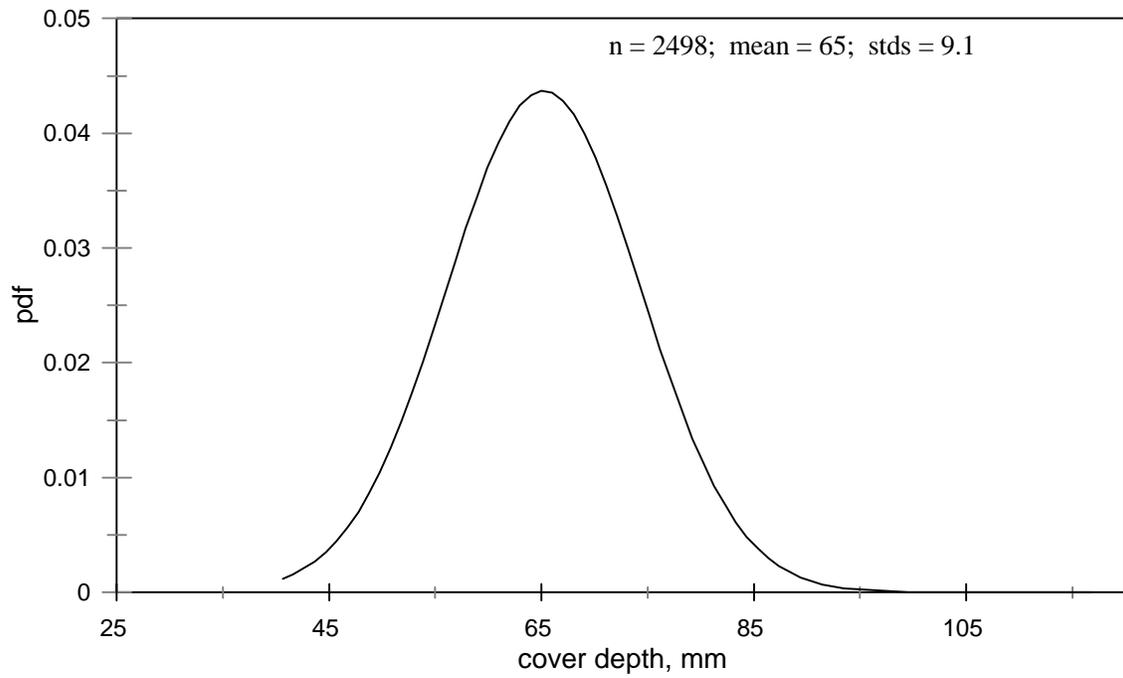
Figure 11.   Cover Depth Measurement Distribution (Phase I and Phase II).
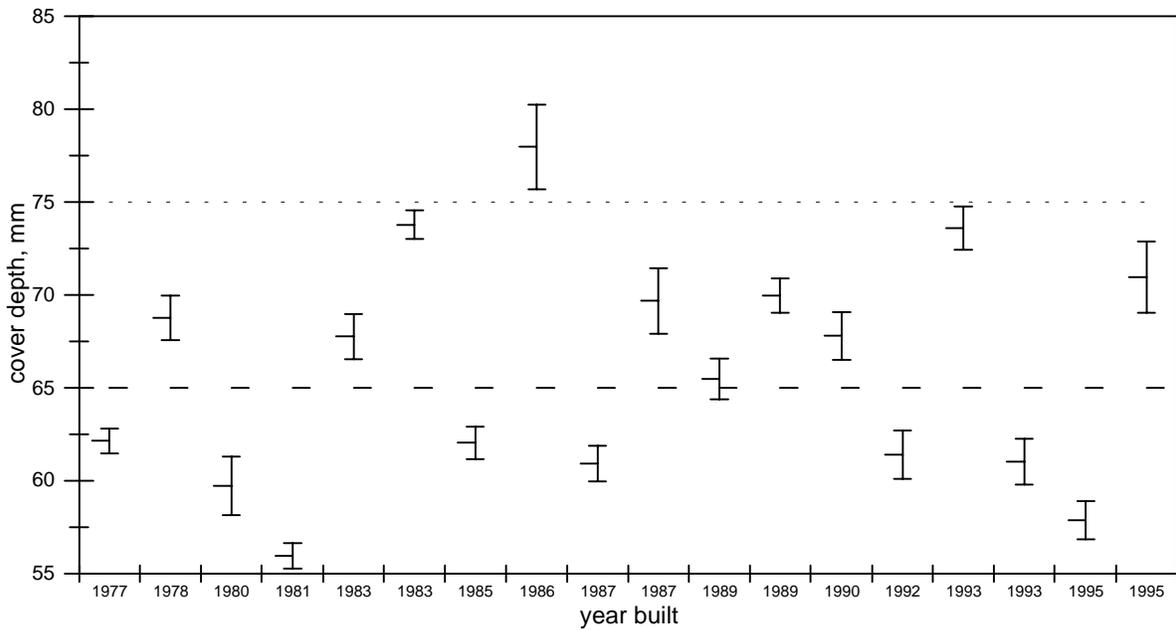
Figure 12.   Average Bridge Deck and VDOT Specification Limits 95% Confidence Intervals.

49

The span on each bridge with the lowest cover depth was identified and the lowest 12 percentile cover depth was determined. Of the 18 decks, 7 decks had the lowest 12 percentile cover depth of less than 50 mm, 8 decks ranged between 51 and 65 mm, and one deck had a lowest 12 percentile cover depth of 66 mm, Figure13.
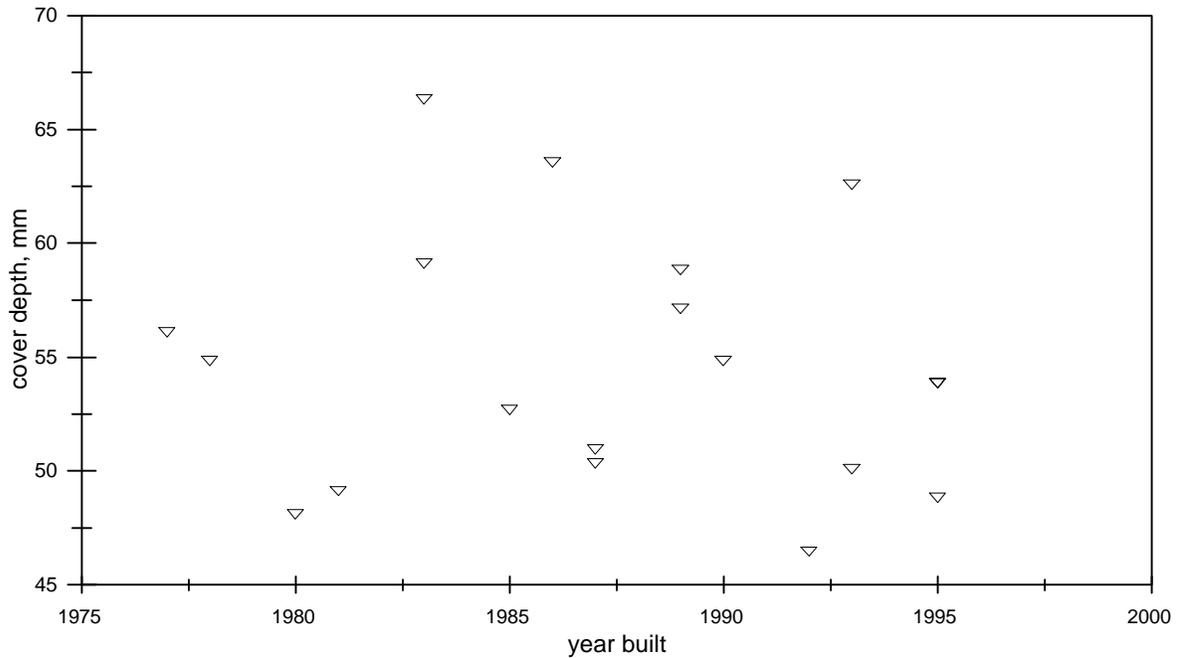
Figure 13.   Span with the Lowest 12th Percentile Cover Depth for Each Bridge Deck.

6.1.2 Visual Condition, Carbonation and Delaminations

The visual condition of all the decks was good, no spalling with very little cracking. The cracking in the right lane was longitudinal, parallel to main beams or girders. The deck concrete was not measurably carbonated, less than 1 mm. No delaminations were detected at core locations. The only bridge deck where delaminations were detected was in the Phase I of the project on SN 8003 built in 1979 and located in Blacksburg, Virginia.

6.2 Laboratory Evaluation

Series of tests were performed on each extracted core. The test regime included an examination of the hardened concrete properties and an evaluation of the condition of the epoxy coating and the steel surface under the coating.

6.2.1 Concrete

Concrete cores drilled from the bridge decks, selected for this research, were visually examined prior to bar extraction. All cores had similar visual appearance. The coarse aggregate used was a crushed stone, angular in shape, with a maximum size of about 25 mm. The fine aggregate was manufactured sand. The only exception was the concrete from four bridge decks, SN1006 and SN1004 built in 1993, SN1001 built in 1992, and SN1019 built in 1990, which had crushed gravel as the coarse aggregate and natural sand as the fine aggregate. The aggregates were well graded and uniformly distributed. The cement matrix was gray in color with a normal amount of entrained and entrapped air. Concrete in all cores was well consolidated. Observed surface cracks were shallow and the widths ranged from 0.007 to 0.025 mm.

6.2.1.1 Rapid Permeability

Rapid chloride permeability testing was performed on concrete cores obtained from the bridge decks. Two concrete disks were cut from each core to allow for determination of concrete permeability for the surface and base concrete.

For the surface concrete, seven structures had an average charge passed of 1000 coulombs, six structures ranged between 1000 and 2000 coulombs, and the remaining five structures average

surface concrete charge passed was greater than 2000 but less than 3000 coulombs, see Figure 14.
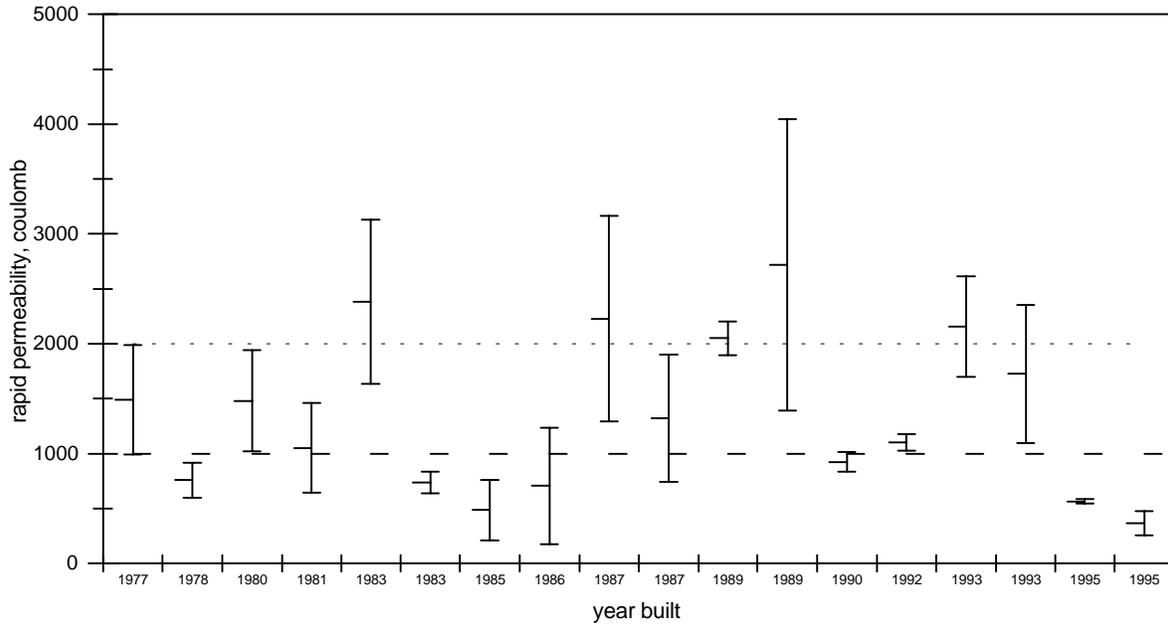
Figure 14.   Rapid Chloride Permeability Test Results, 95% Conf. Interval, Surface Specimens.

Two structures had an average base concrete charge passed less than 1000 coulombs, 5 were between 1000 and 2000 coulombs, 2 greater than 2000 but less than 3000, 4 between 3000 and 4000 coulombs, 4 between 4000 and 5000 coulombs and 1 greater than 6000 coulombs, see Figure 15.
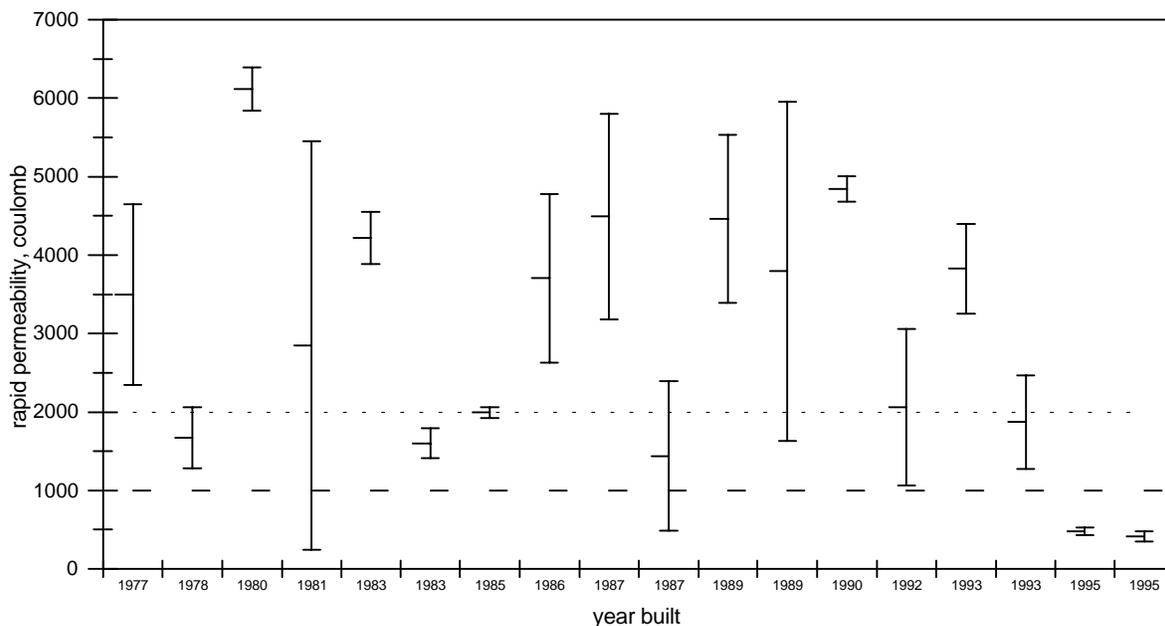
Figure 15.   Rapid Chloride Permeability Test Results, 95% Conf. Interval, Base Specimens.

6.2.1.2 Chlorides

The four decks with the lowest average near surface chlorides were SN's 6005, 1004-6, 1006, and 2022 built in 1989, 1993, 1993, and 1989, respectively, with a chloride content of 0.74, 0.84, 0.86, and 0.89 kg/m^3. The decks with the highest near surface chlorides were SN's 1015, 2068, 1004-3 and 1056 built in 1987, 1978, 1983 and 1977, respectively, with a chloride content of 5.77, 5.01, 4.46 and 3.97 kg/m^3, see Table 7. Also shown in Table 7 are the near surface chloride content standard deviations and coefficients of variation. The standard deviation values for the bridge decks with the lowest chloride contents were 0.35, 0.32, 0.55 and 0.40, respectively, with the coefficients of variation equal to 47, 38, 64, and 45 %. The standard deviations and coefficients of variation observed for the bridge decks with the highest chloride concentrations were 2.31 and 40 %, 1.30 and 26 %, 0.77 and 17 %, and 1.18 and 30 %, respectively.

53

Table 7.   Average Chloride Content @ 13 mm Concrete Depth.

Structure Number	Year Built	Samples	Chloride Content @ 13mm, kg/m^3 of concrete		
		#	average	std.dev.	coef. var.
1056	1977	12	3.97	1.18	30
2068	1978	11	5.01	1.30	26
1032	1980	12	1.32	0.42	31
2021	1981	12	1.09	0.69	63
1004	1983	12	4.46	0.77	17
1020	1983	9	2.36	1.57	67
2262	1985	12	2.16	0.77	36
1029	1986	12	1.32	0.87	66
1015	1987	10	5.77	2.31	40
6161	1987	12	1.59	0.62	39
6005	1989	11	0.74	0.35	47
2022	1989	9	0.89	0.40	45
1019	1990	10	1.70	0.81	48
1001	1992	12	2.54	0.81	32
1004	1993	12	0.84	0.32	38
1006	1993	12	0.86	0.55	64
6243	1995	13	1.17	0.66	56
1136	1995	12	1.40	0.87	62

6.2.1.3 Moisture Content, Absorption, and Saturation

The average moisture content and average absorption of concrete was determined at top and
bottom mat of reinforcement. The percent moisture and absorption are normally distributed,

Figures 16 and 17. Percent average moisture content for the top reinforcement concrete was in the range of 4.0 to 5.5 %, with the exception of one bridge deck , SN1136, built in 1995, which exhibited a moisture content of almost 6.0 %, Figure 18. Percent average absorptions were within the range of 5.4 to 6.5 %.
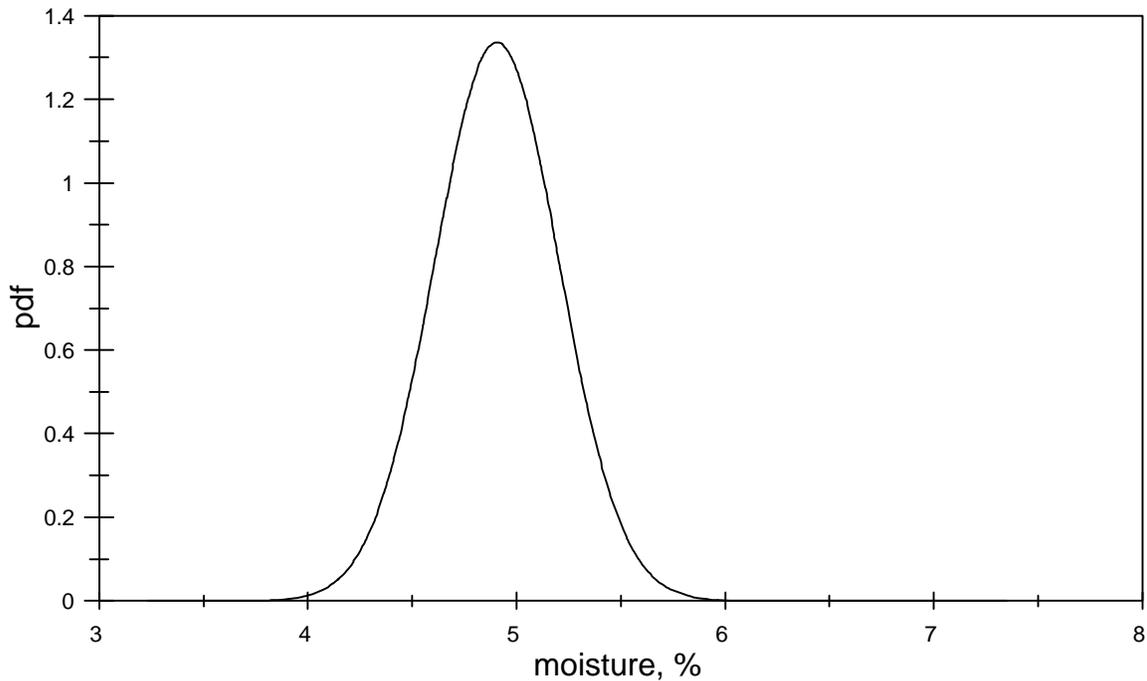
Figure 16. Moisture Content Distribution.

Average percent moisture content at the truss bar depth was generally within the range of 3.5 to 5.0 %. However, SN1015 built in 1987 and SN1136 built in 1995, had higher moisture contents of 5.4 and 5.8 %, respectively, Figure 19. The percent average absorption was between 5.0 and 6.0 %, except for one structure, SN1136, which had an average absorption value of 6.9 %. In general, the concrete moisture and absorption contents of top and bottom reinforcing mats agreed with each other, Figures 18 and 19.

The average saturation for top bars and truss bars was in the range of 72 to 92 %, Figure 20. The higher variability in saturation values was observed for truss bar concrete.
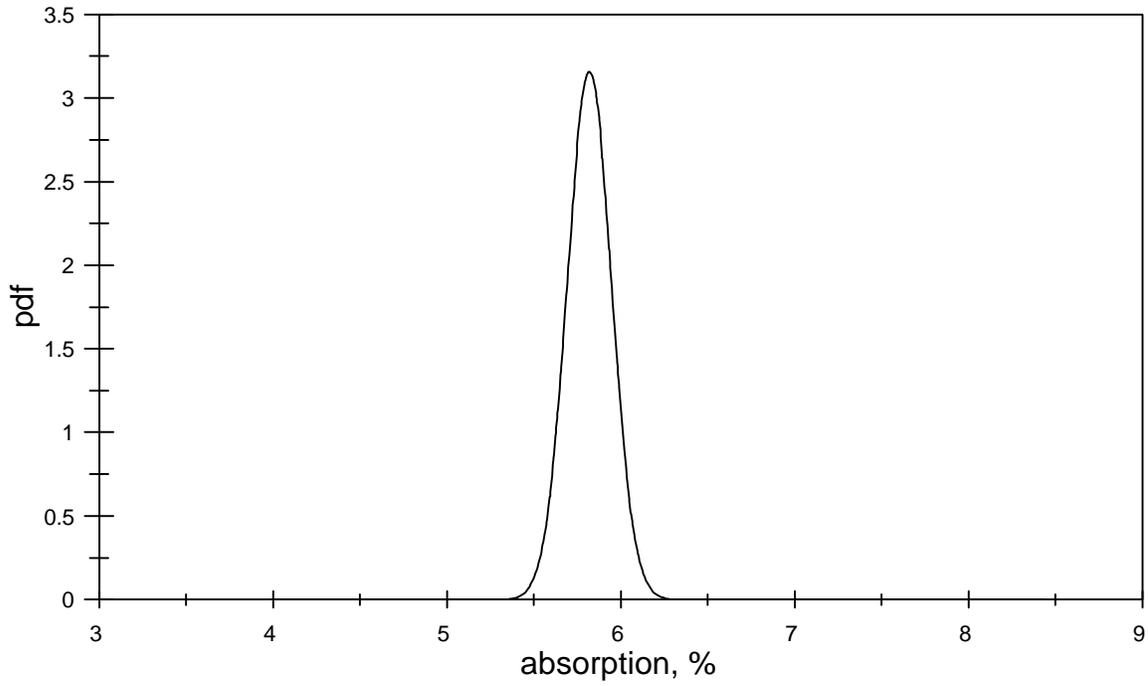
Figure 17. Absorption Distribution.
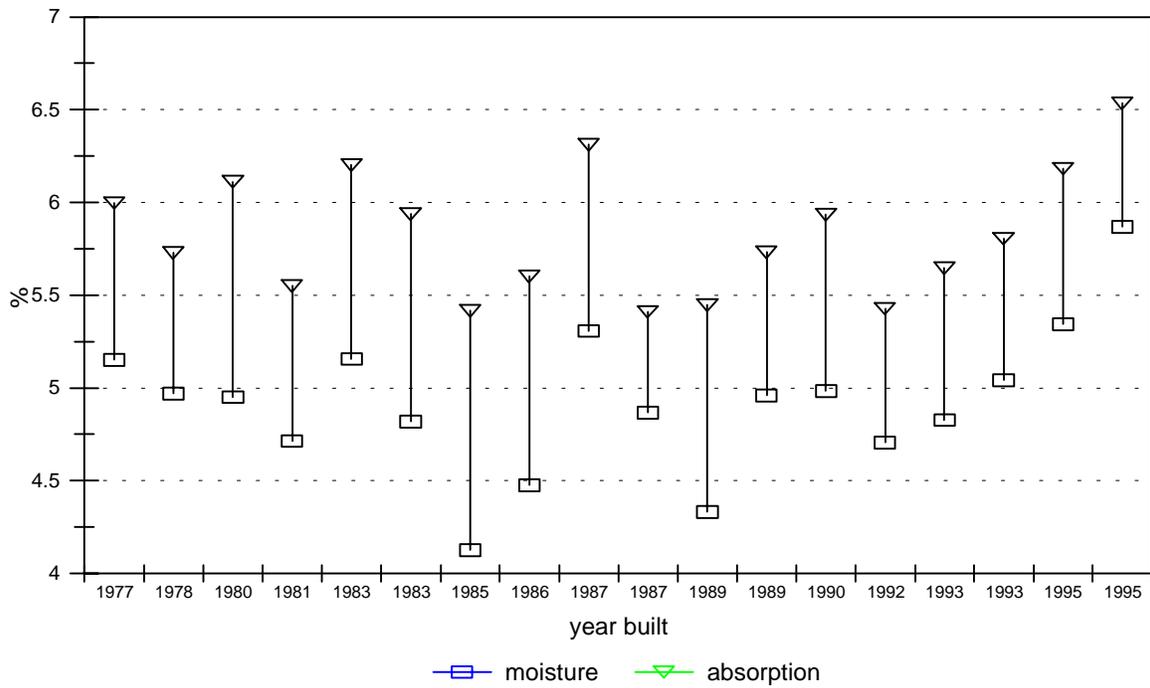
Figure 18. Average Moisture and Absorption, Top Bars.

56
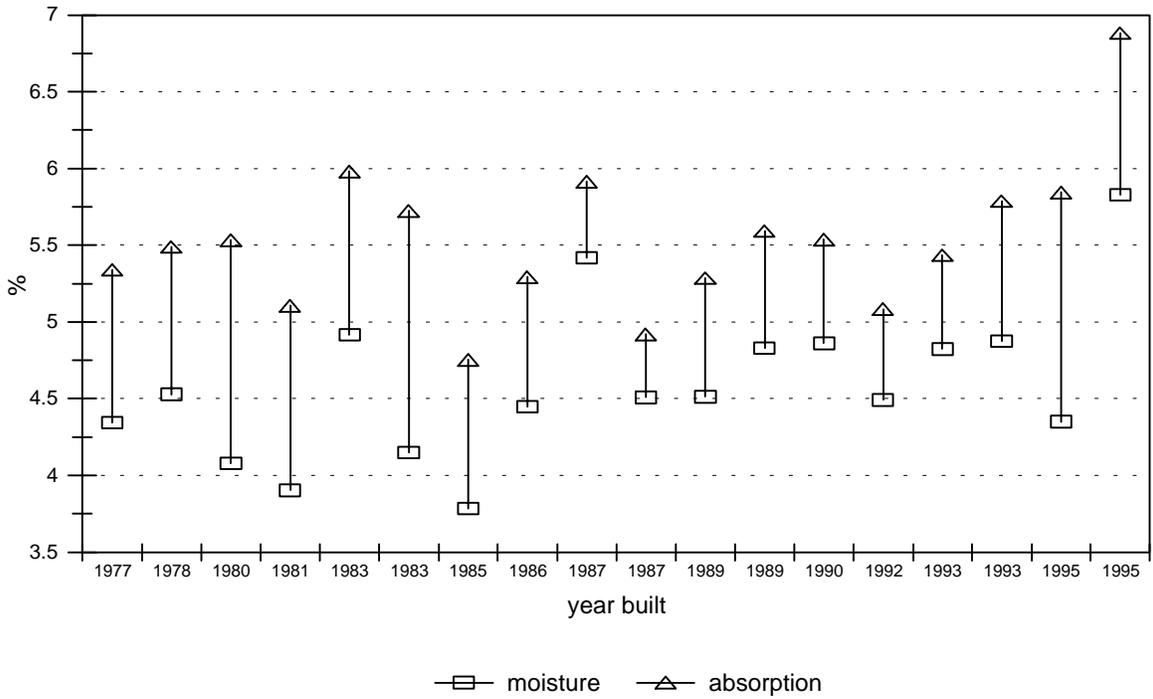
Figure 19. Average Moisture and Absorption, Truss Bars.
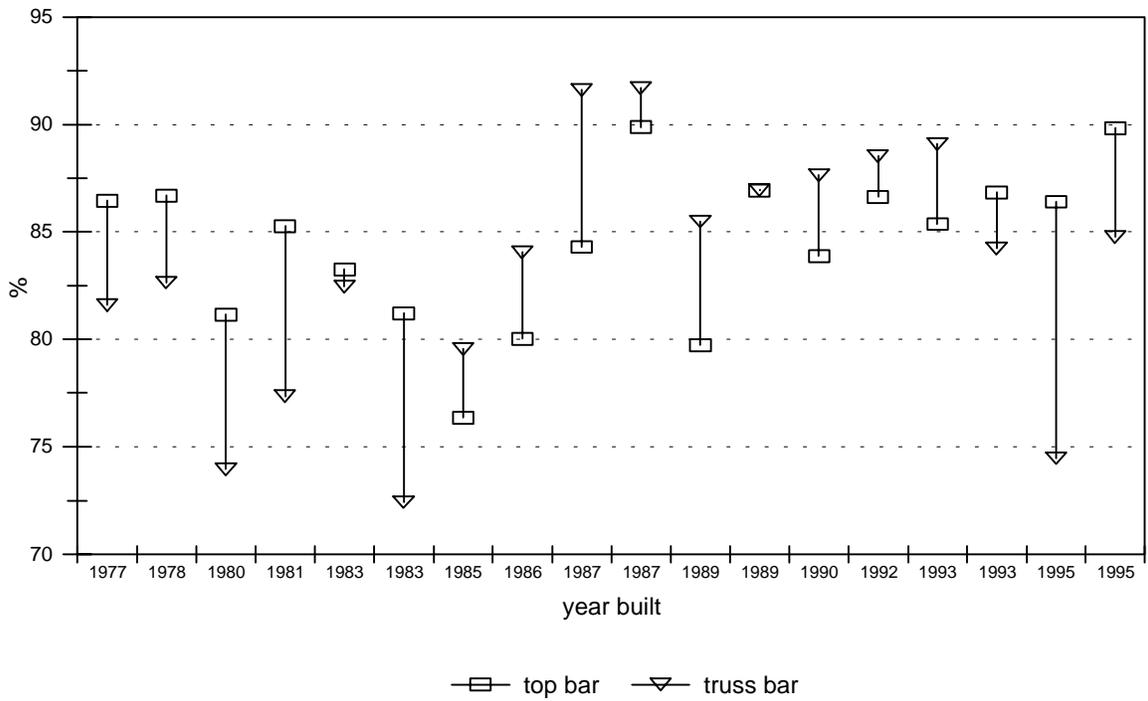
Figure 20. Average Saturation, Top and Truss Bars.

6.2.2   ECR

ECR specimens, approximately 102 mm long, obtained from each concrete core were evaluated in the laboratory testing phase of the research. A total length of 0.9 to 1.2 m of ECR from the top mat and about 0.2 to 0.3 m from the bottom mat, for each bridge deck, was examined. Tested epoxy-coating had two colors: green or red-brown. Brown coating was from four older structures: SN1056 built in 1977, SN2021 built in 1981, and SN1020 and SN1004 built in 1983.

6.2.2.1 Damage

Visual examination was performed on ECR specimens and percent damaged area was calculated, with 1 mm^2 accuracy. Type of damage detected in the epoxy-coating included mashed, dent and scraped spots, as well as cracks and blisters. Results of visual inspection are presented in Figures 21 and 22.

Damage observed on top and bottom bars was below the specification limit of maximum 1 % in each 0.3 m of the bar, see Figure 21. Average damage for the top bars was between 0.05 and 0.5 %, and within the range of 0 to 0.2 % for the truss bars, Figure 22.

6.2.2.2 Holes

Number of holes in the epoxy-coating was determined during the visual inspection of ECR specimens. For the ECR specimens from the top mat, the average number of holes was equal to 0, with the exception of two bridge decks, SN2262 built in 1985 and SN1006 built in 1993, where the average number of holes was 0.07 and 0.34 holes per meter, respectively, Figure 23. For the truss bars, holes were detected only in one set of specimens, SN2068, built in 1978. The average number of holes was 1.09 holes per meter, see Figure 24.
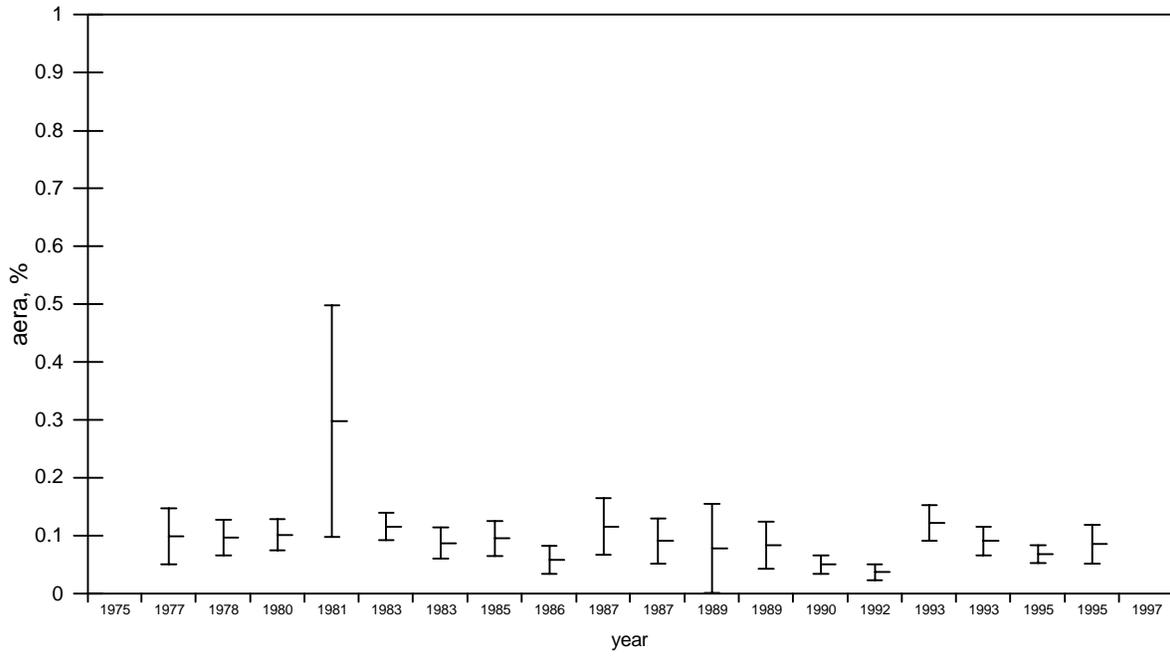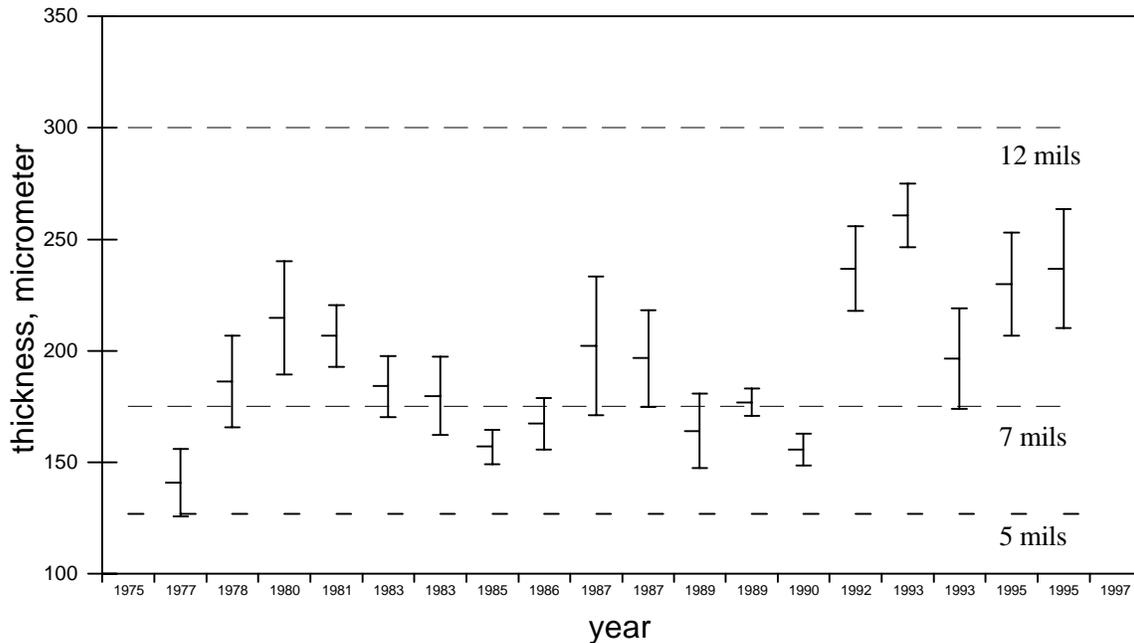
Figure 21.   Average Coating Damage, 90% Confidence Interval, Top Bars.
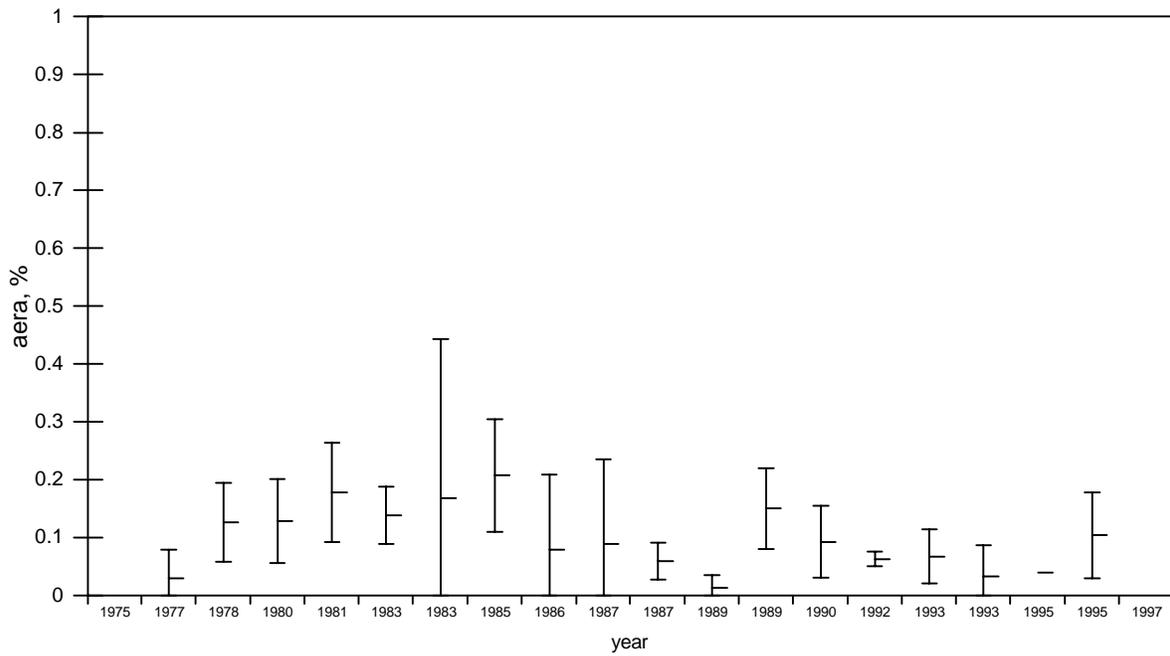
Figure 22.   Average Coating Damage, 90% Confidence Interval, Truss Bars.
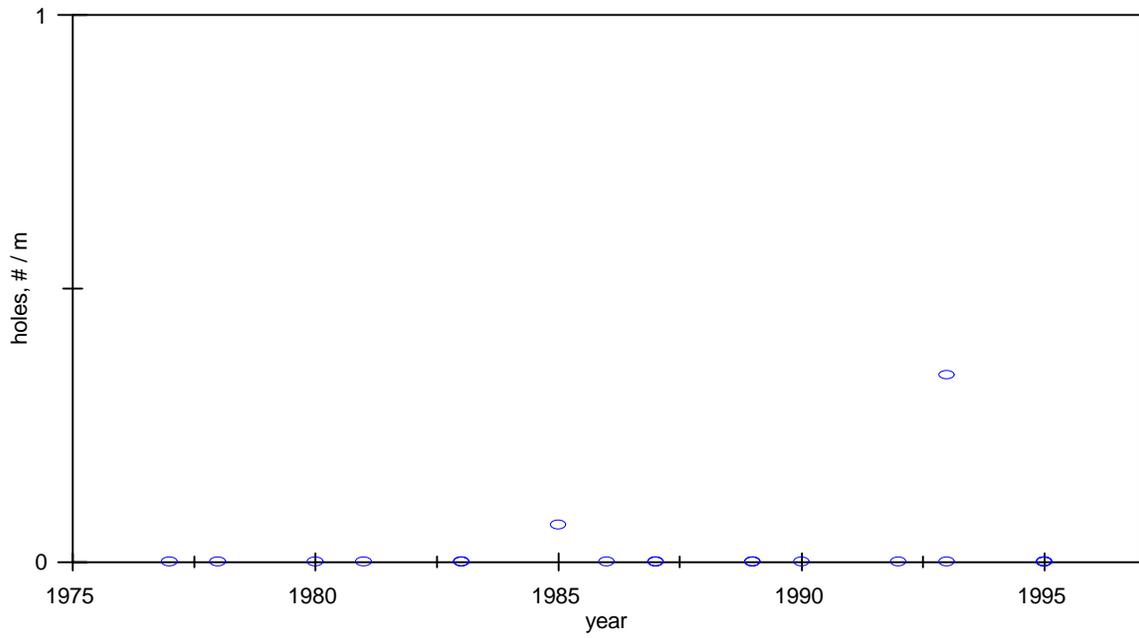
Figure 23.   Average Number of Holes, Top Bars.
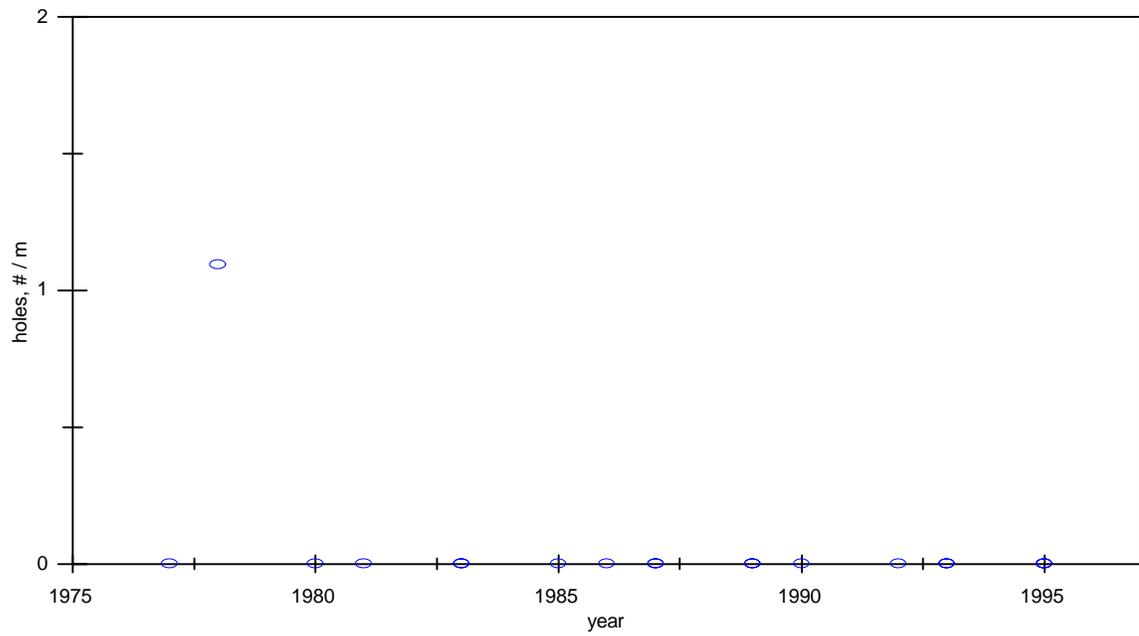
Figure 24.   Average Number of Holes, Truss Bars.

6.2.2.3 Holidays

Number of holidays per meter was examined on each ECR specimen. Average number of holidays was also determined for every bridge deck, Figures 25 and 26. Top bar inspection showed one bridge deck built in 1977, SN1056, that had an average of 44 holidays per meter in the epoxy-coating, and one structure, SN1020 built in 1983, with an average holiday number per meter equal to 3, Figure 25. Both values are above the specification limit from 1995, which recommends 3 holidays per meter. However, the specimens from SN1020 built in 1983 met the specification limit of 6 holidays per meter, dated 1981, in use at the time of construction. Average number of holidays per meter for the other bridge decks was in the range of 0 to 3, Figure 25.
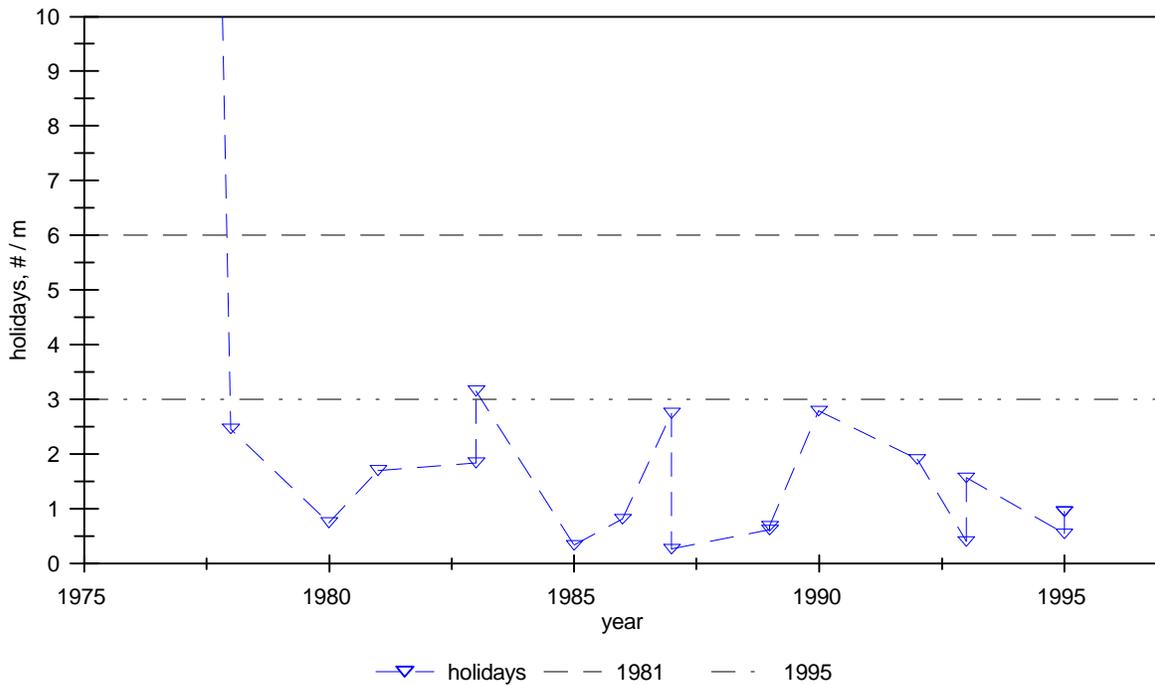
Figure 25. Average Number of Holidays, Top Bars.
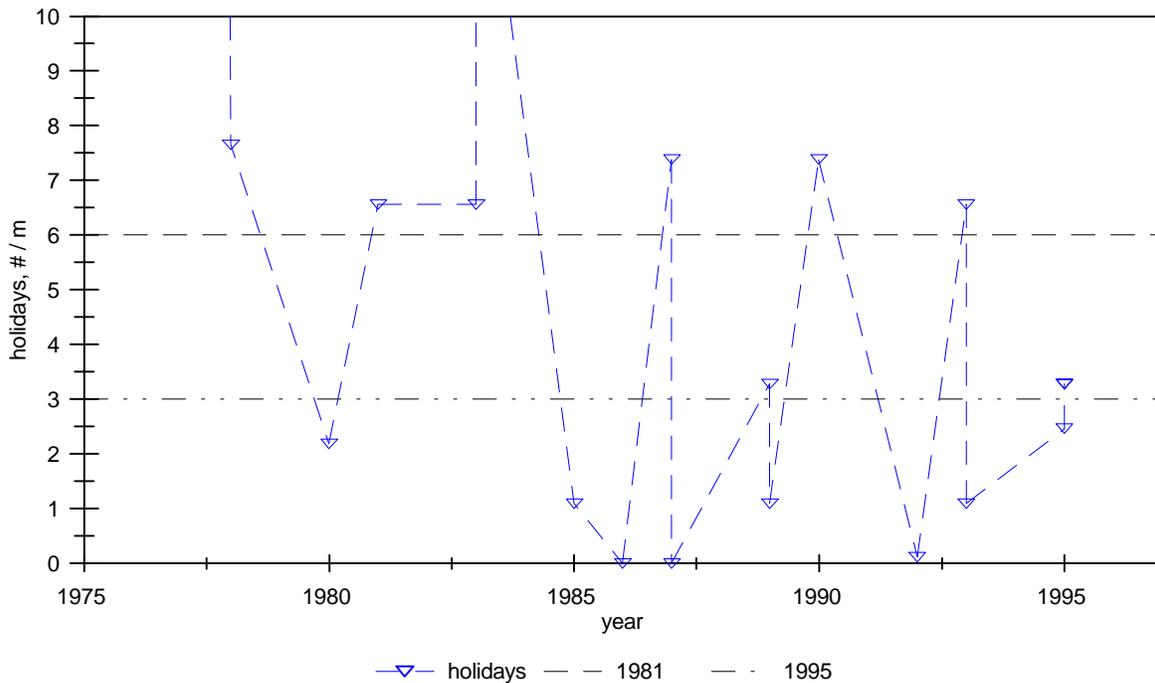
Figure 26.   Average Number of Holidays, Truss Bars.

ECR specimens from truss bars have higher variability in number of holidays per meter which is probably related to the small sample size, 2 or 3 specimens from each bridge deck., Figure 26. Three structures had number of holidays equal or close to zero, SN1029 built in 1986, SN1987 built in 1987, and SN1001 built in 1992. Five structures met the current specification limit of 3 holidays per meter, SN1032 from 1980, SN2262 from 1985, SN2022 from 1989, SN1006 from 1993, and SN6243 built in 1995. Two sets of specimens from SN6005 and SN1136, built in 1989 and 1995, respectively, were slightly above the new specification limit, 3 holidays per meter, but met the older specification limit, 6 holidays per meter. Average number of holidays for specimens extracted from the other eight structures exceeded both specification limits. Especially bridge decks, SN1056 built in 1977 and SN1020 built in 1983 had the highest average number of holidays of 246 and 15 per meter of bar, respectively, Figure 26.

6.2.2.4 Thickness

Coating thickness measurements were determined from 12 locations on the bar, 6 readings from between deformations and on each bar side. Average coating thickness was then calculated for each specimen and for every bridge deck, and compared with the different specification limits.

The average of all readings on top bar specimens from 13 of the 18 decks were within the specification range of 175 to 300 μm. The other five bridge decks, SN1056 built in 1977, SN2262 built in 1985, SN1029 built in 1986, SN6005 built in 1989, and SN1019 built in 1990, which had average coating thicknesses between 125 and 175 μm, Figure 27. Within the group of truss bar specimens, five bridges, SN1056 built in 1977, SN2021 built in 1981, SN2262 built in 1985, SN1029 built in 1986, and SN1006 built in 1993, average coating thickness was below the lower specification limit of 175 μm, but greater than 125 μm, Figure 28.

Figure 27.   Average Coating Thickness, 90% Confidence Interval, Top Bars.

63
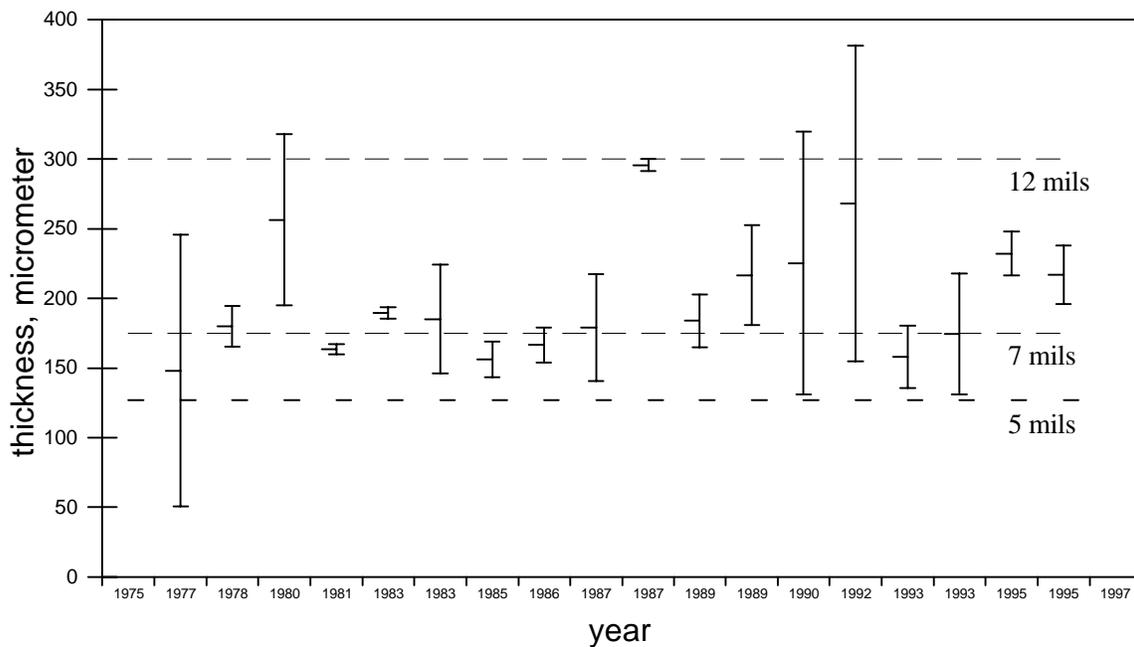
Figure 28.   Average Coating Thickness, 90% Confidence Interval, Truss Bars.

A coating thickness of 125 μm is the lowest thickness allowed for ECR according to ASTM A 775 - 95. If a single recorded measurements is below the value of 125 μm, the bar is rejected. Using this approach, during the testing procedure, some ECR specimens were discarded from further evaluation because of their low thicknesses. Average coating thicknesses of the rejected top bar and truss bar specimens are presented in Figures 29 and 30. Percent ECR specimens that were discarded from the experiment based on the measured coating thickness are shown in Figures 31 and 32. Number of rejected bars varied among evaluated bridge decks between 0 and 70 % for top and truss bars. No general trend regarding the low coating thickness was observed for top bars and truss bars, respectively. New average coating thicknesses were determined after excluding rejected bars, Figures 33 and 34. However, the general tendency for the average coating thickness stayed unchanged.
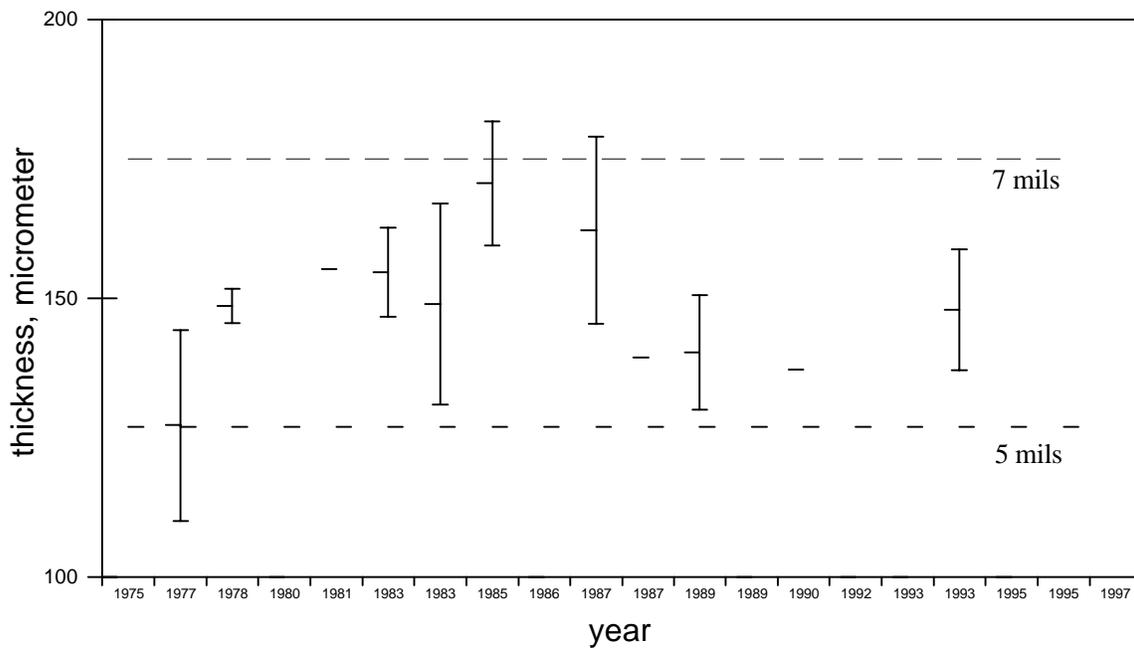
Figure 29.   Average Coating Thickness, Rejected Top Bars, 90% Conf. Interval.
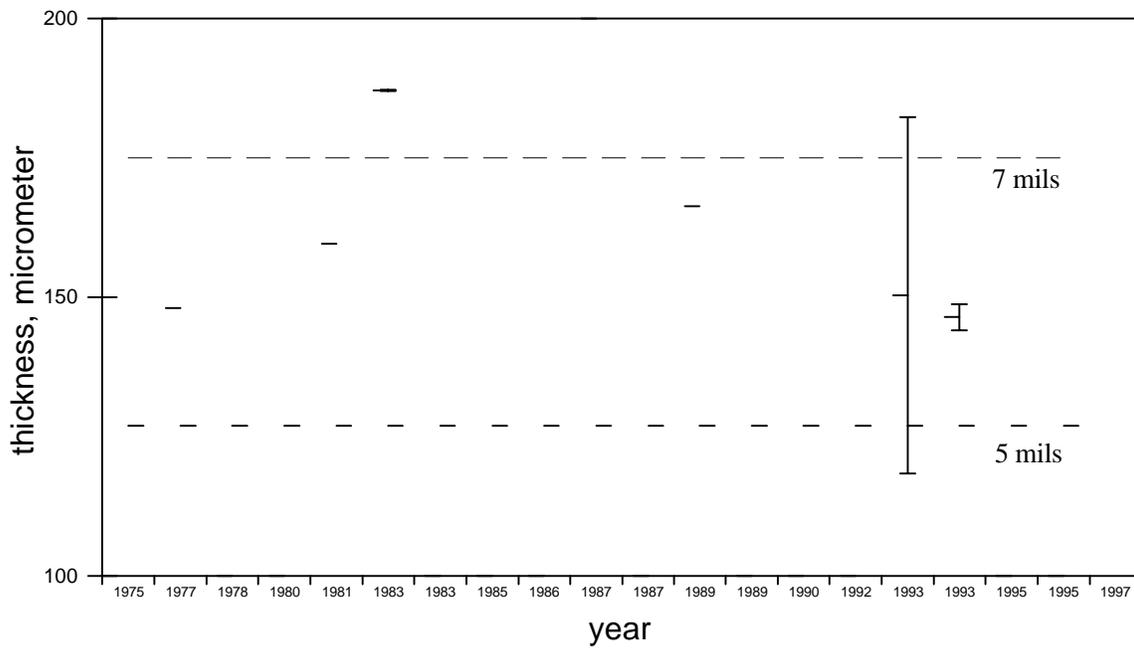
Figure 30.   Average Coating Thickness, Rejected Truss Bars, 90% Conf. Interval.

65
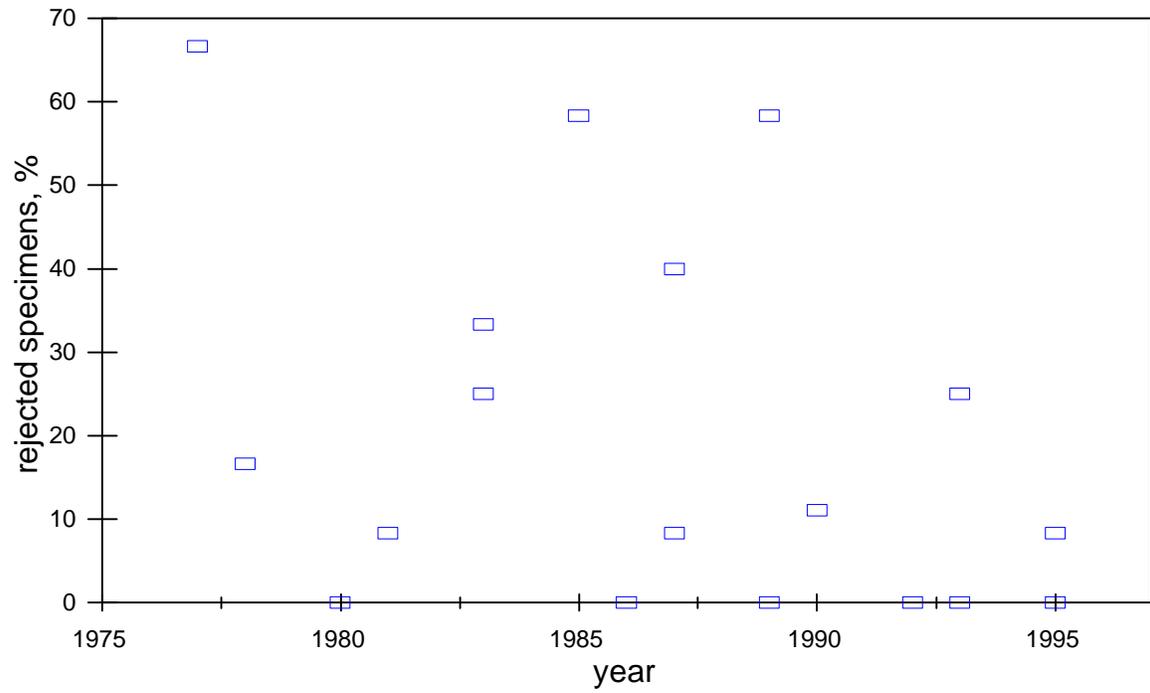
Figure 31.   Percent Rejected Top Bars.
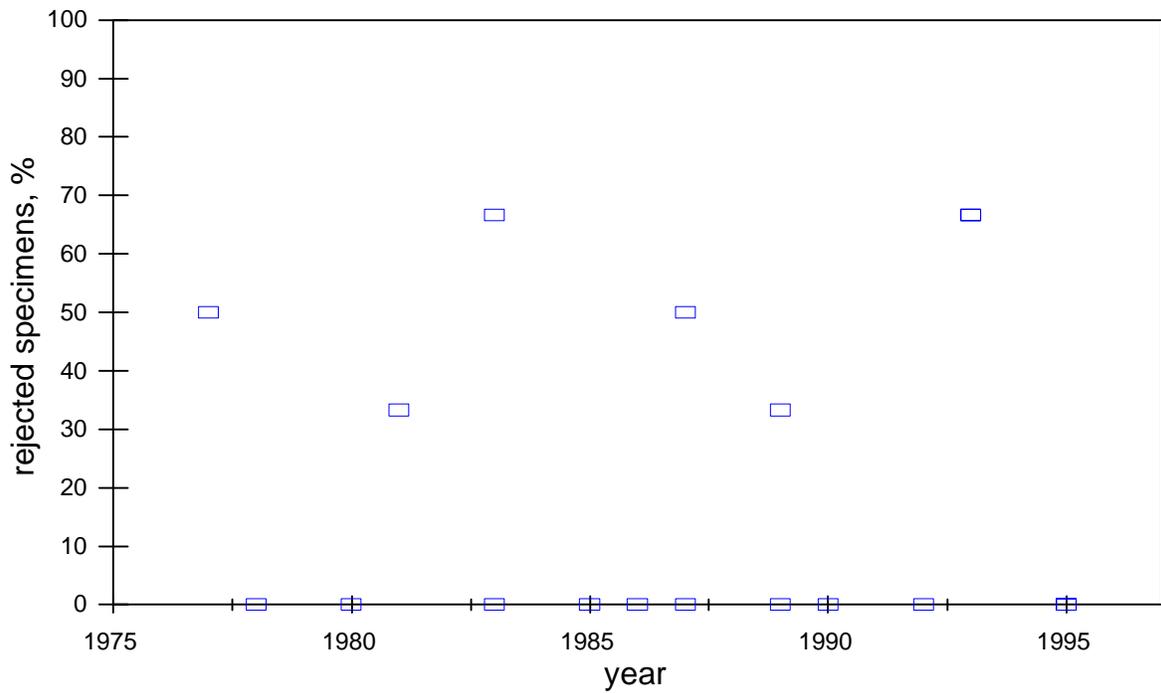
Figure 32.   Percent Rejected Truss Bars.

66
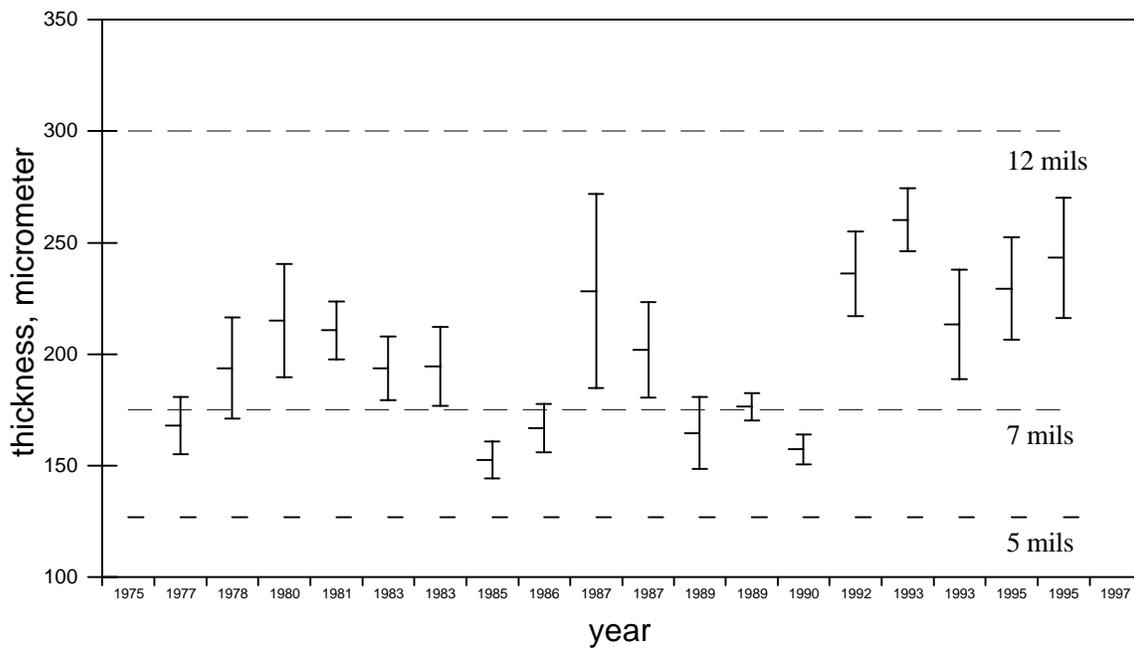
Figure 33.　　Average Coating Thickness, Accepted Top Bars, 90% Conf. Interval.
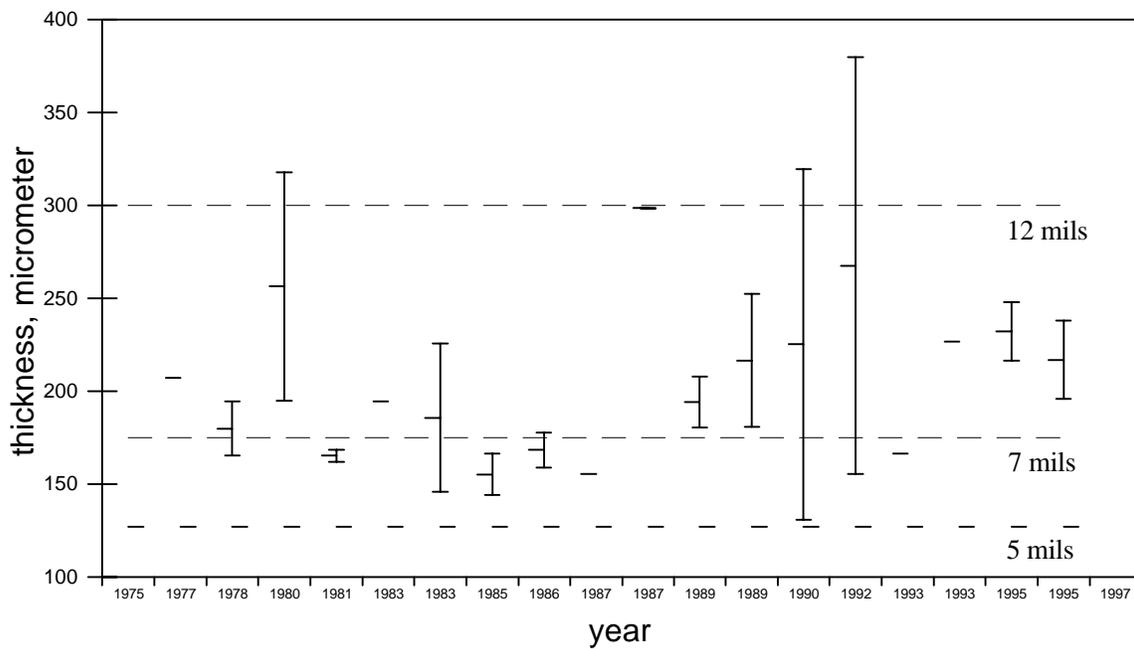
Figure 34.　　Average Coating Thickness, Accepted Truss Bars, 90% Conf. Interval.

67

6.2.2.5 Adhesion

Adhesion of epoxy-coating to reinforcing steel was determined using the knife-peel test described in the Method & Material section. ECR specimens rejected because of their low coating thickness were discarded from adhesion testing. Only three of tested bridge decks had an average adhesion value equal to 1, SN1020 built in 1983, SN6243 and SN1136 built in 1995, Figure 35. Average adhesion values equal or greater than 3 were observed for the following bridge decks: SN1032 built in 1980, SN2021 built in 1981, SN1029 built in 1986, SN1019 built in 1990, SN1001 built in 1992, and SN1004 and SN1006 built in 1993. In the case of truss bars, average adhesion values were above 3 for all bridge decks except, SN1004 and SN1020 built in 1983, SN6161 built in 1987, SN1006 built in 1993, and SN6243 and SN1136 built in 1995, Figure 36. Percent of average adhesion values equal or greater than 3 was also determined, Figures 37 and 38. For top mat ECR specimens, the percent of average adhesion values equal or greater than 3 was between 10 and 90, except structures, SN1004 and SN1020 built in 1983, SN2262 built in 1985, and SN6243 and SN1136 built in 1995, Figure 37. Similar observations were made for the truss bars, with the percent of average adhesion equal or higher than 3, ranging between 30 and 100, with an exception of SN1004 and SN1020 built in 1983, SN6161 built in 1987, SN1006 built in 1993, and SN6243 and SN1136 built in 1995, Figure 38.

The visually observed color of the steel under the peeled epoxy-coating was noted and numerical values were assigned to the observed colors, see Table 8. A correlation was established between the color of the steel surface under the coating and the adhesion values, Figures 39 and 40. The linear relationship had R^2 values of 0.88 for the top bars and 0.7 for the truss bars.

Photographs, Figure 41 to 45, represent various colors of the steel surface underneath the coating described in Table 8.
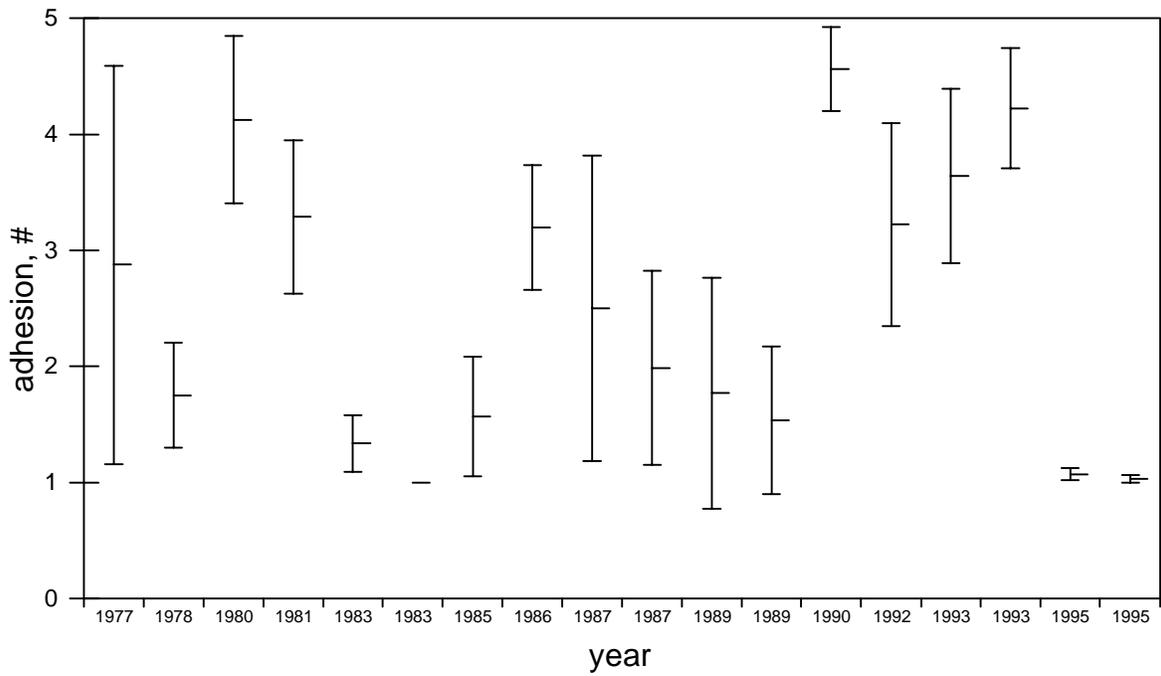
Figure 35.　　　Average Coating Adhesion, Thickness Accepted Top Bars, 90% C.I..
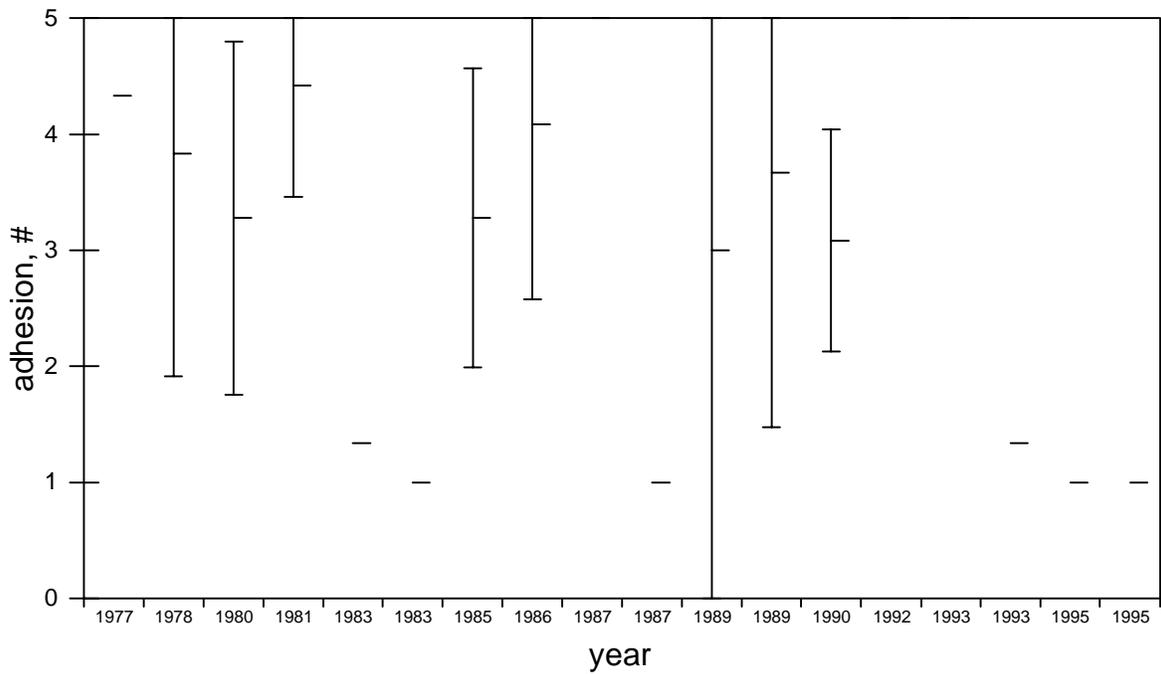
Figure 36.　　　Average Coating Thickness, Thickness Accepted Truss Bars, 90% C.I.
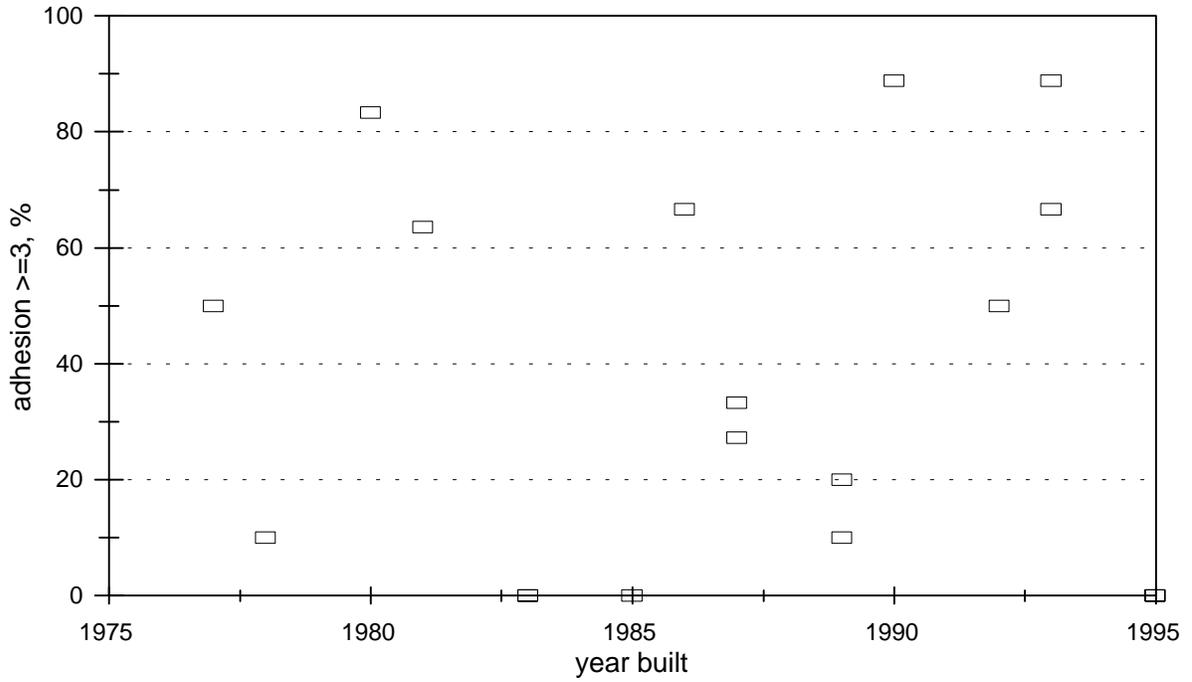
Figure 37.   Percent of Average Adhesion ≥ 3, Top Bars.
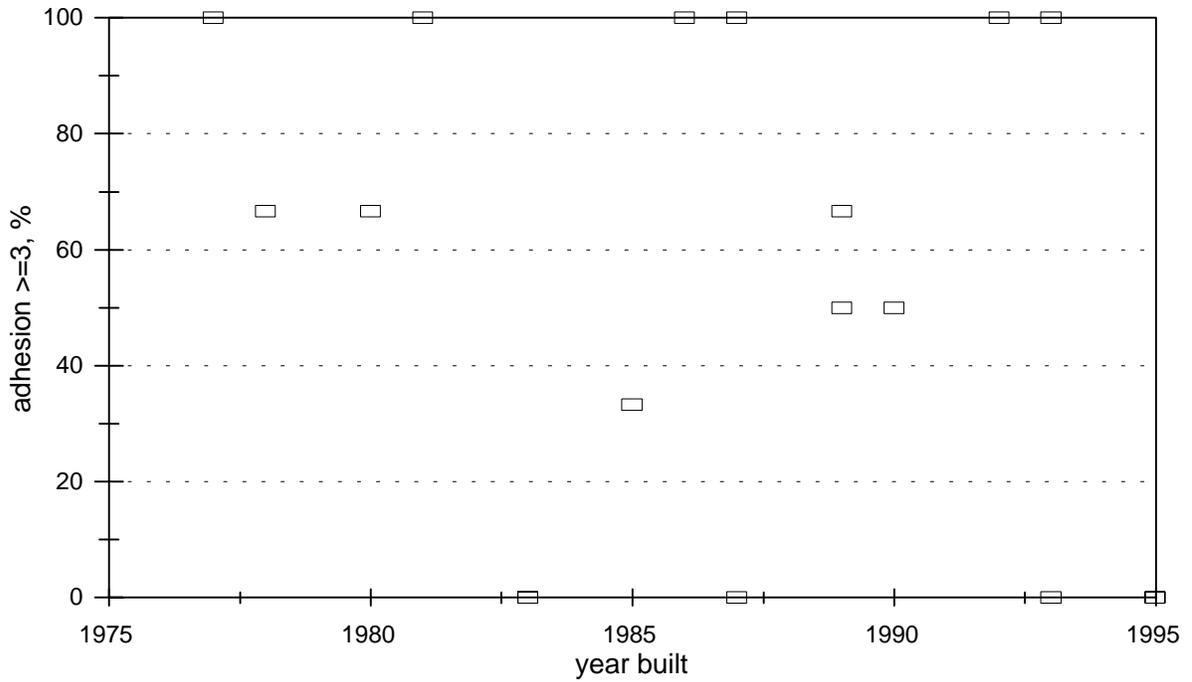
Figure 38.   Percent of Average Adhesion ≥ 3, Truss Bars.

70
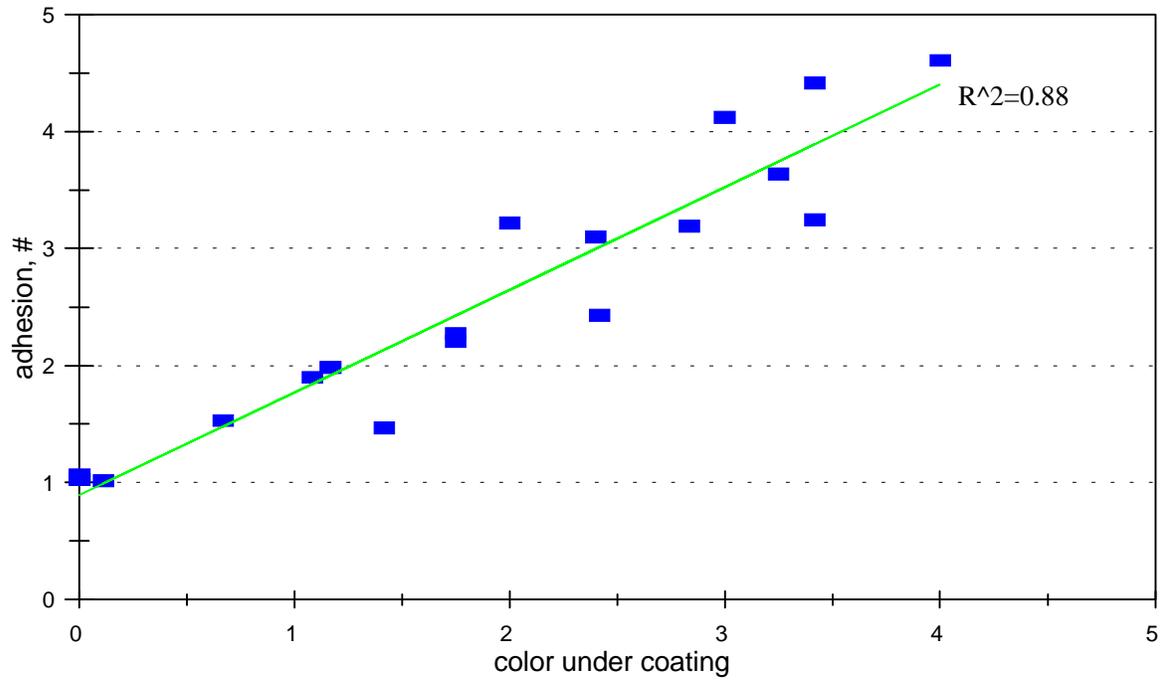
Figure 39.   Average Adhesion and Steel Color Relation, Top Bars.
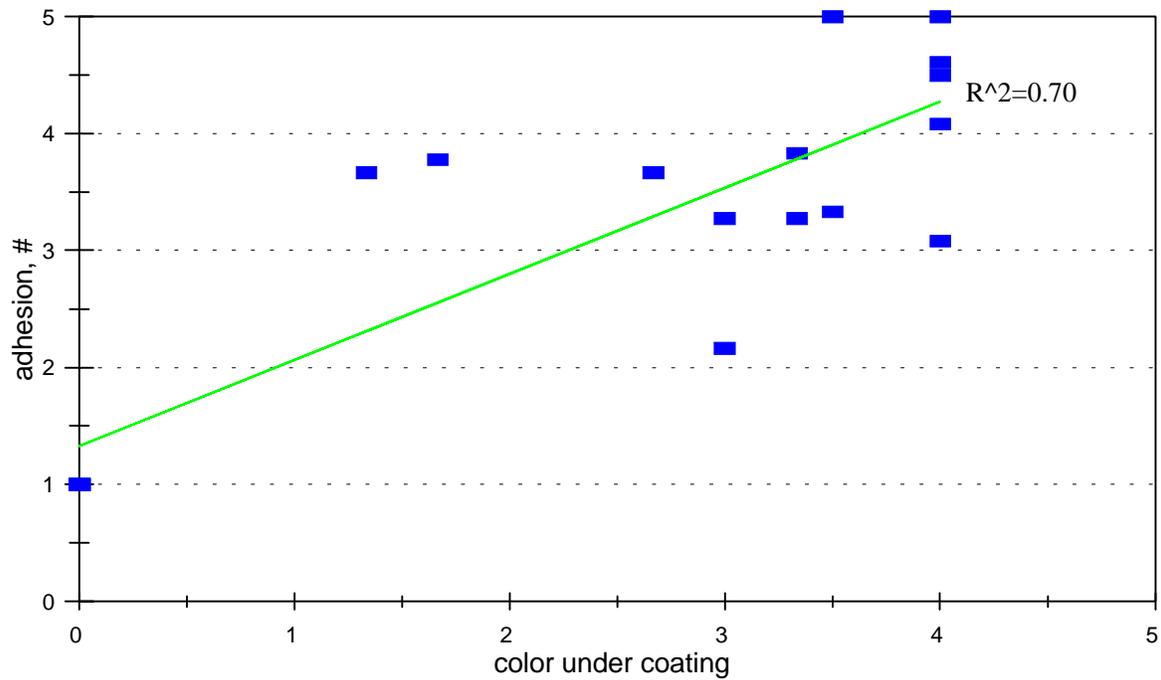
Figure 40.   Average Adhesion and Steel Color Relation, Truss Bars.

Table 8.   Steel Color under the Coating.

Number	Steel Color
1	shining
2	gray, shining
3	dark gray, shining
4	black, shining
5	black
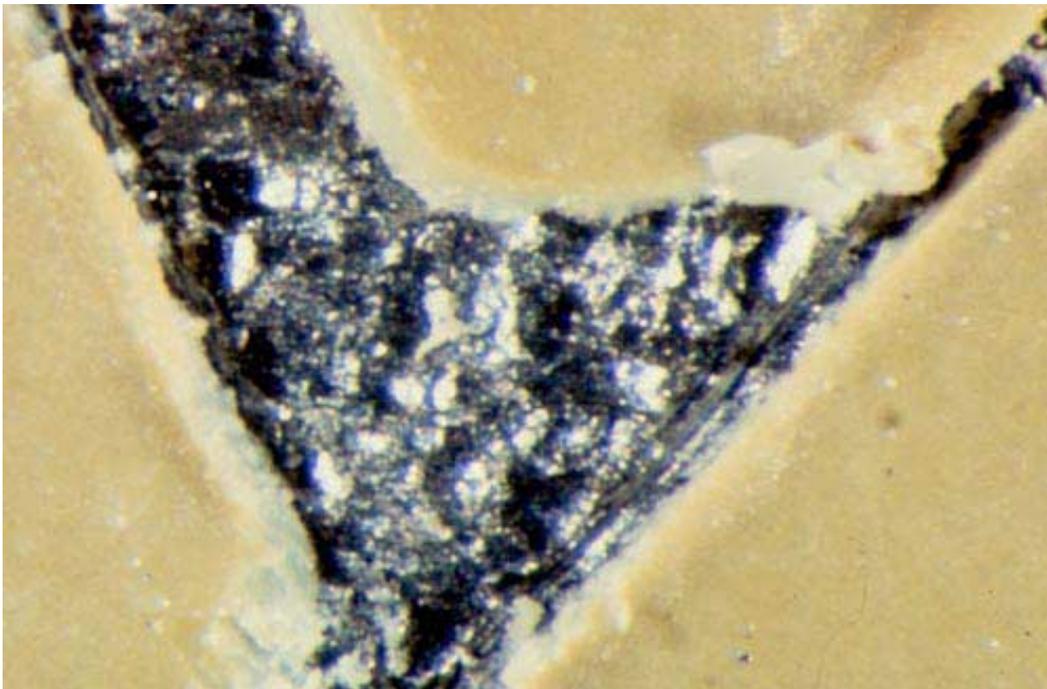
Figure 41.   Shining Steel Surface Underneath Coating.
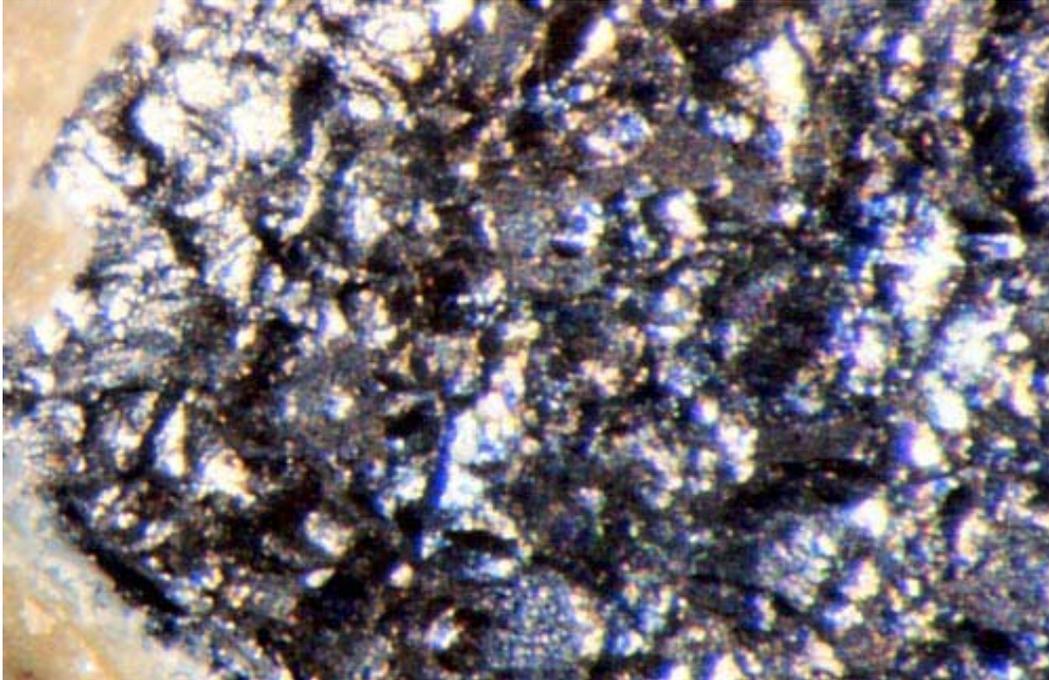
Figure 42.   Gray, Shining Steel Surface Underneath Coating.
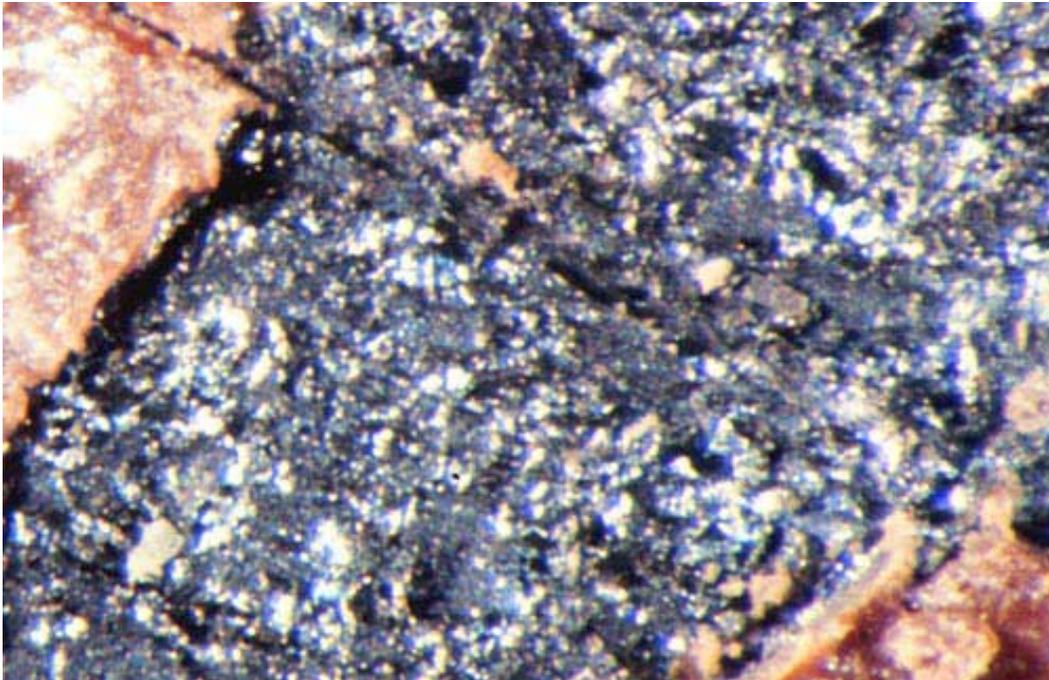
Figure 43.   Dark Gray, Shining Steel Surface Underneath Coating.

Figure 44.   Black, Shining Steel Surface Underneath Coating.
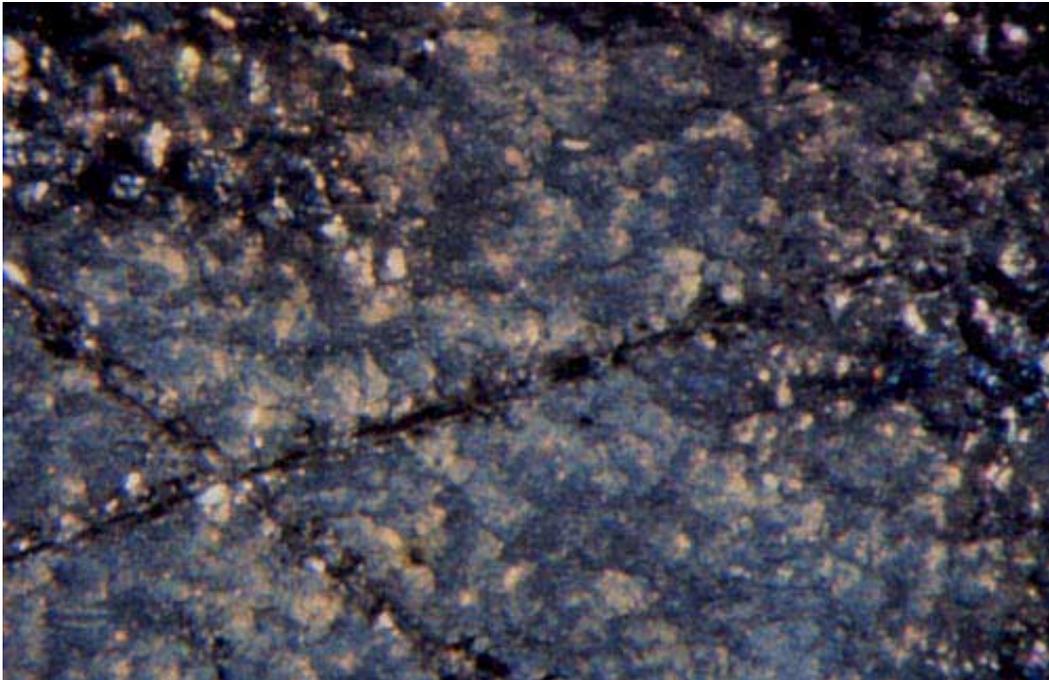
Figure 45.   Black Steel Surface Underneath Coating.

Chemical analysis of steel surfaces representing the different colors was performed using two techniques, EDAX (Energy Dispersion Analysis of X-rays) and XPS (X-ray Photoelectron Spectroscopy). The results of these tests are presented in Tables 6 and 7. XPS samples approximately 5 nm, about 10 layers of molecules , of the specimen surface. X-ray analyses were made immediately after making a fresh cut in the epoxy-coating subsequently peeling the coating. Iron, Fe, oxygen, O, and carbon, C, were three elements with the highest detected concentration, 0.56 to 6.28, 11.90 to 39.30, and 40.15 to 83.60, identified in the XPS analysis, Table 9.

Table 9.　　　XPS (X-ray Photoelectron Spectroscopy) Analysis Results.

Element	Concentration, % atomic				
	shining (1)	gray, shining (2)	dark gray (3)	black, shining (4)	black (5)
Fe	6.3	4.5	4.6	0.6	3.9
Cu	0.7	0.7	3.0	< 0.2	0.9
Sn	0.7	1.2	0.6	< 0.2	< 0.2
Si	1.5	0.8	3.7	3.5	8.3
Ca	0.2	< 0.2	0.8	< 0.2	0.8
Na	< 0.2	< 0.2	2.0	< 0.2	2.9
K	< 0.2	< 0.2	1.5	< 0.2	2.2
O	29.4	25.0	37.9	11.9	39.3
N	1.1	0.6	< 0.2	0.4	1.6
C	60.1	67.2	45.9	83.6	40.2
metal / oxygen	0.3	0.3	0.2	0.1	0.1

Traces of other metals, Cu, Sn, and alkalies, Ca, Na, K, were also present. Thickness of the layer analyzed by EDAX technique is about 100 μm, 1000 times deeper than the XPS penetration. Testing the same type of a freshly exposed reinforcing steel surface using EDAX, provided similar

results, with iron, Fe, and oxygen, O, having the highest weight percent, 83.68 to 97.65, and 0.66 to 5.4, respectively, Table 10. Traces of following metals and alkalies were also detected: Mn, Cr, Ti, Ni, Cu, Al, Na, Ca, and K.

Table 10.   EDAX (Energy Dispersion Analysis of X-rays) Analysis Results.

Element	Weight, %				
	shining (1)	gray, shining (2)	dark gray (3)	black, shining (4)	black (5)
Fe	97.7	93.9	92.1	93.6	83.7
Mn	1.7	2.1	1.1	2.3	n/a
Cr	0.7	1.2	0.5	n/a	< 0.2
Ti	n/a	0.7	n/a	0.6	n/a
Ni	n/a	n/a	n/a	0.2	n/a
Al	n/a	n/a	< 0.2	n/a	0.4
Si	n/a	0.3	0.6	n/a	6.7
Cu	n/a	0.4	2.7	0.8	2.5
Ca	n/a	0.3	n/a	n/a	n/a
K	n/a	n/a	n/a	0.4	1.3
O	n/a	1.0	3.2	2.3	5.4
metal / oxygen	n/a	95.5	30.6	43.1	16.0

6.2.3 EIS (Electrochemical Impedance Spectroscopy) and LP (Linear Polarization)

Electrochemical Impedance Spectroscopy (EIS) and Linear Polarization (LP) measurements were collected from 3 ECR top mat specimens from 18 bridge decks. Each specimen was selected from a different span of the bridge.

Polarization resistance measurements were performed in the range of -20 mV and +20 mV with the respect to E_{corr} using a scan rate of 0.1 mV/sec. An EIS test was conducted after a delay of 15 minutes during which specimens were allowed to return to their rest potential from the polarized condition. EIS measurements were carried out in the frequency range between 5000 Hz and 0.001 Hz.

6.2.3.1 EIS

Nyquist and Bode plots were constructed from the data obtained using the EIS technique. All graphs related to EIS can be found in Appendix B. An attempt was made to determine if impedance measurements can give an indication on the coating performance as a protective barrier against chloride induced corrosion. A correlation between the EIS results and the data collected from various testing procedures performed on ECR was also examined.

Based on the Nyquist plots determined for all tested ECR specimens three main curve shapes were detected, Figures 57A and B, 58A and B and 59A and B. The structure and specimen number that followed a certain Nyquist diagram category are presented together with the low frequency impedance range in Table 11.

No correlation was found between the impedance measurements obtained at 0.001 Hz and the different shapes of the Nyquist diagram. Bode plots presented along with the Nyquist diagrams have a similar shape for all ECR specimens tested using the EIS technique.

Impedance values determined at the low frequency, 0.001 Hz, should differentiate "good" and "bad" coatings. However, no exact values that could be used as the limits for typical coating behaviors have been determined, although some attempts were made to find representative values characterizing various coating performance. Clear, Hartt, McIntyre and Lee suggested in their report three major coating performance groups based on their impedance value: coatings with an

excellent corrosion resistance, overall impedance values greater than 10^8 ohm/cm^2, coatings with an intermediate effectiveness, impedance values between 10^6 and 10^8 ohm/cm^2, and coatings with a poor corrosion resistance, impedance values below 10^6 ohm/cm^2 [29]. Other researchers indicated that impedance measurements greater than 10^5 ohm are typical for an intermediate coating quality, and impedance values lower than 10^5 ohm represent poor quality coatings [A]. It should be mentioned that these correlations were made for a low frequency measurements, for example 0.001 Hz. Impedance values at the frequency of 0.001 Hz obtained in this study were in the range of 10^4 ohm and 10^7 ohm for sixteen out of the eighteen evaluated bridge decks. The only two bridge decks that have experienced higher impedance readings, slightly above 10^8 ohm, were SN6243 and SN1136 constructed in 1995, Figure 46.

Table 11.   ECR Specimens Representing Typical Nyquist Plots.

Nyquist Plot Type	Structure Number	Specimen Number	Z @ 0.001Hz, ohm
N1	1056	12	10^5
	2068	3, 8, 12	10^4 - 10^6
	1032	1, 8, 10	10^5 - 10^7
	1004-3	4	10^5 - 10^6
	1020	1, 4, 8	10^5 - 10^6
	2262	3	10^6 - 10^7
	1029-9	7, 9	10^5 - 10^6
	1015	3, 5, 8	10^4 - 10^6
	6161	8, 10	10^6 - 10^7
	6243	4, 7, 12	10^6 - 10^8
	6005	3	10^6
	1019	5, 7	10^5 - 10^6

Table 11.   ECR Specimens Representing Typical Nyquist Plots (cont.).

Nyquist Plot Type	Structure Number	Specimen Number	Z @ 0.001Hz, ohm
N2	1056	2, 8	$10^5 - 10^6$
	1004-3	8, 10	$10^5 - 10^6$
	2262	7	$10^5 - 10^6$
	6005	8, 12	$10^5 - 10^8$
	2022	1, 4, 8	$10^5 - 10^7$
	1019	3	$10^4 - 10^5$
	1001	3, 5, 11	$10^5 - 10^7$
	1136	5	$10^4 - 10^5$
N3	2021	3, 8, 9	$10^4 - 10^5$
	2262	9	$10^5 - 10^6$
	1029-9	4	$10^6 - 10^7$
	6161	3	$10^5 - 10^6$
	1004-6	1, 8, 12	$10^4 - 10^5$
	1006	4, 6, 11	$10^4 - 10^6$
	1136	1, 10	$10^6 - 10^8$

Impedance values determined at 0.001 Hz were plotted against various ECR properties: coating thickness, percent area damage, holiday number, coating adhesion, and color of steel underneath the coating. No correlation was found between the impedance, Z, and coating thickness. An increase in coating thickness was not followed by a higher impedance value. For the thickness equal to 200 μm the highest and the lowest impedance values were observed, 10^8 ohm and 10^4 ohm, respectively, Figure 47.
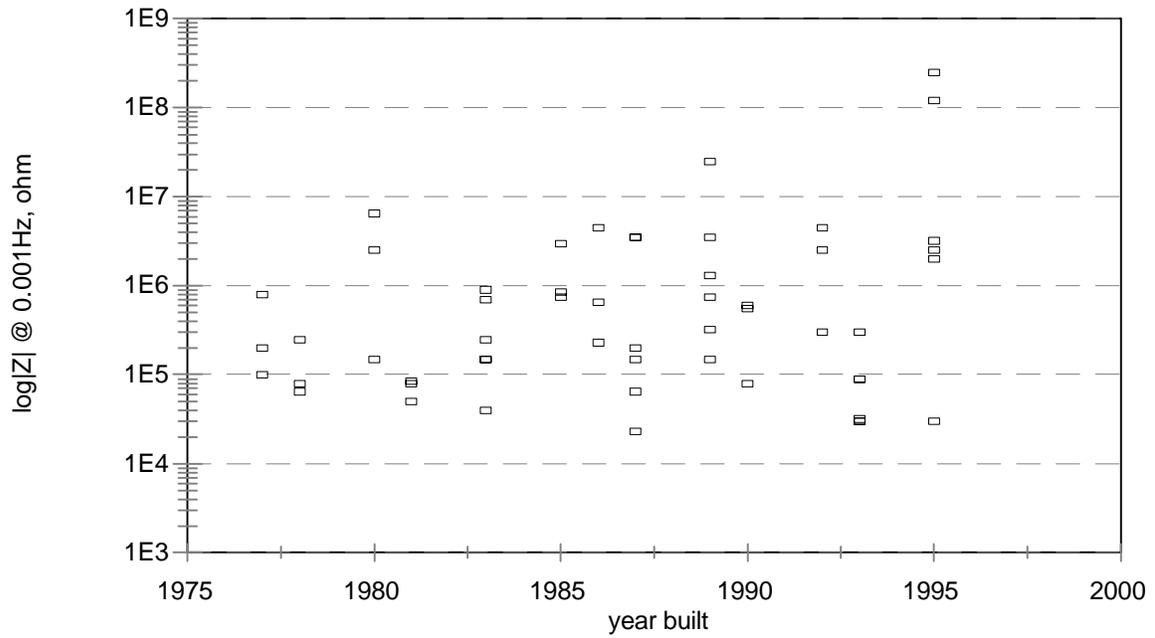
Figure 46. Impedance Data for 18 Bridge Decks.
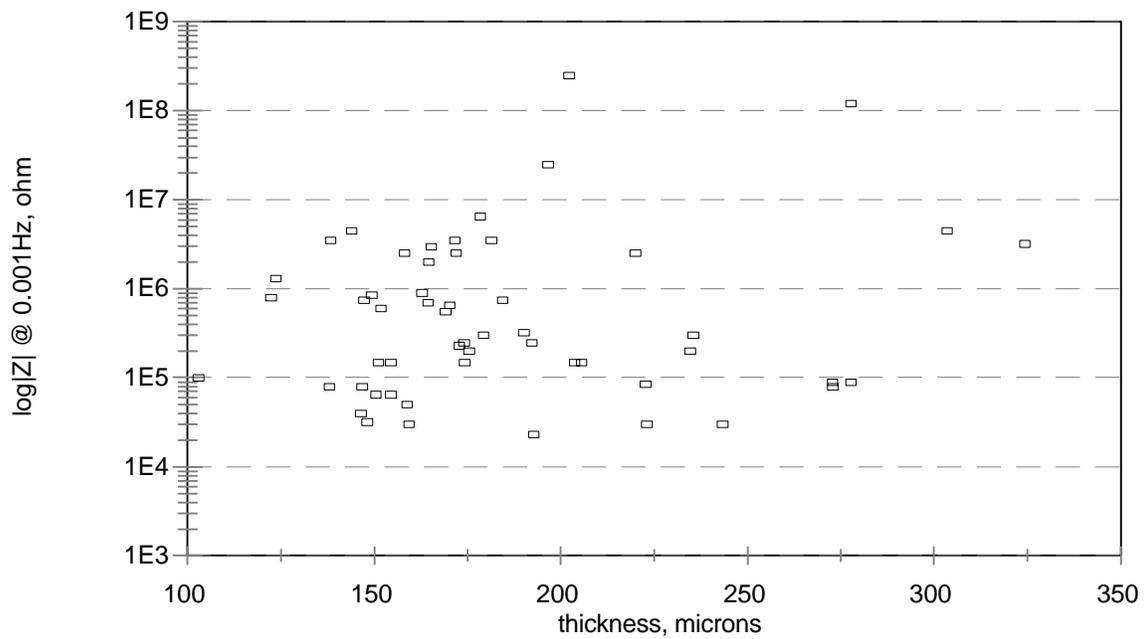
Figure 47. Impedance at Low Frequency, 0.001Hz, vs. Coating Thickness.

Better correlation was detected for the low frequency impedance and the percent area damaged of ECR specimens. Although the data seemed to be scattered they give an overall impression of the decreasing impedance, Z, with an increased damage in the coating. The highest impedance, 10^8 ohm, was observed for the specimens with almost a non visible damage and the lowest, 10^4 ohm, was determined for a 0.65 % area damage, Figure 48 Similar correspondence was detected for the measured coating impedance and number of holidays in the coating. The highest impedance values were typical for ECR specimens with no holidays and had gradually decreased with a growing holiday number, Figure 49.
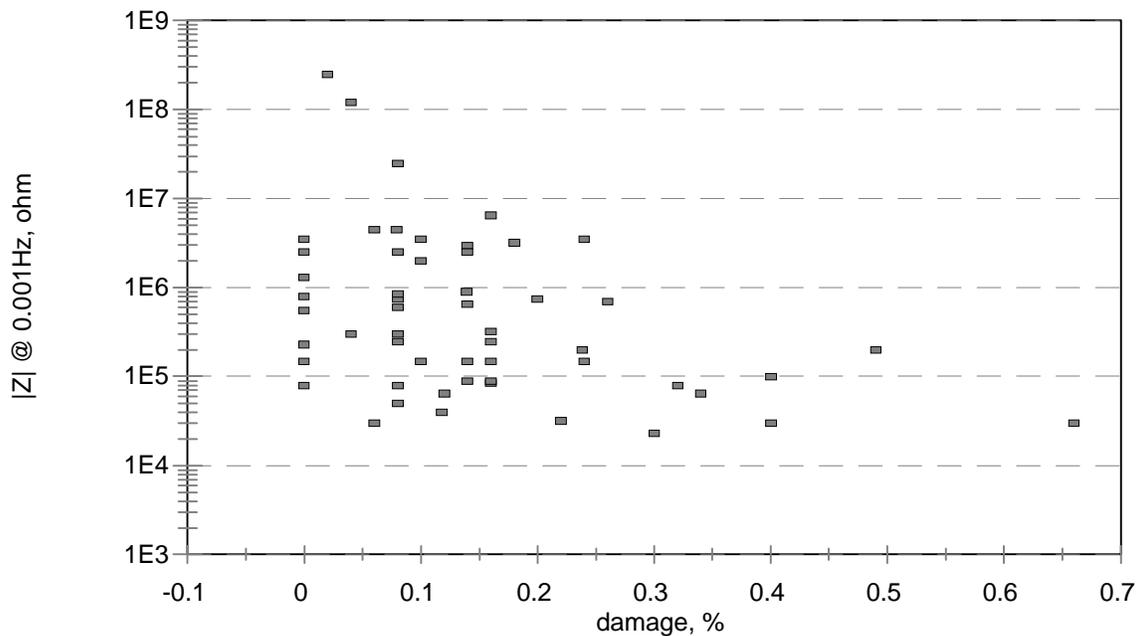
Figure 48. Impedance at Low Frequency, 0.001Hz, vs. Percent Area Coating Damage.
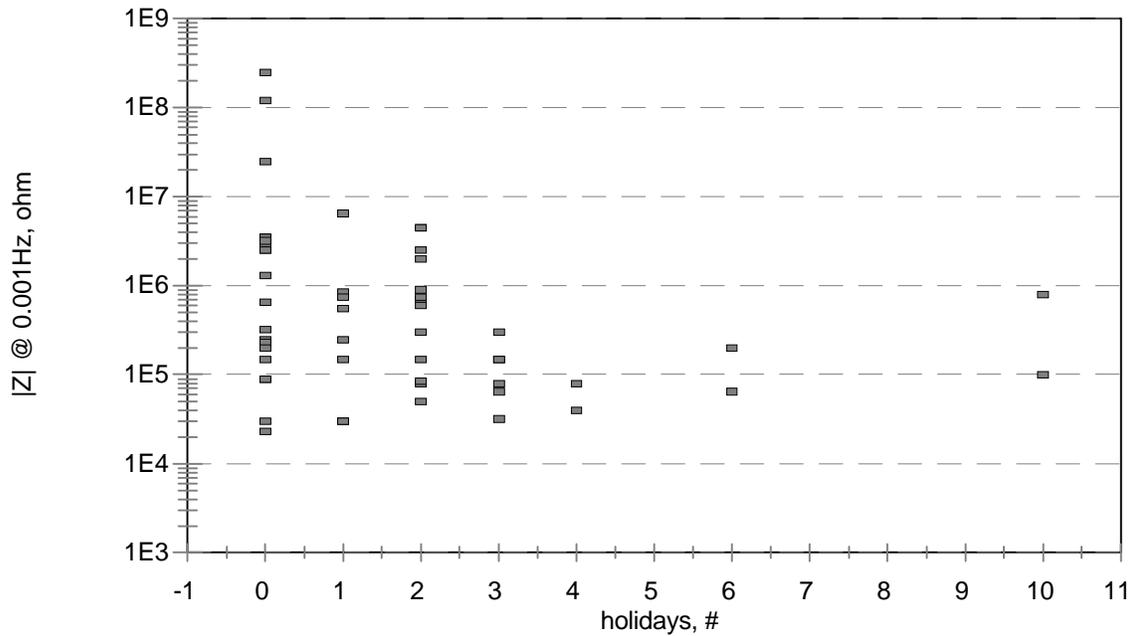
Figure 49. Impedance at Low Frequency, 0.001Hz, vs. Number of Holidays in Coating.

A comparison between the low frequency impedance and coating adhesion demonstrated lower frequency values for higher adhesion numbers, which represent the loss of adhesion of the coating to the steel surface. The maximum impedance of 10^8 ohm was measured for the adhesion value of 1 and the lowest impedance, 10^4 ohm, for the adhesion equal to 5, Figure 50. A similar trend was observed for the low frequency impedance and a color of a steel surface under the coating where the higher impedance values represented a more shining steel surface and lower impedance measurements were characteristic of steel surface covered with an oxide layer, Figure 51.
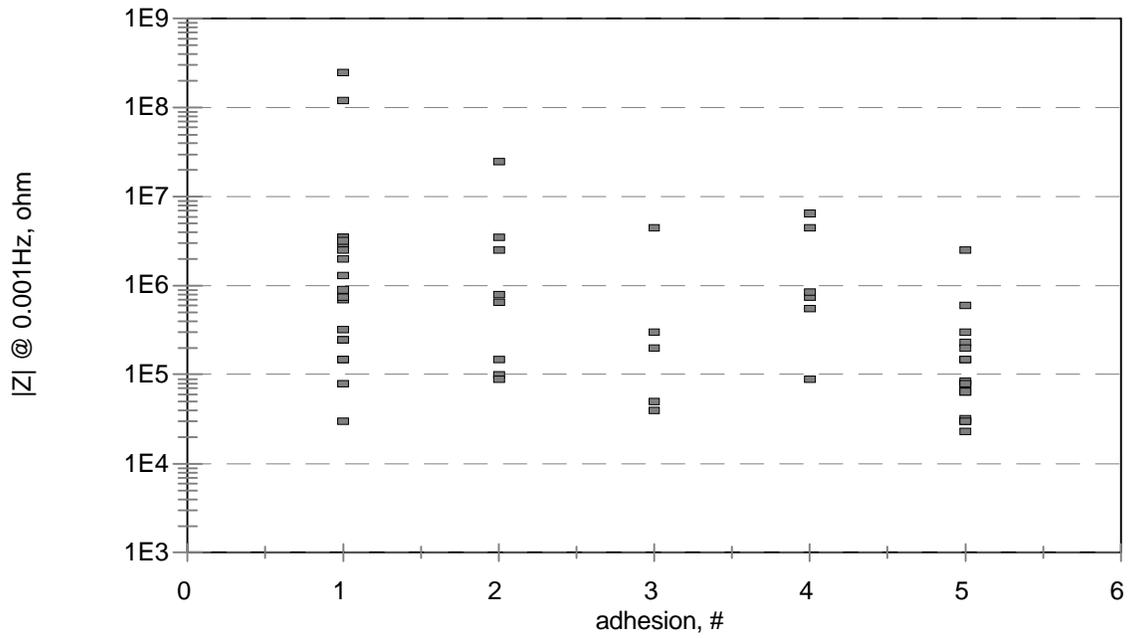
Figure 50. Impedance at Low Frequency, 0.001Hz, vs. Coating Adhesion.
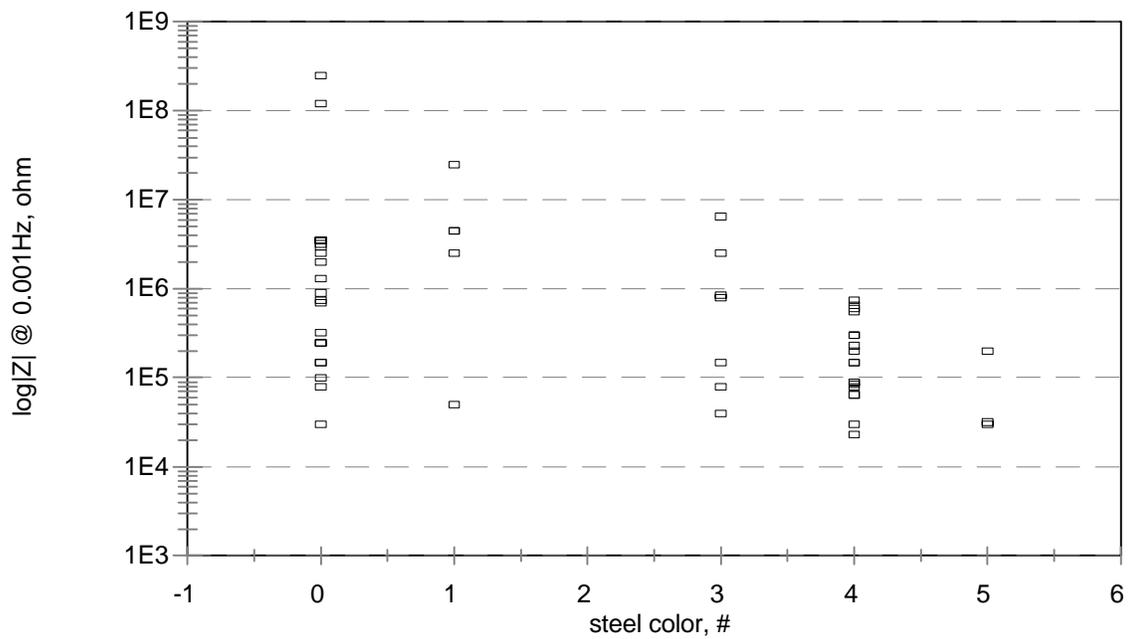
Figure 51. Impedance at Low Frequency, 0.001 Hz, vs. Color of Steel Underneath Coating.

6.2.3.2 LP

Polarization resistance was determined for all ECR specimens. The values ranged from 10^5 ohm cm^2 to 10^9 ohm cm^2. Polarization resistance was also compared with the impedance data measured at the lowest frequency of 0.001 Hz. The results are presented in Table 12.

Table 12.   Polarization Resistance Results, Average Values.

structure number	year built	log Rp, ohm cm2	log Z @ 0.001 Hz, ohm
1056	1977	6.57	5.56
2068	1978	6.10	5.12
1032	1980	7.04	6.48
2021	1981	5.84	4.86
1004-3	1983	6.10	5.05
1020	1983	6.76	5.79
2262	1985	7.12	6.19
1029-9	1986	6.84	6.25
1015	1987	5.66	4.90
6161	1987	6.99	6.38
6005	1989	7.23	6.95
2022	1989	7.04	6.18
1019	1990	6.59	5.61
1001	1992	7.37	6.39
1004-6	1993	5.76	4.85
1006	1993	5.66	5.08
6243	1995	7.77	7.93
1136	1995	8.26	7.61

Corrosion current values calculated from the polarization resistance data were in the range of 0 mA/cm^2 to 10^{-7} mA/cm^2 for the majority of tested ECR specimens with the corrosion potential values between -300 mV and -50 mV, Figure 52. Obtained corrosion rates were equal to zero for all ECR specimens, Figure 53.

6.3 Statistical Analysis

Statistical analysis was performed using the results of various testing procedures applied to ECR specimens and concrete cores obtained from 18 bridges in Virginia.   The analysis consisted of two parts. The first part included the evaluation of an influence of various characteristics on the adhesion of the epoxy coating to the steel surface. The second part concentrated on an examination of the relation between the impedance values measured using the electrochemical impedance spectroscopy (EIS) technique and other properties of ECR specimens.

Statistical evaluation was performed using a multiple linear regression. Average values were incorporated into the analysis to ensure the independence of all variables included in the model.

6.3.1 Adhesion

Adhesion of the epoxy coating to the reinforcing steel surface is expected to influence the field performance of ECR. Coating thickness, damage, holidays, holes, moisture and chloride concentration present in concrete, as well as the color of the steel surface underneath the coating were expected to affect the adhesion. Absorption was excluded from the statistical model based on its correlation with moisture, Figure 54.
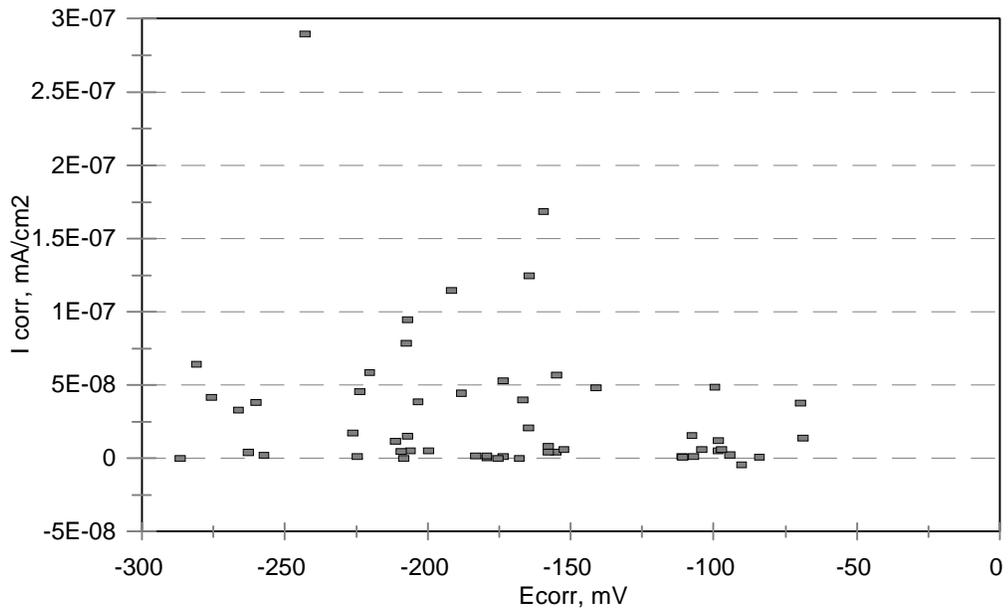
Figure 52. Polarization Resistance Results, Corrosion Current vs. Corrosion Potential.
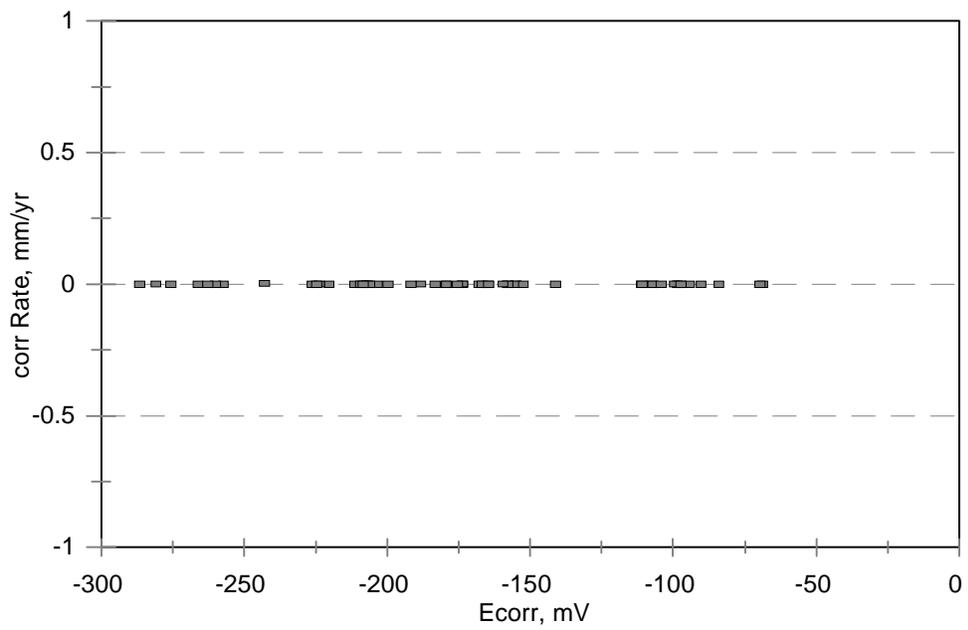
Figure 53. Polarization Resistance Results, Corrosion Rate vs. Corrosion Potential.
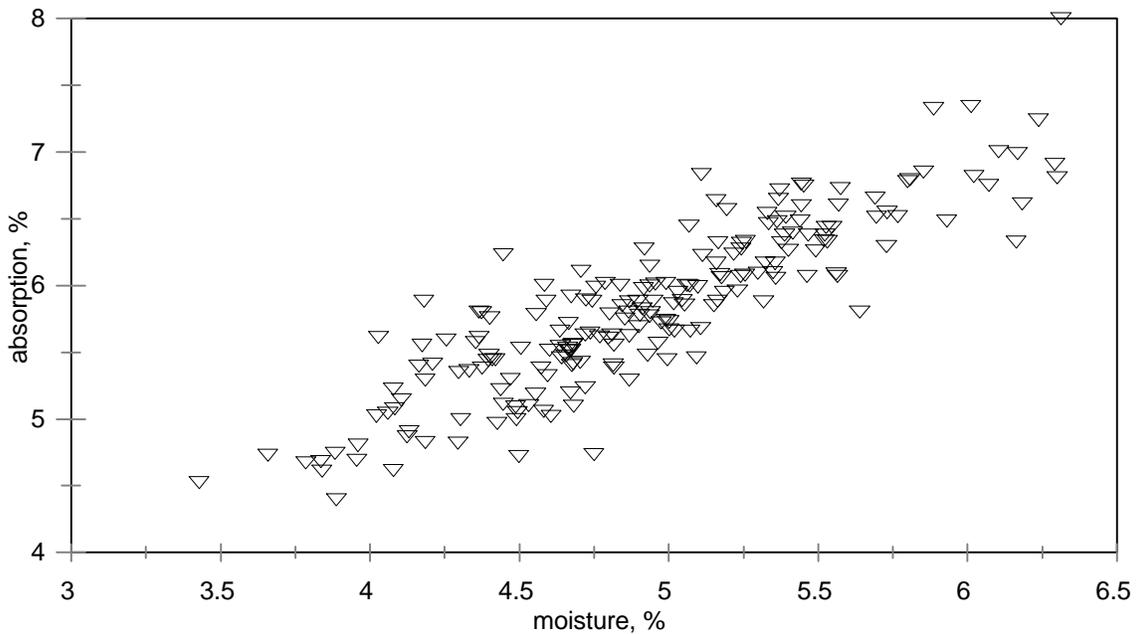
Figure 54. Absorption vs. Moisture, All Data, $R^2 = 1$.

All coating and concrete properties were introduced into the statistical model as independent variables and tested using a multiple regression analyses, "stepwise" and "rsquared". Both methods demonstrated three variables, color of the steel under the coating, coating thickness and coating damage, provided the best fit with a model R^2 value equal to 0.906. The partial R^2 values for individual variables were 0.843 for the color of steel underneath the coating and 0.031 for the coating thickness and coating damage, respectively.

6.3.2 Coating Impedance

The determination of the coating impedance was suggested as a method for the evaluation of the performance of the ECR. Impedance values of the epoxy coating obtained using the EIS technique were tested against the coating damage, holidays, holes, thickness, and steel color

underneath the coating. All properties of the concrete were excluded from the model since coating impedance was presented as the difference between the lowest and the highest frequencies. The impedance at the lowest frequency, 0.001 Hz, represents coating and at the highest frequency, 5000 Hz, characterizes concrete, thus the concrete impedance was removed from the total impedance.

The multiple regression analyses, "stepwise" and "rsquared", indicated two variables influencing the impedance, color of the steel underneath the coating and coating damage, with the model R^2 value of 0.431. The partial R^2 values for these variables were 0.341 and 0.091, respectively.

6.4 Life Cycle Costs

Initial costs for elements used in the bridge deck construction and maintenance: epoxy-coated reinforcement (ECR), black steel (BS), A4 concrete, low permeable (LP) A4 concrete, corrosion inhibitor (CI), DCI-S, 10 l/m^3 of concrete, and latex modified concrete (LMC), are presented in Table 13. Table 14 contains initial costs for newly constructed bridge decks for various systems. The highest initial costs for the bridge deck, 11.76 \$/ft^2, 11.55 \$/ft^2, and 11.54 \$/ft^2 were obtained for the ECR-LP A4 concrete system, the BS-LP A4 concrete-CI system, and ECR-A4 concrete system, respectively. The two lowest initial cost belonged to the BS-A4 concrete system and the BS-LP A4 concrete system, and were equal to 10.96 \$/ft^2 and 11.18 \$/ft^2, Table 14.

The present value of the life-cycle cost, using a 5 % interest rate, for 75 year design life was determined for all systems, Table 15. Based on service life estimates, several systems do not require any maintenance during the 75 year design life. Among them were ECR and BS with LP concrete, BS with A4 concrete and CI, and BS with LP concrete and CI. It was also recognized that the ECR-A4 concrete and BS-A4 concrete systems will need a latex modified concrete (LMC) overlay. The service life of the LMC overlay is equal to 24 years [68]. The placement times for the LMC overlay varied depending on the system and were based on the calculated service life

estimates, Table 15. The present cost of a LMC overlay was obtained using 3.4 % inflation rate. The life-cycle cost evaluation of the systems requiring LMC overlays was estimated for two cases: with and without the traffic control costs.

Table 13.　　　Initial Costs for Bridge Deck, 1997.

Item	Initial Cost
ECR	0.62 $/lb
BS	0.49 $/lb
A4 concrete	355.00 $/cy
LP A4 concrete	364.00 $/cy
CI (DCI-S, 2 gal/cy)	7.50 $/gal
LMC overlay w/o traffic control	5.22 $/sf
LMC overlay with traffic control	11.10 $/sf

Table 14.　　　Initial Costs for Bridge Deck, Various Systems, 1997.

Systems	Initial Cost, $/ft^2
ECR + A4 concrete	11.54
ECR + LP A4 concrete	11.76
BS + A4 concrete	10.96
BS + LP A4 concrete	11.18
BS + A4 concrete + CI	11.33
BS + LP A4 concrete + CI	11.55

The life-cycle cost analysis indicated the highest total cost of 12.30 $/ft^2 and 13.15 $/ft^2 for the ECR with A4 concrete system, without and with the traffic control respectively. The lowest total cost of 11.18 $/ft^2 was determined for the BS-LP A4 concrete system without the traffic control, Table 15.

Table 15.   Life Cycle Cost for 75 Year Design Life.

System	Initial Cost, $/ft^2	LMC overlay placement, years	Total Cost, $/ft^2 w/o [a]	w [b]
ECR + A4 concrete [*]	11.54	45 & 69	12.30	13.15
		50 & 75	11.99	12.54
		55	11.90	12.30
		60	11.82	12.13
		65	11.76	12.00
ECR + LP A4 concrete	11.76	n/a	11.76	---
BS + A4 concrete	10.96	40 & 64	11.93	13.02
BS + LP A4 concrete	11.18	n/a	11.18	---
BS + A4 concrete + CI	11.33	n/a	11.33	---
BS + LP A4 concrete + CI	11.55	n/a	11.55	---

[a] -   traffic control not included
[b] -   traffic control included
[*]   Assumes 5, 10, 15, 20 and 25 years of added corrosion protection provided by ECR, respectively.

Chapter 7. DISCUSSION

7.1 Field Survey

Evaluated concrete bridge decks had either simply supported spans or a continuous structure. A majority of the bridges were constructed using stay-in-place forms. Surface cracks observed on the bridge decks were caused primarily by shrinkage of concrete. Longitudinal cracks, related to the negative moment and/or shrinkage, were also found. No delaminations were detected with the exception of one structure, SN8003, from Phase I of the project [51].

Cover depth measurements, obtained from the evaluated concrete bridge decks, were normally distributed with the mean of 65.2 mm and the standard deviation equal to 9.13 mm, Figure 11. They were either slightly below or above the VDOT Hydraulic Cement Specifications of 64 mm clear cover, Figure 12. Only for one tested structure, SN6005 (1989), was the measured cover depth higher than 75 mm.

7.2 Laboratory Evaluation

Laboratory evaluation included various testing procedures described in more details in the Method & Materials Section. All of them were introduced into this study to inspect the quality and performance of the ECR, used currently in bridge decks in Virginia and other states, as the main corrosion protection method.

7.2.1 Concrete

Visual examination of concrete cores, drilled from evaluated bridge decks, demonstrated sound, well consolidated concrete, with a normal amount of entrained and entrapped air. Coarse and fine aggregate were well graded and uniformly distributed. No carbonation in concrete was detected.

Observed surface cracks were related to shrinkage cracking in concrete only.

Based on the rapid chloride permeability test results, most surface concrete samples indicated very low or low chloride ion penetrability since the measured charge transfer was either below 1000 Coulombs or between 1000 and 2000 Coulombs, respectively. Out of the eighteen tested bridge decks a moderate chloride ion permeability was detected for the following structures only: SN1004 (1993), SN2022 and SN6005 (1989), SN1015 (1987), and SN1004 (1983), Figure 14. These findings vary to some degree from the rapid chloride permeability data obtained for the base concrete samples. Except the very low and low and moderate chloride penetrability, the high chloride ion permeability, above 4000 Coulombs, was detected for the following bridge decks: SN1019 (1990), SN6005 (1989), SN1015 (1987), SN1004 (1983) and SN1032 (1980), Figure 15.

In general, the observed trend of the measured charge transfers through the bridge deck samples would suggest, that the base concrete demonstrates a higher chloride ion penetrability than the surface concrete within one bridge deck. This phenomenon is probably related to the lower permeability of the surface concrete as a result of finishing practices.

Average chloride content in concrete at the depth of 13 mm was determined for each bridge deck, Figure 55. Based on the obtained chloride content values at 13 mm a chloride concentration at the reinforcing steel depth was calculated using the following equation [70], Figure 56. An equation found using the lowest significant level, standard deviation, and results from a linear regression

$$y = 0.246 \ x^{0.95} \tag{10}$$

where y is the chloride content (lbs/yd^3) at the bar level and x is the chloride content (lbs/yd^3) at 13 mm depth. The computed chloride concentrations at the reinforcing steel depth were below the chloride corrosion threshold limit in concrete for all bridge decks except four: SN1015 (1987), SN1004 (1983), SN2068 (1978), and SN1056 (1977), Figure 55.
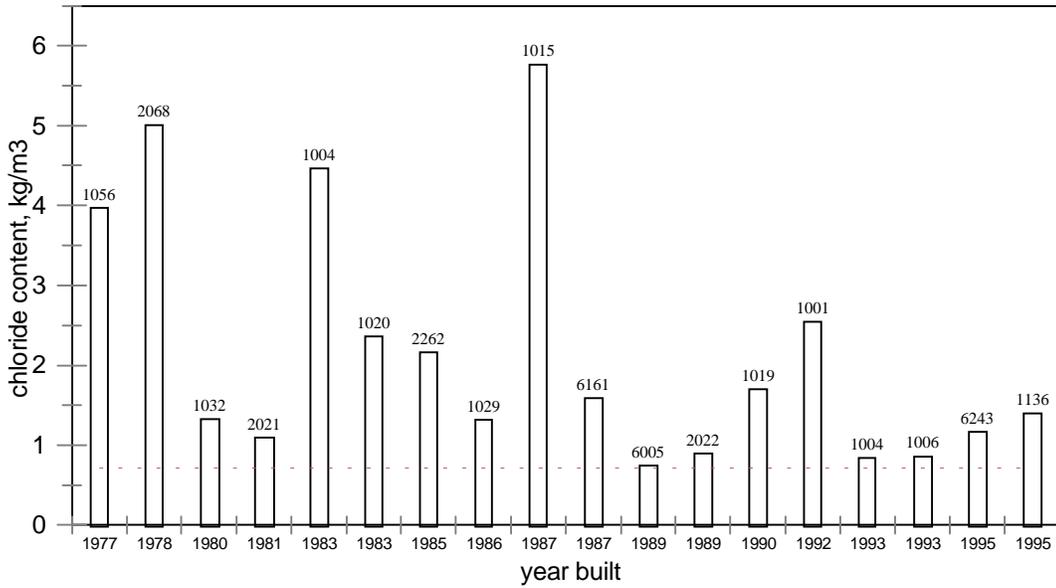
Figure 55. Average Chloride Content at 13 mm Depth.
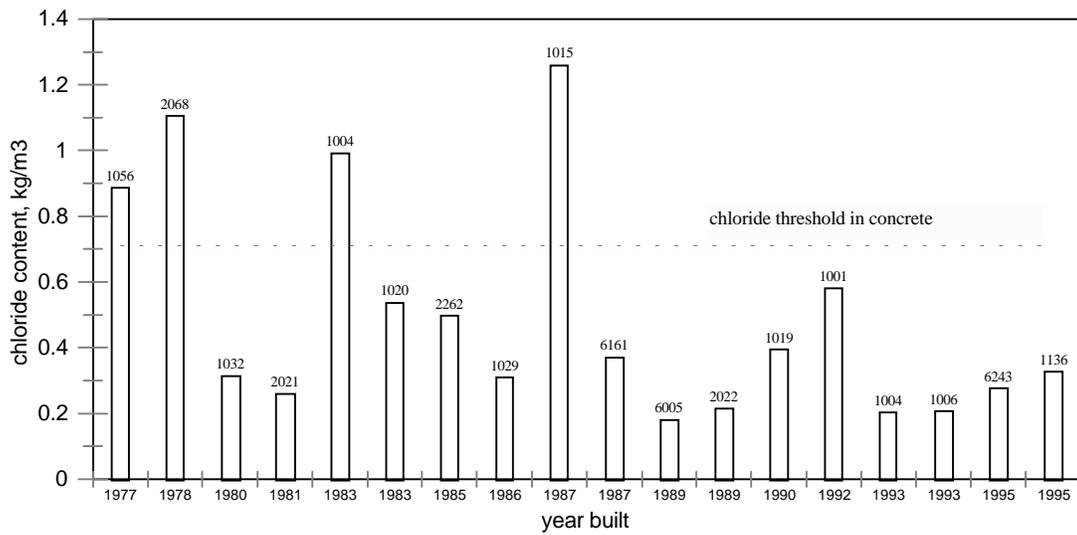
Figure 56. Average Chloride Content at Bar Depth.

93

The moisture content and absorption values of tested concrete bridge decks were relatively uniform for the concrete samples from the top reinforcement level and the truss bar level, between 5.4% and 6.5%, and between 3.5% to 5.5%, respectively, Figures 18 and 19. The determined saturation values for the evaluated bridge decks, in the range of 72% to 92%, agreed with the moisture content and absorption trend, Figure 20. The fairly uniform percent saturation at the top reinforcement verified also findings of the earlier study conducted on bridge decks in Pennsylvania [47].

7.2.2 ECR (Epoxy-Coated Reinforcement)

Visual inspection performed on each ECR specimen and coating continuity examination, demonstrated the small percent area damage and low number of holidays. The calculated damage was below 1% of the total surface area in each 0.3 m of the bar for all evaluated bridge decks, top and bottom reinforcing steel, Figures 21 and 22. The measured number of holidays for the top reinforcement met the current specification limit of 3 holidays per meter for all but two inspected bridge decks, Figure 25. One of them, SN1020 (1983) met the previous specification limit, from 1981, of 6 holidays per meter. However, the number of holidays for the other bridge deck, exceeded both specification requirements. In the case of the tested truss bars, based on the obtained number of holidays, ten out of eighteen bridge decks met the current or previous specification limits, Figure 26. The higher variability in the holiday number seems to be related mostly to the smaller sample size of the examined truss bar specimens, two or three from each bridge deck.

The number of holes was used as an additional characteristic assigned to evaluate the epoxy-coating. The obtained average number of holes was smaller than 1 for all tested top bars and for the most of the inspected truss bars, with the exception of one bridge deck, SN2068 (1978), Figures 23 and 24.   ASTM specification does not include holes as a separate type of coating

damage. However, the author strongly believes that holes should be identified as a special type of coating damage because of their size, which places them somewhere between holidays and more severe imperfections (mashes, dents, scrapes, cracks, and blisters).

Average coating thickness measured on tested ECR specimens met the specification limit of 175 to 300 μm, Figures 23 and 24. All specimens with the thickness values below 125 μm were excluded from further inspection, according to the ASTM A 775 - 95.

ECR specimens rejected because of their low coating thickness, less than 125 μm, where also discarded from the knife-peel test. Adhesion testing allowed the determination of the bond strength between the epoxy coating and the steel surface after the exposure of the coating to the highly alkaline, pH 13, concrete environment for a number of years. The loss of adhesion was not detected for the top reinforcement specimens from the following bridge decks: SN1020 (1983), SN6243 (1995) and SN1136 (1995). The top mat specimens obtained from other bridge decks experienced a decrease in the adhesion strength. Their average adhesion values ranged from 2 to 5, Figure 25.   In the case of the truss bar specimens, the strong adhesion bond was detected for the following structures: SN1004 (1983), SN1020 (1983), SN6161 (1987), SN1006 (1993), SN6243 (1995), and SN1136 (1995), Figure 26. The rest of the evaluated truss bar specimens demonstrated an average adhesion value between 3 and 5.

Although, adhesion loss was observed for the top and bottom mat specimens used in bridge decks constructed in various times, there was no cor relation between the structure age and the decreasing strength of the adhesive bond of the epoxy coating to the reinforcing steel surface. Among the inspected top mat specimens the average adhesion value was 5 for two bridges constructed in 1993, SN1006 and SN1004, Figure 25. At the same time, the strong adhesion bond, a number 1 or 2 adhesion rate, was detected for the specimens obtained from the bridge deck constructed in 1978, SN2068, Figure 25. A similar spread in the average adhesion values was observed for the truss bar specimens, Figure 26.

During the adhesion testing a different color of the steel surface underneath the coating was observed. The color ranged from the shining, almost white, steel to various shades of gray and black. Assigning numbers to all detected colors and analyzing them together with the adhesion values between 1 and 5, demonstrated a linear relation, with the R^2 of 0.88, for the top bars, and 0.7, for the truss bars, Figures 29 and 30. Further investigation of steel surfaces, varying in color, using EDAX (Energy Dispersion Analysis) and XPS (X-ray Photoelectron Spectroscopy), has defined a group of chemical elements on the exposed steel surface, Tables 12 and 13. The general tendency, observed during the testing of the chemical composition of the steel surface, suggests that iron and oxygen are the two main components of the surface layer. Their ratio changes with the change in the defined color. The iron content decreases while the shades of gray become darker and turn into black. This process is accompanied by an increasing concentration of oxygen. The examination of the steel surface underneath the epoxy-coating, using EDAX and XPS, indicates that the variation in color is related primarily to the iron oxidation process and its current stage. The other observation made from the surface layer composition analysis is the absence of chloride on any of the tested specimens.

The detected relation between the adhesion loss and the color of steel surface underneath the epoxy-coating suggests the certain mechanism of the coating disbondment. Water migrates through the coating and weakens the adhesion bond between the epoxy coating and the steel surface. Oxygen becomes available for iron to oxidize. Iron oxidation of the coated steel and its progress tends to weaken the adhesive bond leading to a complete adhesion loss. Absence of chloride ions underneath the coating eliminates their participation in destroying the coating-steel bond at this stage of the adhesion loss.

7.2.3 EIS (Electrochemical Impedance Spectroscopy) and LP (Linear Polarization)

7.2.3.1 EIS

Three main curve shapes determined for tested ECR specimens represent a slightly different behavior, Figures 57A, 58A and 59A. The small semicircle at high frequency for the ECR specimen core #3, SN2262, in Figure 57A, indicated a formation of conductive pathways in the coating and the low coating pore resistance, demonstrated by the small diameter of the circle. The larger incomplete semicircle formed at lower frequencies symbolized the charge transfer reaction. The second semicircle was followed than by the diffusion tail, representing the diffusion controlled corrosion process taking place at the metal substrate, Figure 57A. The phase angle shift at the low frequency, present in the phase angle diagram, was attributed to the diffusion process, Figure 57B.
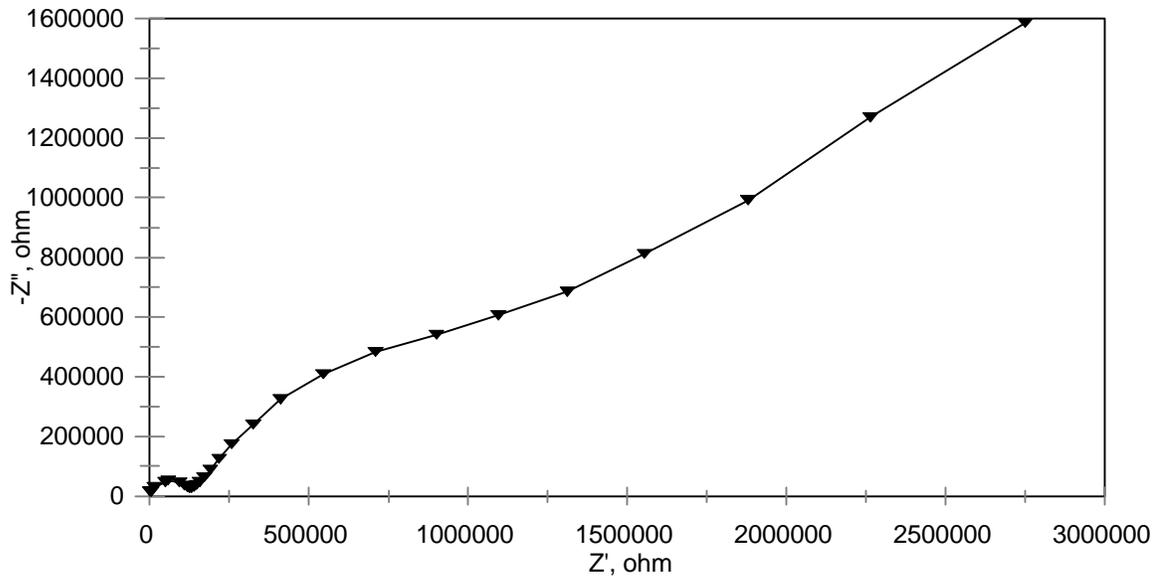
Figure 57A. Type N1 Nyquist Plot, SN2262, Core #3.

EIS, Bode Plot
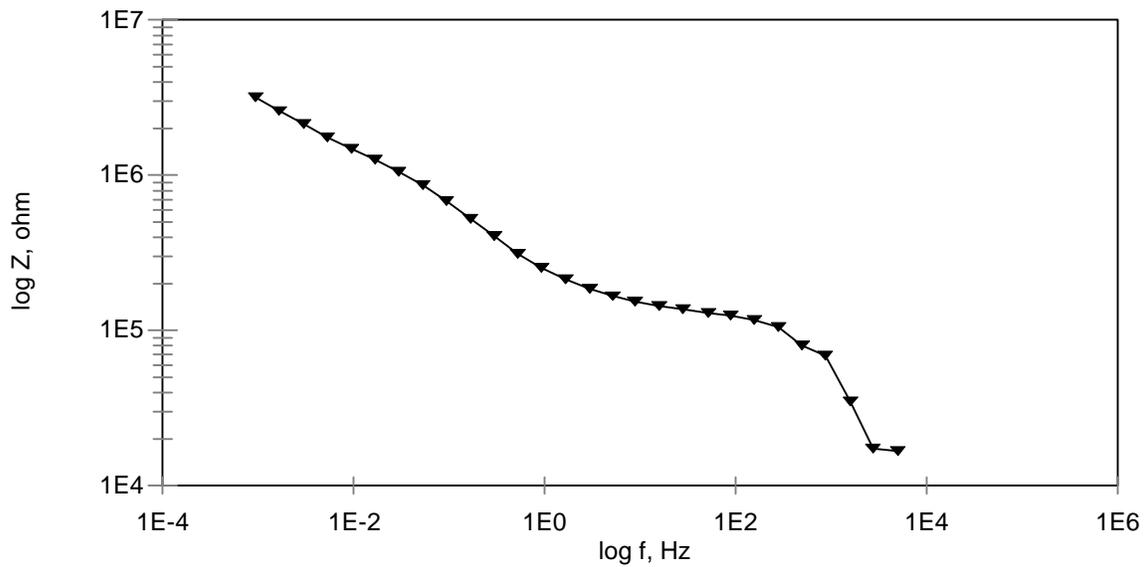
EIS, Phase Angle Plot
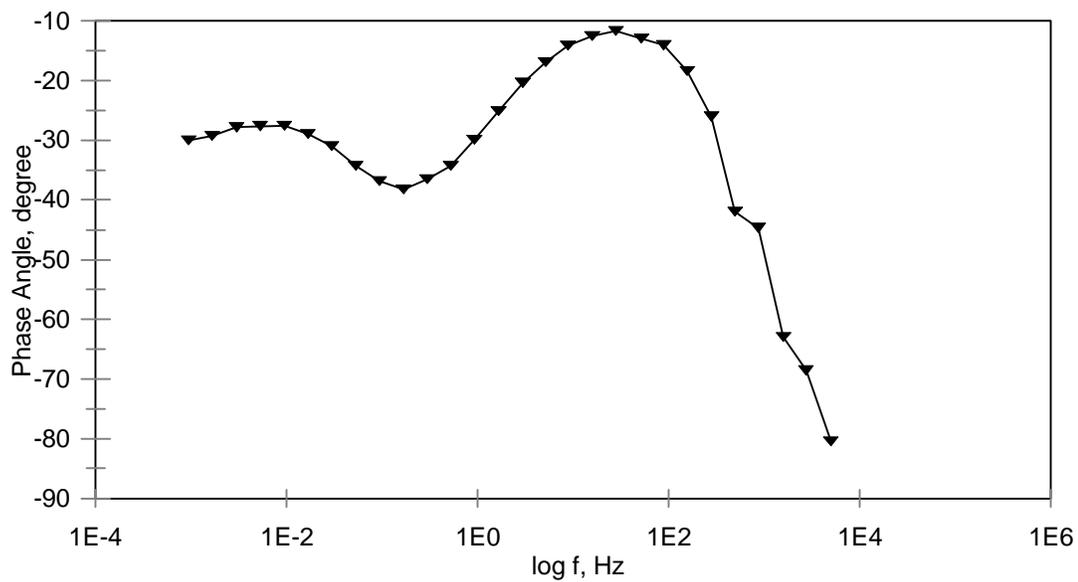
Figure 57B. Bode and Phase Angle Plots, SN2262, Core #3.

EIS, Nyquist Plot
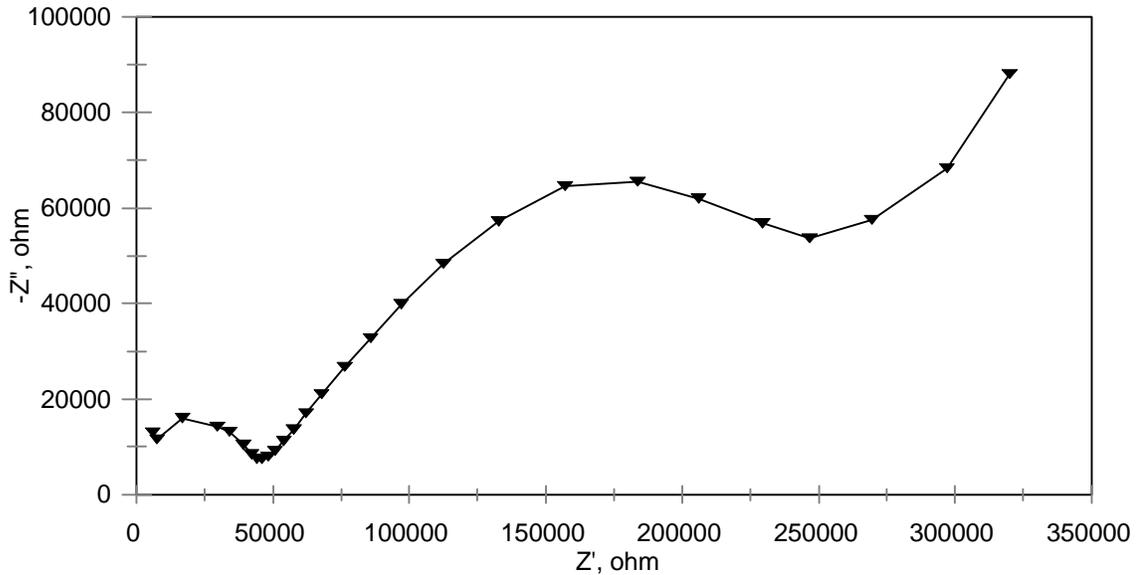
Figure 58A. Type N2 Nyquist Plot, SN2022, Core #8.

The second type of the Nyquist diagram, N2, observed during the EIS testing procedure, demonstrates a permeable coating with a higher coating resistance which could be seen from the larger diameter of the high frequency semicircle, Figure 58A. The low frequency semicircle, clearly visible this time, and a small diffusion tail for the tested core #8, SN2022, ECR specimen, revealed the corrosion process at the metal surface attributed mainly to the charge transfer reaction. Again the phase angle shift at the low frequency was related to the diffusion process, Figure 58B.

Figure 59A demonstrates a completely different behavior. The high frequency semicircle has not formed at this time suggesting a full permeability of the coating. An incomplete charge transfer circle and a diffusion tail represented a corrosion process taking place at the metal surface and being controlled by these two phenomenon. This statement can be supported by the constant phase angle observed from the phase angle plot, Figure 59B.

EIS, Bode Plot
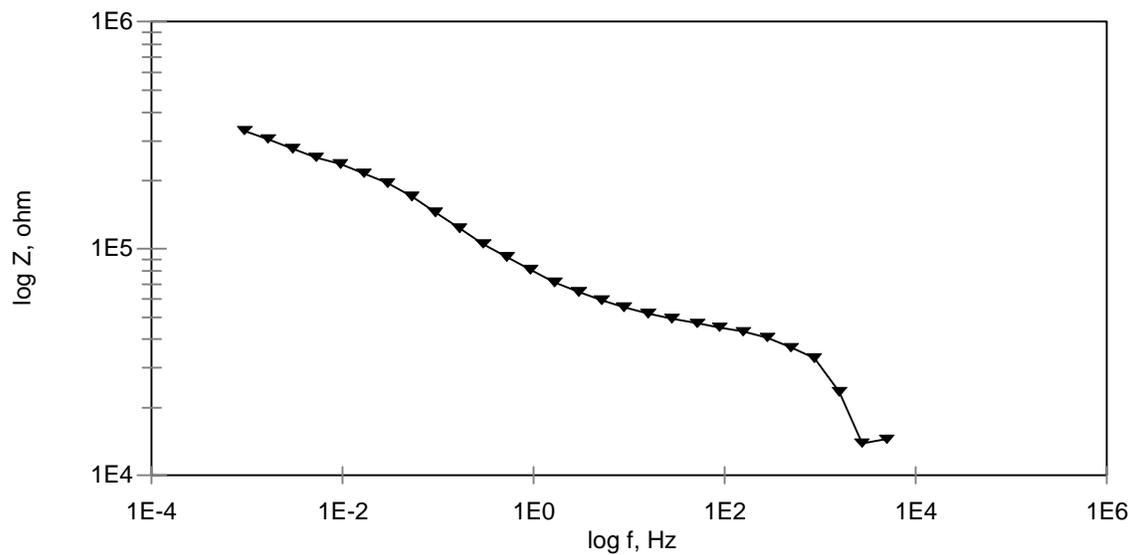
EIS, Phase Angle Plot
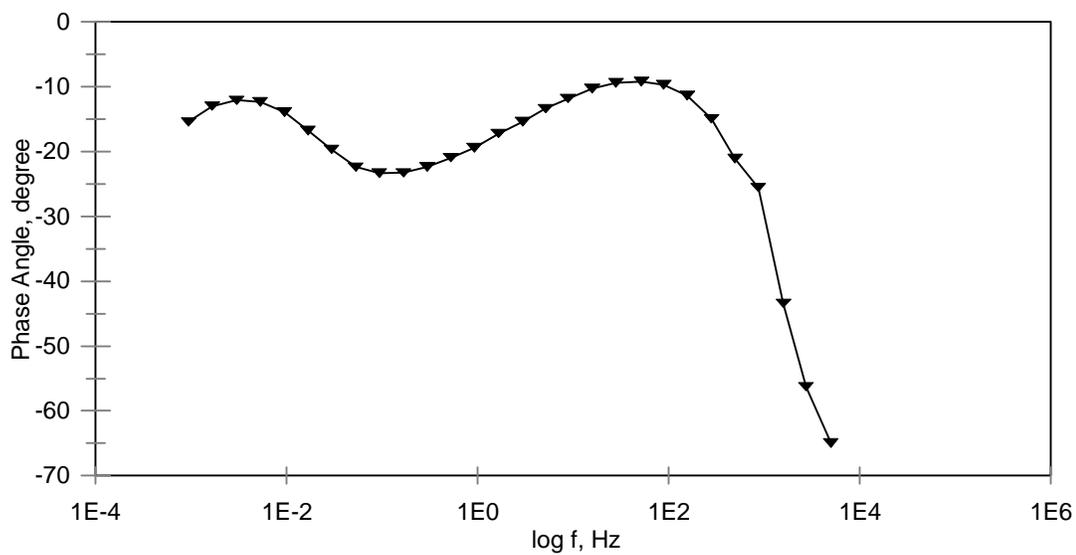
Figure 58B. Bode and Phase Angle Plots, SN2022, Core #8.

EIS, Nyquist Plot
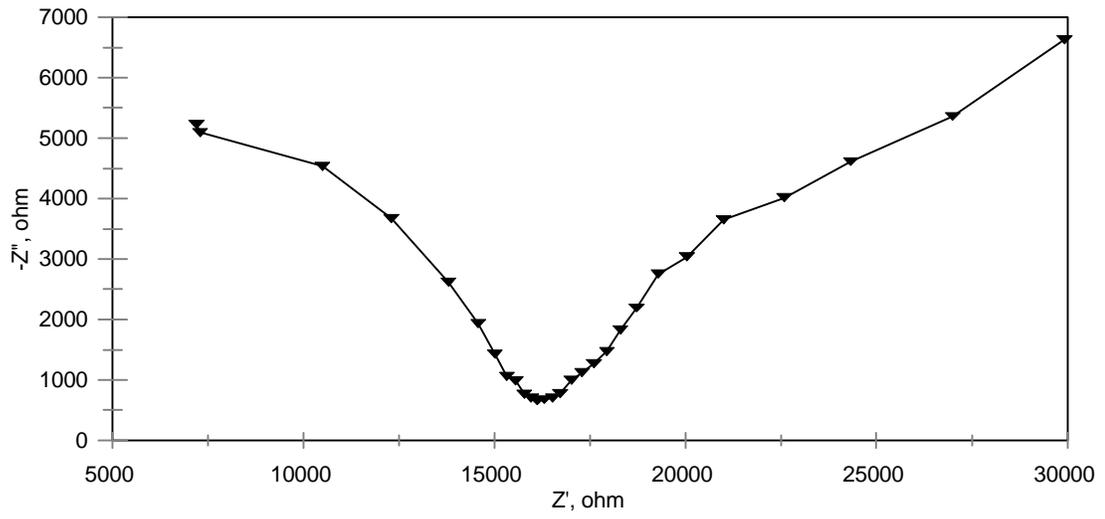
Figure 59A. Type N3 Nyquist Plot, SN1006, Core #6.

EIS, Bode Plot
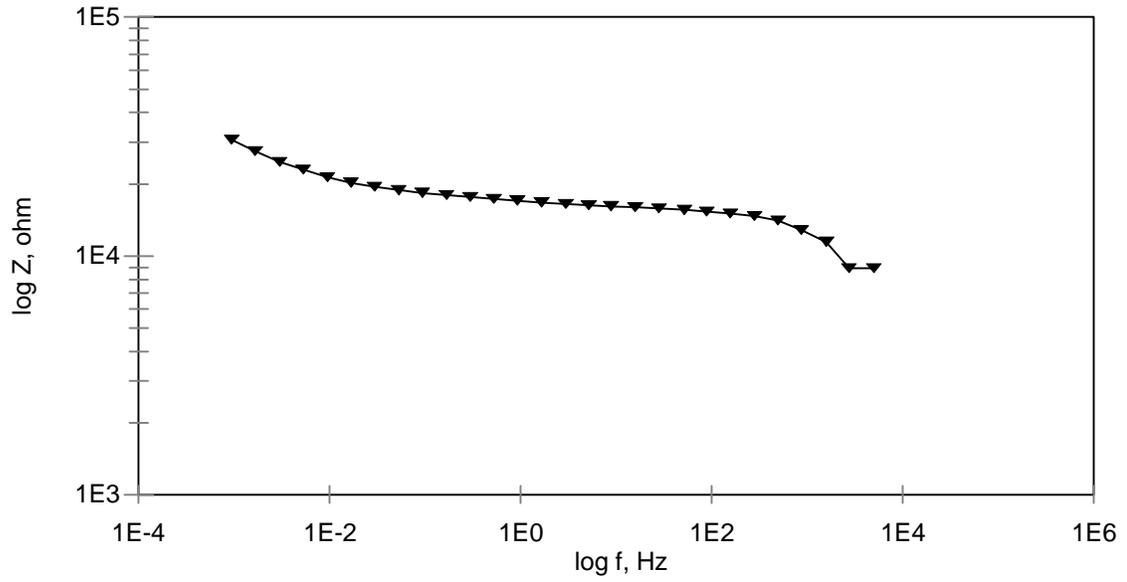
EIS, Phase Angle Plot
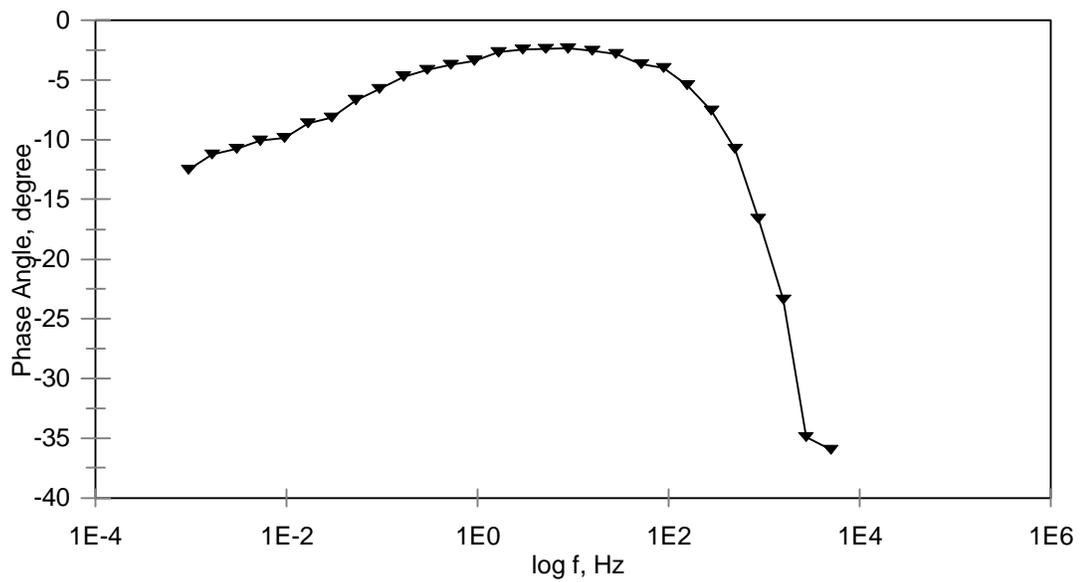
Figure 59B. Bode and Phase Angle Plots, SN1006, Core #6.

7.2.3.2 LP

The comparison of the polarization resistance data and the impedance values measured at the low frequency of 0.001 Hz for 54 ECR specimens embedded in concrete cores, 3 from each bridge deck, gave an indication of a linear relation between these two properties, Figure 60. The only exception was one value with the polarization resistance being relatively higher than the impedance, 10^8 ohm cm^2 and 10^4 ohm, respectively. In general, the findings demonstrate that polarization resistance of ECR is an equivalent of the sum of coating pore resistance, charge transfer resistance, and the diffusion impedance.

Corrosion rates obtained from the polarization resistance measurements may not be the correct values, since the technique works properly with systems where the only significant anodic reaction is metal oxidation [69]. The corrosion mechanism that generates on the steel surface underneath the epoxy coating seems to be more complicated than a typical metal oxidation process.
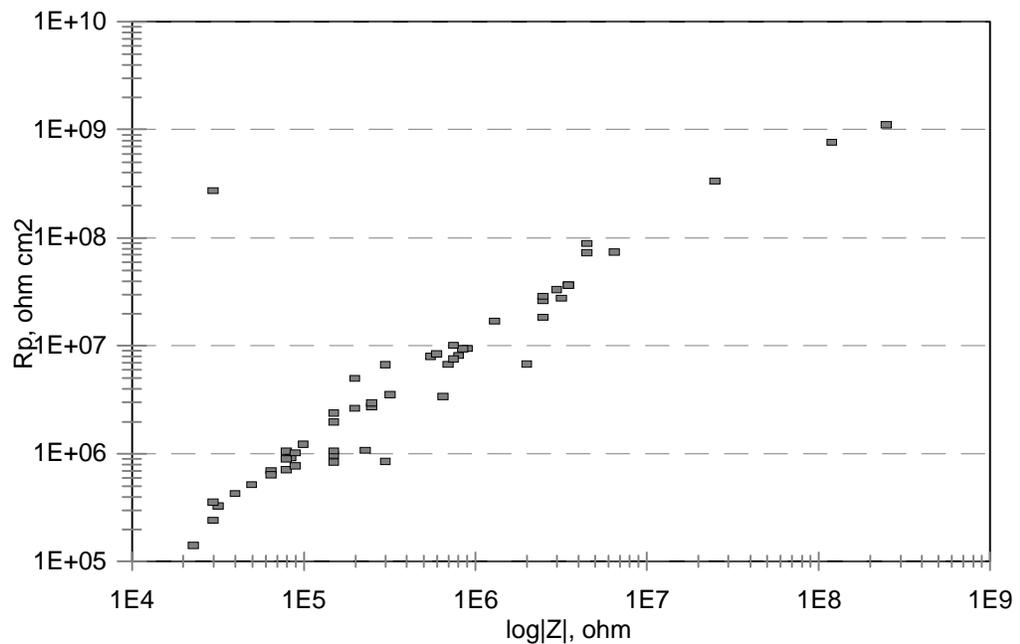
Figure 60. Polarization Resistance, R_p, vs. Impedance, $|Z|$, at 0.001Hz.

103

7.3 Statistical Analysis

Results of the multiple regression analysis of variables influencing the adhesion of the epoxy coating to the reinforcing steel surface demonstrated the best model using the three independent variables, color of the steel underneath the coating, coating thickness and coating damage. However, based on their partial R^2 values the steel color underneath the coating becomes the most important characteristic in the model. The partial R^2 value of 0.843 for the color of the steel underneath the coating predominates the R^2 values of 0.031 of the other two independent variables. These results are in the agreement with simple linear regression findings presented in Figures 61, 62, and 63.
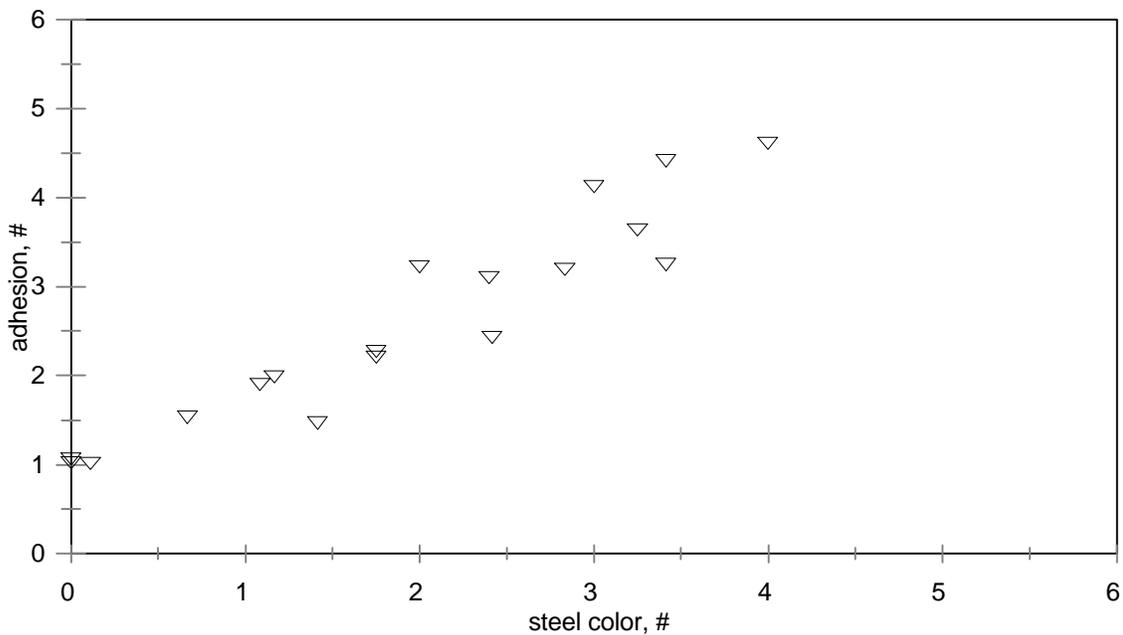
Figure 61. Adhesion vs. Steel Color, Average Values, $R^2 = 0.896$.
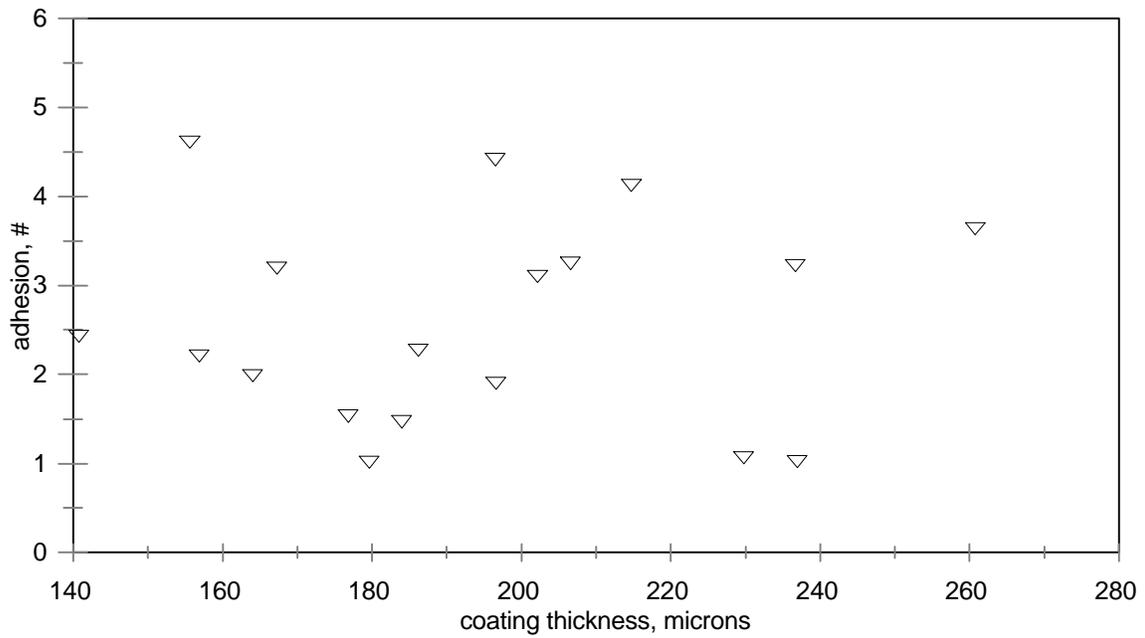
Figure 62. Adhesion vs. Coating Thickness, Average Values, $R^2 = 0.001$.
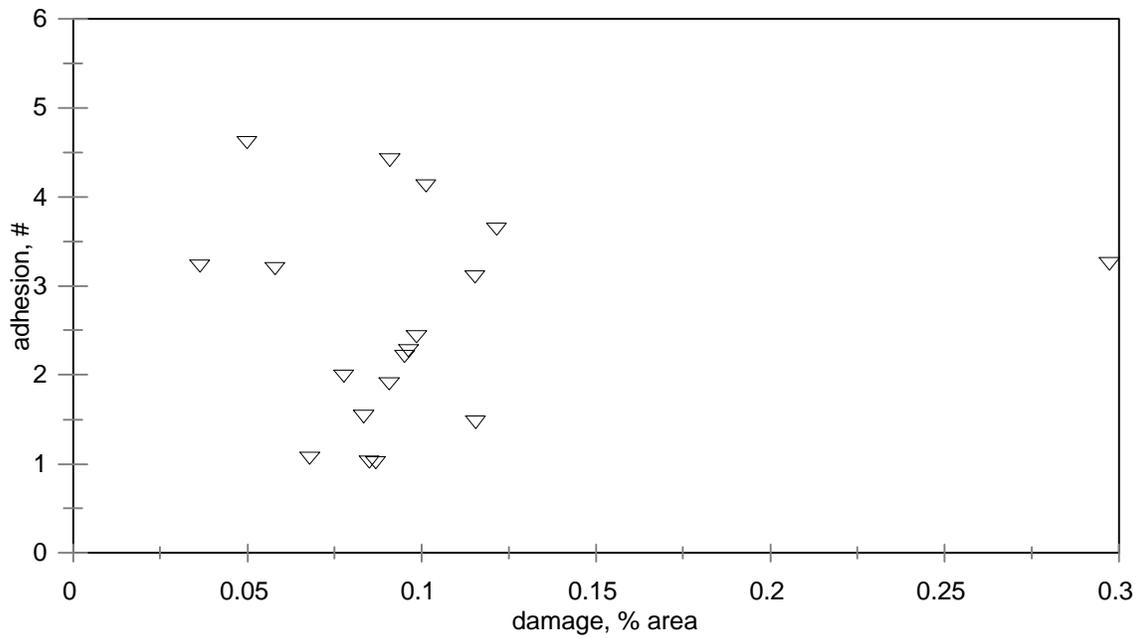
Figure 63. Adhesion vs. Damage, Average Values, $R^2 = 0.008$.

The multiple regression analysis introduced to test the influence of the various coating properties on its impedance values gave the model R^2 value of 0.431 with the two chosen variables, color of the steel underneath the coating and coating damage. Again, the partial R^2 values of 0.341 for the steel color underneath the coating and 0.091 for the coating damage indicate the coating impedance being controlled by the color of the steel surface underneath the coating. Again, the findings agreed with the results of the simple linear regression, Figures 64 and 65.
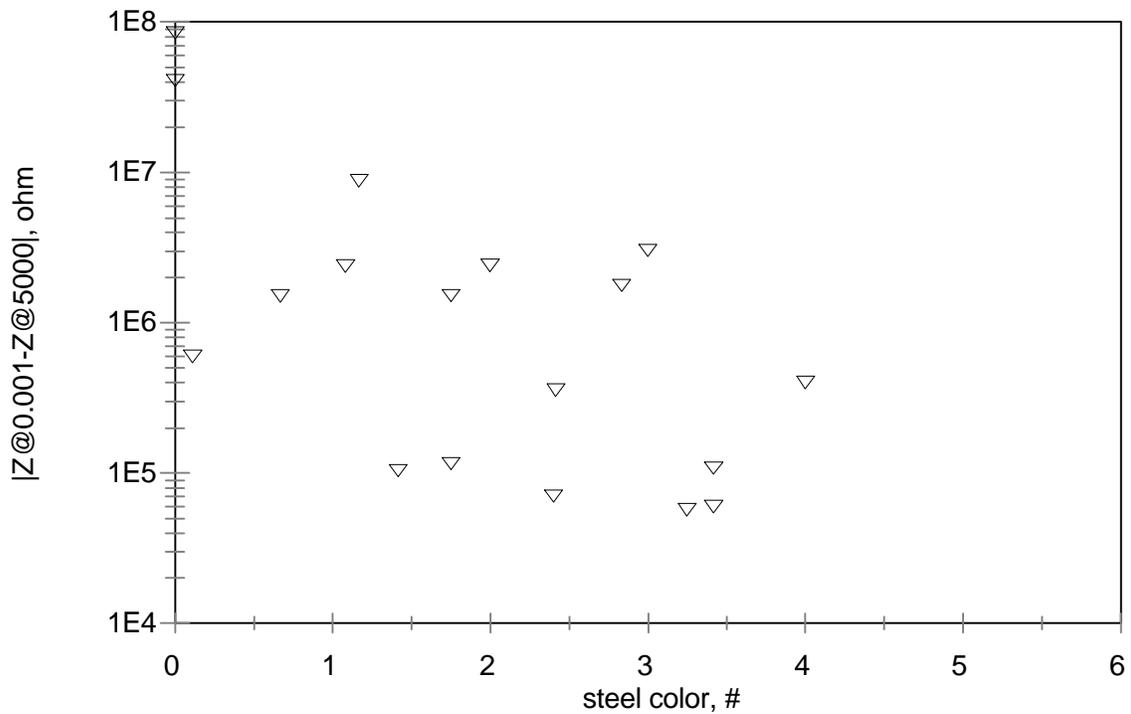
Figure 64. Coating Impedance vs. Steel Color, Average Values, $R^2 = 0.396$.
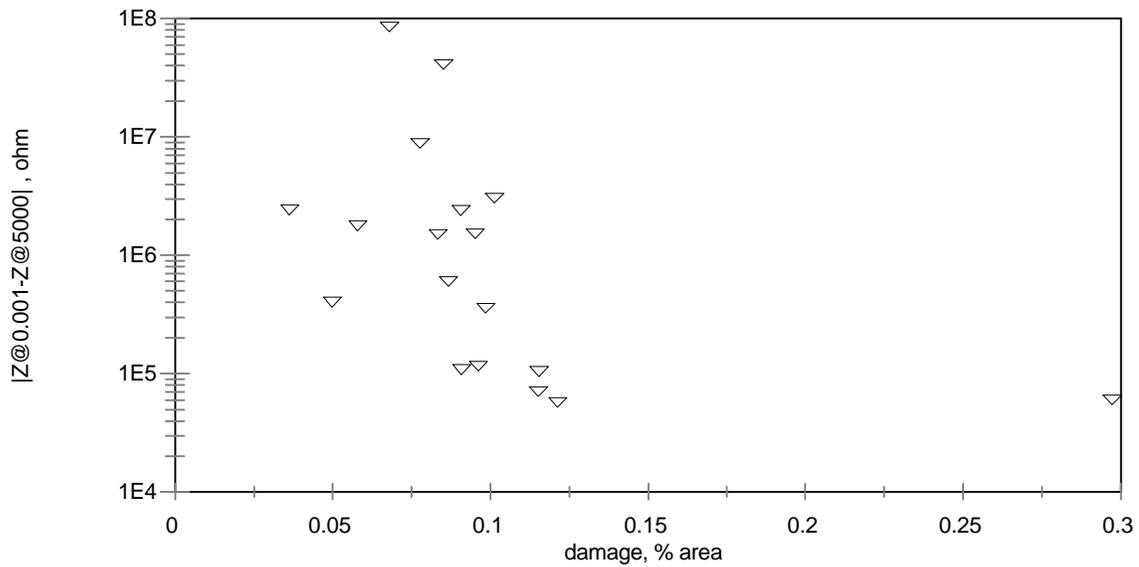
Figure 65. Coating Impedance vs. Damage, Average Values, $R^2 = 0.032$.

7.4 Cost Effectiveness

Life cycle cost analysis for 75 year design life was performed on bridge decks containing epoxy-coated reinforcement (ECR), black steel (BS), A4 concrete, low permeable (LP) A4 concrete, corrosion inhibitor (CI), and their combinations. Total costs, with and without traffic control, were determined for various concrete bridge deck systems, Table 15. The highest total cost of 13.15 $/ft^2 was obtained for the ECR-A4 concrete with LMC overlay placements at 45 and 69 years of the service life. In comparison, the total cost determined for the BS-A4 concrete system with LMC overlay placements at 40 and 64 years of the service life, including the traffic control expenses, was equal to 13.02 $/ft^2.

The evaluation of total costs of concrete bridge deck systems, traffic control costs excluded from the analysis, indicated BS-LP A4 concrete, BS-A4 concrete-CI, and BS-LP A4 concrete-CI systems as more cost effective than ECR-A4 concrete or ECR-LP A4 concrete, Table 15.

Chapter 8. CONCLUSIONS

8.1 Bridge Decks

Evaluated bridge decks were in a good overall condition. No severe cracking damage, no carbonation, and no delaminations were detected. The concrete was sound, well consolidated, with a normal amount of entrained and entrapped air. Coarse and fine aggregates were well graded and uniformly distributed. Inspected concrete demonstrated also low chloride penetrability, based on the rapid chloride permeability test results and obtained chloride concentrations at 13 mm, using chemical analysis of concrete powdered samples.

Measured cover depths were normally distributed and close to the VDOT Hydraulic Cement Specifications of 64 mm clear cover depth. They also seemed to provide the desired protection for the reinforcing steel. The standard deviation of 9.1 mm agrees with findings of others and demonstrates the capability of the present construction techniques of placing the steel in bridge decks at the desired location.

8.2 ECR (Epoxy-Coated Reinforcement)

Although the coating on tested ECR specimens was in overall good condition, detected damage and measured coating thickness met the specification limits, the obtained adhesion values revealed concern on the long term performance of ECR in the concrete environment. The time for corrosion initiation to cracking and delamination in the case of bar reinforcing steel is about 5 years in Virginia [71]. An adhesion loss of the epoxy-coating to the reinforcing steel surface was detected for the ECR specimens embedded in the 4 year old bridge decks. At the same time, it was found that this disbondment was not caused by the presence of chloride ions on the steel surface or the excessive coating damage. The loss of adhesion was related to water penetrating the coating and accumulating at the metal/coating interface, and its peeling stress exceeding the

adhesive bond strength [54] and oxidation of the steel surface.

Electrochemical Impedance Spectroscopy (EIS) measurements revealed that most of the tested ECR specimens became permeable while in moist concrete bridge decks. In Virginia, concrete exhibits more than 72 percent saturation. The charge transfer and diffusion controlled corrosion process have also developed at the metal-coating interface which would explain the observed change in color of the steel surface underneath the coating.

The above stated findings would imply that epoxy-coating will not stay intact and sustain its good adhesion to the steel surface upon the arrival of chloride ions at the bar depth. The protective properties of the epoxy-coating against chloride induced corrosion will be destroyed and the corrosion process underneath the epoxy-coating can progress similar to that of a bare reinforcing steel corrosion or in an acidic environment and thus at a more rapid rate than bare reinforcing steel.

This research supports the conclusions drawn from the Phase I of this project [51] and provides more information on the performance characteristics of ECR used in concrete bridge structures in Virginia.

8.3 Statistical Analysis

The multiple regression analyses applied to examine the influence of various ECR and concrete properties on the adhesion of the epoxy coating to the steel surface indicated the predominant role of the color of the steel underneath the coating. Similar results were obtained while testing variables controlling coating impedance. Again, the color of the steel underneath the coating was found to be the most important characteristic of ECR affecting the coating impedance values.

8.4 ECR and Alternate Systems Based on Cost-Effectiveness Analysis

Adhesion loss of the epoxy-coating to the steel surface, in a moist concrete environment, before the chloride arrival and a possibility of a corrosion process underneath the coating suggest that ECR will not provide any or little additional service life for concrete bridge decks. Other systems, which will provide longer protection with a higher degree of reliability against chloride induced corrosion of steel in concrete, should be considered.

Economical analysis of various systems has demonstrated that the most cost effective practice would be the use of bare reinforcing steel (BS) with the following types of concrete: low permeable (LP) A4 concrete, A4 concrete plus corrosion inhibitor (CI), or low permeable (LP) A4 concrete plus corrosion inhibitor (CI). According to the cost effective estimation, presented in this study, these three systems will provide savings for concrete bridge decks, in comparison to the ECR-A4 concrete system, by 1.12, 0.97 and 0.75 $/ft^2, respectively, Table 15. The use of BS-LP A4 concrete and BS-LP A4 concrete-CI systems instead of the ECR-LP A4 concrete gives also savings of 0.58 and 0.15 $/ft^2, respectively. Presented values were obtained for the systems containing the latex modified concrete (LMC) overlay and excluding the traffic control costs.

Chapter 9. RECOMMENDATION FOR FURTHER RESEARCH

Adhesion testing (bond strength testing)of the epoxy-coating to the steel surface, using the knife-peel test, should become a standard procedure for the evaluation of ECR. However, additional research should be performed on the determination of the adhesion value at which epoxy-coating will not maintain its protective properties against chloride induced corrosion.

The author strongly believes that in the scale of 1 to 5, the adhesion rate of 3 is the limit after which coating disbondment will progress rapidly and upon chloride ions arrival corrosion, underneath the coating, will develop in the same manner as for the adhesion values of 4 or 5. However, a laboratory study on monitoring the chloride induced corrosion development and progress should be performed to support this claim.

Field performance evaluation of other corrosion protection systems, suitable for concrete bridge decks, including bare steel plus low permeable A4 concrete, bare steel plus A4 concrete and corrosion inhibitor, bare steel plus low permeable concrete and corrosion inhibitor, should be conducted and compared with the results obtained from the ECR study.

REFERENCES

[1]   Hausmann, D.A. (1967). "Steel Corrosion in Concrete. How Does It Occur?." *Materials Protection*, November, pp. 19-23.

[2]   Arup, H. (1983). "The mechanism of the protection of steel by concrete." *Corrosion of Reinforcement in Concrete Construction*, edit. A.P. Crane, Ellis Horwood Limited, England, Ch.10, pp.151-157.

[3]   Fraczek, J. "A Review of Electrochemical Principles as Applied to Corrosion of Steel in a Concrete or Group Environment," *Corrosion, Concrete, and Chlorides - Steel Corrosion in Concrete: Causes and Restrains*, SP-102, American Concrete Institute, Detroit, Michigan.

[4]   Dillard, J.G., J.D. Glanville, W.D. Collins, R.E. Weyers, and I.L. Al-Qadi (1993). *Concrete Bridge Protection and Rehabilitation: Chemical and Physical Techniques, Feasibility Studies of New Rehabilitation Techniques*. SHRP-S-665, Strategic Highway Research Program, National Research Council, Washington, DC.

[5]   Schiessl, P. and R. Bakker (1988). "Measures of Protection," *Corrosion of Steel in Concrete,* edit P. Shiessl.. Report of the Technical Committee 60-CSC RILEM, The International Union of Testing and Research Laboratories for Materials and Structures, Ch. 5, pp.73.

[6]   Treadaway, K.W.J., B.L. Brown, and R.N. Cox (1978). "Durability of Galanized Steel in Concrete." *Corrosion of Reinforcing Steel in Concrete*, A symposium sponsored by ASTM Committee G-1 on Corrosion of Metals, pp.102-131.

[7]   Clifton, J.R., H.F. Beeghly, F. Hugh, and R.G. Mathey (1974). *Nonmetallic Coatings for Concrete Reinforcing Bars*. National Bureau of Standards, Report No. FHWA-RD-74-18, Washington, DC, Federal Highway Administration.

[8]   Clifton, J.R., H.F. Beeghly, F. Hugh, and R.G. Mathey (1975). *Nonmetallic Coatings for Concrete Reinforcing Bars*. National Bureau of Standards, Building Science Series - 65, Washington, DC, Federal Highway Administration.

[9]   Clifton, J.R. (1976). "Protection of Reinforcing Bars with Organic Coatings." *Materials Performance*, Vol.15, No.5, pp. 14-17.

[10]   Zemajtis, J., R.E. Weyers, M.M. Sprinkel, and W.T. McKeel, Jr. (1996). *Epoxy-Coated Reinforcement - A Historical Performance Review*. VTRC 97-IR1, Virginia Transportation Research Council, pp. 4.

[11]   Manning, D.G. (1996). "Corrosion performance of epoxy-coated reinforcing steel: North America experience." *Construction and Building Materials*, Vol. 10, No. 5, pp. 349-365.

[12]   (1979) Durability of concrete bridge decks. NCHRP Synthesis of Highway Practice 57, Transportation Research Board, Washington, D.C., pp. 61.

[13]   Babei, K. and N.M. Hawkins (1987). *Evaluation of Bridge Deck Protective Strategies*. National Cooperative Highway Research Program Report 297, Washington, DC.

[14]   Gustafson, D.P. (1990). "Steel Reinforcement." *ASTM Standardization News*, Vol. 18, No. 12, pp. 38-42.

[15]   Babei, K. and N.M. Hawkins (1988). "Evaluation of Bridge Deck Protective Strategies." *Concrete International*, pp. 56-66.

[16]   Kilareski, W.P. (1977). "Epoxy Coating for Corrosion Protection of Reinforcement Steel. Chloride Corrosion of Steel in Concrete. " *ASTM STP 629*, Philadelphia, PA, pp. 82-88.

[17]   Virmani, Y.P., K.C. Clear, and T.J. Pasko, Jr. (1983). *Time-to-Corrosion of Reinforcing Steel in Concrete Slabs, Volume 5: Calcium Nitrate Admixtures or Epoxy-Coated Reinforcing Bars as Corrosion Protection Systems*. Report No. FHWA/RD83/012, Interim Report, Washington, DC, Federal Highway Administration.

[18]   Pfeifer, D.W., J.R. Langren, and A. Zoob (1987). *Protective Systems for New Prestressed and Substructure Concrete. Report No.* FHWA/RD-86/193, Washington, DC, Federal Highway Administration.

[19]   Treadway, K.W.J., and H. Davies (1989). "Performance of Fusion-Bonded Epoxy-Coated Steel Reinforcement." *Structural Engineer*, Vol. 67, No. 6, pp. 99-108.

[20]   Romano, D.C. (1988). *Preliminary Investigation of Epoxy-Coated Reinforcing Steel Disbondement: Causes and Effects.* Florida Department of Transportation, Materials Office, Gainsville, FL.

[21]   Sagues, A.A., and A.M. Zayed (1989). *Corrosion of Epoxy-Coated Reinforcing Steel in Concrete - Phase 1.* Report No. FL/DOT/SM089-419, Florida Department of Transportation, Materials Office, Gainsville, FL.

[22]   Sagues, A.A., and A.M. Zayed (1989). "Corrosion of Epoxy-Coated Reinforcing Steel in Concrete." Paper No. 379, *Corrosion 89*, New Orleans Convention Center, New Orleans, LA.

[23] Sohanghpurwala, A.A., and K.C. Clear (1990). "Effectiveness of Epoxy Coatings in Minimizing Corrosion of Reinforcing Steel in Concrete." Paper No. 89, *Transportation Research Board*, 69th Annual Meeting, Washington, DC.

[24] Sohanghpurwala, A.A., and K.C. Clear (1990). "Effectiveness of Epoxy Coatings in Minimizing Corrosion of Reinforcing Steel in Concrete." *Transportation Research Record*, No. 1268, pp. 193-204.

[25] Sagues, A.A. and R.G. Powers (1990). "Effect of Concrete Environment on the Corrosion Performance of Epoxy-Coated Reinforcing Steel." Paper No. 311, *Corrosion 90*, Las Vegas, NV.

[26] Concrete Reinforcing Steel Institute (1992). "CSRI Performance Research: Epoxy-Coated Reinforcing Steel." Interim Report.

[27] Sagues, A.A. (1991). *Mechanism of Corrosion of Epoxy-Coated Reinforcing Steel in Concrete.* Report No. FL/DOT/RMC/0543-3296.

[28] Rasheeduzzafar, F.H. Dakhil, M.A. Bader, and M.M. Khan (1992). "Performance of Corrosion Resisting Steels in Chloride-Bearing Concrete." *ACI Materials Journal*, Vol. 89, No. 5, pp. 439-448.

[29] Clear, K.C., W.H. Hartt, J. McIntyre, and Seung Kyoung Lee (1995). *Performance of Epoxy-Coated Reinforcing Steel in Highway Bridges*. NCHRP Report 370, National Cooperation Highway Research Program, Washington, DC.

[30] Cork, H.A. (1977). "Coating Treatment for Reinforcing Steel." *Concrete (London)*, Vol. 11, No. 1, pp. 31-33.

[31] Kobayashi, K., and K. Takewaka (1984). "Experimental Studies on Epoxy-Coated Reinforcing Steel for Corrosion Protection." *The Journal of Cement Composites and Lightweight Concrete*, Vol. 6, No. 2, pp. 99-116.

[32] Satake, J., M. Kamakura, K. Shirakawa, N. Mikami, and N. Swamy (1983). "Long-Term Corrosion Resistance of Epoxy-Coated Reinforcing Bars." *Corrosion of Reinforcement in Concrete Construction*, Ellis Horwood Ltd., UK, Chapter 21.

[33] Salparanta, L. (1988). "Corrosion Prevention of Concrete Reinforcement by Epoxy Coating." *Nordic Concrete Research*, No. 7, pp. 250-258.

[34] Yeomans, S.R. (1994). "Performance of Black, Galvanized, and Epoxy-Coated Reinforcing Steels in Chloride-Contaminated Concrete." *Corrosion*, Vol. 50, No. 1, pp. 72-81.

[35] Miura, T., H. Itabashi, and I. Iwaki (1997). "Study on Allowable Coating Damage of Epoxy-Coated Reinforcing Bars." *ACI Materials Journal*, Vol. 94, No. 4, pp. 267-272.

[36] McKeel, W.T., Jr. (1977). *Evaluation of Epoxy-Coated Reinforcing Steel*. VHTRC 77R56, Virginia Highway Research Council, Charlottesville, VA.

[37] McKeel, W.T., Jr. (1988). *Evaluation of Epoxy-Coated Reinforcing Steel*. Federal Highway Administration, Virginia Division.

[38] Munjal, S.K. (1981). *Evaluation of Epoxy-Coated Reinforcing Steel in Bridge Decks*. Report No. FHWA-MD-82/03, Maryland State Highway Administration.

[39] Hegen, M.G. (1982). *Bridge Deck Deterioration and Restoration - Final Report*. Report No. FHDA-MN-RD-83/01, Minnesota Department of Transportation.

[40] Weyers, R.E. and P.D. Cady (1987). "Deterioration of Concrete Bridge Decks from Corrosion of Reinforcing Steel." *Concrete International*, Vol. 9, No. 1, pp. 15-20.

[41] Malesheski, G., D. Maurer, D. Mellott, and J. Arellano (1989). *Bridge Deck Protective Systems*. Report No. FHWA-PA-88-001 + 85-17, Pennsylvania Department of Transportation, Harrisburg, PA.

[42] Malesheski, G. (1989). *Bridge Deck Protection with Epoxy and Galvanized Rebars Pennsylvania Experience*. NACE Northeast Regional Meeting, Baltimore, MD.

[43] Read, J.A. (1989). "FBECR. The Need For Correct Specification and Quality Control." *Concrete (London)*, Vol. 23, No. 8, pp. 23-27.

[44] Weyers, R.E. (1995). *A Protocol for the Evaluation of Existing Bridges Containing Epoxy-Coated Reinforcing Steel*. NCHRP Project 10-37B, National Cooperative Highway Research Program, National Research Council, pp.46-47.

[45] Clear, K.C. (1994). "Effectiveness of epoxy-coated reinforcing steel - Final Report. Canadian Strategic Highway Research Program." Ottawa, ON, pp.128.

[46] Clear, K.C. (1992). "Effectiveness of epoxy-coated reinforcing steel - Interim Report. Canadian Strategic Highway Research Program." Ottawa, ON, pp.79.

[47] Perregaux, G.R. and D.R. Brewster (1992). "In-service performance of epoxy-coated steel reinforcement in bridge decks." *Technical Report 92-3*, New York DOT, Albany, NY, pp. 11.

[48]   Cillis, H.J. and M.G. Hagen (1994). "Field examination of epoxy coated rebars in concrete bridge decks." *Report No. MN/RD-94-14*, Minnesota DOT, St. Paul, MN, pp. 4.

[49]   North Carolina DOT (1993). *A report on the performance of epoxy coated reinforcement steel in substructures of coastal bridges in North Carolina.* Raleigh, NC, pp. 8.

[50]   West Virginia DOT (1994). *Evaluation of bridge decks using epoxy coated reinforcement.* Research Report MIR 1261603, Charleston, WV, pp. 11.

[51]   Weyers, R.E., et al. (October 1997). *Final Report: Field Investigation of the Corrosion Protection Performance of Bridge Decks and Piles Constructed with Epoxy-Coated Reinforcing Steel in Virginia.* Report No. VTRC 98-R4, Virginia Transportation Research Council.

[52]   de Wit, J.H.W. (1995). "Inorganic and Organic Coatings." *Corrosion Mechanisms in Theory and Practice*, edited by P. Marcus and J. Oudar, Marcel Dekker, Inc., New York.

[53]   Ledheiser, Jr., H. (1983). "Towards a Better Understanding of Corrosion Beneath Organic Coatings." *Corrosion NACE*, Vol. 39, pp. 189-200.

[54]   Leidheiser, H. and W. Funke (1987). "Water disbondement and wet adhesion of organic coatings on metals: A review and interpretation," *J. Oil & Colour Chemists' Assoc.*, 70, No. 5, pp.121-132.

[55]   Sagues, A.A. et al. (1994). *Corrosion of Epoxy-Coated Rebar in Florida Bridges.* University of South Florida, College of Engineering.

[56]   Pyc, W.A., R.E. Weyers and M.M. Sprinkel (1998). Corrosion Protection Performance of Corrosion Inhibitors and Epoxy-Coated Reinforcing Steel in a Simulated Concrete Pore Water Solution. Report No. VTRC 98-R42, Virginia Transportation Research Council, pp. 40.

[57]   Jones, D.A. (1992). *Principles and Prevention of Corrosion*, Macmillan Publishing Company, New York, pp. 107-111.

[58]   Chen, H., and H.G. Wheat (1996). "Evaluation of Selected Epoxy-Coated Reinforcing Steels." *Corrosion 96*, The NACE International Annual Conference and Exposition.

[59]   Gileadi, E. (1993). *Electrode Kinetics for Chemists, Chemical Engineers, and Materials Scientists.* VCH Publisher, Inc., New York.

[60] Clear, K.C. (1995). "Performance of Epoxy Coated Reinforcing Steel in Highway Bridges." *NCHRP Report 370*, Transportation Research Board National Research Council, National Academy Press, Washington, D.C.

[61] Berke, N.S., and A. Rosenberg (1989). "Technical Review of Calcium Nitrite Corrosion Inhibitor in Concrete." *Transportation Research Record 1211*, TRB, National Research Council, Washington, D.C., pp. 18-26.

[62] Pyc, W.A. (1997). *Performance Evaluation of Epoxy-Coated Reinforcing Steel and Corrosion Inhibitors in a Simulated Concrete Pore Water Solution.* M.S. Thesis, Virginia Polytechnic Institute and State University, Blacksburg.

[63] Ozyildirim, C., and W. Halstead (1988). "Resistance to Chloride Ion Penetration of Concretes Containing Fly Ash, Silica Fume, or Slag." *Permeability of Concrete,* Whiting D. and A. Walitt, eds., ACI SP-108, American Concrete Institute, Detroit, pp. 35-62.

[64] Berke, N.S. (1988). "Microsilica and Concrete Durability." *Transportation Research Record 1204*, TRB, National Research Council, Washington, D.C., pp. 21-26.

[65] Ozyildirim, C., and W. Halstead (1994). "Improved Concrete Quality with Combinations of Fly Ash and Silica Fume." *ACI Materials Journal*, Vol. 91, No.6, pp. 587-595.

[66] Gjørv, O.E. (1995). "Effect of Condensed Silica Fume on Steel Corrosion in Concrete." *ACI Materials Journal*, Vol. 92, No. 6, pp. 591-598.

[67] Whiting, D. (August 1981). *Rapid Determination of the Chloride Ion Permeability of Concrete*. Final Report No. FHWA/RD-81/119, Federal Highway Administration, NTIS No. PB 82140724.

[68] Weyers, R.E., B.D. Prowell, M.M. Sprinkel, and M. Vorster (1993). *Concrete Bridge Protection, Repair, and Rehabilitation Relative to Reinforcement Corrosion: A Methods Application Manual*. SHRP-S-360, Strategic Highway Research Program, National Research Council, pp.254, 268.

[69] Liu, Y. and R.E. Weyers "Modeling the Time-to-Corrosion Cracking in Chloride Contaminated Reinforced Concrete Structures." *ACI* accepted paper.

[70] Larsen, E.P. (1993). *Service Life Determination of Concrete Bridge Decks and Bridge Deck Overlay Systems.* M.S. Thesis, Virginia Polytechnic Institute and State University, Blacksburg.

[71] Liu, Y. (1996). *Modeling the Time-to-Corrosion Cracking of the Cover Concrete in Chloride Contaminated Reinforced Concrete Structures*. Ph.D. Dissertation, Virginia Polytechnic Institute & State University, Blacksburg.

Appendix A:

FIELD SURVEY AND LABORATORY TESTING RESULTS

Table A1   Cover Depth Measurements

Structure #	Constr. year	Span (Section) #	Readings #	Cover Depth mm				
				Mean	Std. Dev.	12 percentile	95% Conf. Limit	
1056	1977	NB	60	58	7.06	50	60	62
		SB	60	63	5.80	57		
2068	1978	1	40	69	5.34	63	72	75
		2	40	80	3.48	76		
		3	40	72	3.60	67		
1032	1980	1	40	75	7.30	67	68	71
		2	40	59	7.38	50		
		3	40	75	3.78	70		
2021	1981	1	40	60	3.27	56	60	62
		2	40	59	7.05	51		
		3	40	64	3.96	59		
1004	1983	1	40	71	4.22	66	73	75
		2	40	77	2.97	74		
		3	40	73	3.31	69		
1020	1983	1	30	66	6.06	59	67	69
		2	30	72	5.22	66		
		3	30	65	3.83	61		
2262	1985	1	30	59	7.84	50	57	59
		2	30	56	6.23	49		
		3	30	58	4.22	53		
		4	30	58	3.75	54		

Table A1   Cover Depth Measurements (cont.)

Structure #	Constr. year	Span (Section) #	Readings #	Cover Depth mm				
				Mean	Std. Dev.	12 percentile	95% Conf. Limit	
1029	1986	1	40	83	3.09	80	69	73
		2	40	60	5.37	54		
		3	40	69	5.85	63		
1015	1987	1	30	67	6.79	59	58	61
		2	40	56	6.29	48		
		3	30	59	6.61	51		
6161	1987	1	40	54	4.52	49	55	57
		2	40	55	2.98	52		
		3	40	58	2.77	55		
6005	1989	1	40	71	3.51	67	76	80
		2	40	71	6.41	64		
		3	40	92	12.23	77		
2022	1989	1	30	57	3.87	53	61	63
		2A	30	63	3.36	59		
		2B	30	67	3.53	63		
		3	30	61	2.20	58		
1019	1990	1	40	66	3.11	62	60	63
		2	40	53	5.83	46		
		3	40	65	4.17	60		
1001	1992	1	40	68	5.00	62	67	69
		2	40	62	6.02	55		
		3	40	74	4.78	68		

Table A1   Cover Depth Measurements (cont.)

Structure #	Constr. year	Span (Section) #	Readings #	Cover Depth mm				
				Mean	Std. Dev.	12 percentile	95% Conf. Limit	
1004	1993	1	30	73	2.70	69	69	71
		2	30	66	6.33	59		
		3A	30	68	4.44	63		
		3B	30	73	2.44	70		
1006	1993	1	30	73	3.10	69	64	67
		2A	30	60	2.64	57		
		2B	30	61	3.11	57		
		3	30	68	3.23	64		
6243	1995	1	40	63	7.05	55	68	70
		2	40	72	5.53	65		
		3	40	72	2.82	68		
1136	1995	1	40	62	4.80	56	61	63
		2	40	63	3.01	59		
		3	40	62	3.42	58		

Table A2.   Concrete Properties, Truss Bars

Structure #	Constr. year	Rapid Permeability Coulombs		Moisture %	Absorption %	Saturation %
		surface	base			
1056	1977	1489	3498	4.35	5.34	81.60
2068	1978	758	1670	4.53	5.49	82.65
1032	1980	1479	6114	4.08	5.53	73.95
2021	1981	1053	2850	3.90	5.11	77.34
1004	1983	2383	4218	4.92	5.98	82.47
1020	1983	735	1603	4.15	5.72	72.44
2262	1985	483	1995	3.79	4.75	79.56
1029	1986	706	3704	4.45	5.29	84.05
1015	1987	2226	4493	5.42	5.92	91.60
6161	1987	1322	1441	4.51	4.92	91.70
6005	1989	2051	4465	4.51	5.29	85.49
2022	1989	2718	3795	4.83	5.59	86.96
1019	1990	924	4845	4.86	5.54	87.63
1001	1992	1103	2061	4.49	5.08	88.52
1004	1993	2155	3824	4.83	5.44	89.08
1006	1993	1725	1870	4.88	5.79	84.24
6243	1995	565	482	4.35	5.84	74.46
1136	1995	366	411	5.83	6.88	84.77

Table A3.   Concrete Properties, Top Reinforcement

Structure #	Constr. year	Moisture %	Absorption %	Saturation %	Chlorides kg / m^3	
					13 mm	bar depth [a]
1056	1977	5.15	6.00	86.44	3.97	0.89
2068	1978	4.97	5.73	86.70	5.01	1.11
1032	1980	4.95	6.11	81.15	1.32	0.31
2021	1981	4.71	5.55	85.27	1.09	0.26
1004	1983	5.16	6.20	83.26	4.46	0.99
1020	1983	4.82	5.94	81.22	2.36	0.54
2262	1985	4.13	5.42	76.37	2.16	0.50
1029	1986	4.48	5.60	80.02	1.32	0.31
1015	1987	5.31	6.31	84.29	5.77	1.26
6161	1987	4.87	5.41	89.87	1.59	0.37
6005	1989	4.33	5.45	79.73	0.74	0.18
2022	1989	4.96	5.73	86.94	0.89	0.21
1019	1990	4.98	5.93	83.88	1.70	0.39
1001	1992	4.71	5.43	86.63	2.54	0.58
1004	1993	4.83	5.65	85.36	0.84	0.20
1006	1993	5.04	5.80	86.85	0.86	0.21
6243	1995	5.34	6.18	86.40	1.17	0.28
1136	1995	5.87	6.53	89.83	1.40	0.33

[a] -   Chloride content at the bar depth was estimated using the following equation:
$y = 0.246 \ x^{0.95}$ [70].

Table A4.   ECR Testing Results, Epoxy Coating Evaluation

Structure #	Constr. year	Bar	Holidays #	Holes #	Damage % area	Thickness µm mean [b]	std. dev.
1056	1977	1	9	0	0.08	155	17.9
		2	6	0	0.49	176	56.3
		3	12	0	0.00	138	43.6
		4	0	0	0.18	190	32.9
		5	8	0	0.08	142	21.5
		6	100	0	0.10	75	31.8
		7	100	0	0.00	133	37.8
		8	100	0	0.00	122	32.3
		9	100	0	0.04	130	15.6
		10	100	0	0.12	157	27.0
		11	6	0	0.16	167	27.8
		12	100	0	0.04	103	21.94
2068	1978	1	4	0	0.08	140	12.8
		2	6	0	0.06	143	15.2
		3	0	0	0.26	147	23.0
		4	2	0	0.10	286	30.8
		5	5	0	0.16	174	16.8
		6A	0	0	0.00	223	44.5
		7	4	0	0.10	181	31.2
		8	1	0	0.08	174	26.9
		9	0	0	0.14	218	31.5
		10	4	0	0.12	179	14.0
		11	4	0	0.12	220	23.9
		12	6	0	0.34	151	24.8

[b] -   mean of 12 measurements obtained between ribs

Table A4.   ECR Testing Results, Epoxy Coating Evaluation (cont.)

Structure #	Constr. year	Bar	Holidays #	Holes #	Damage % area	Thickness μm mean [b]	std. dev.
1032	1980	1	1	0	0.16	179	13.7
		2	0	0	0.30	332	67.9
		3	1	0	0.10	198	56.5
		4	0	0	0.16	253	25.4
		5	1	0	0.18	180	42.6
		6	0	0	0.00	258	33.9
		7	0	0	0.14	189	14.6
		8	0	0	0.08	158	22.1
		9	6	0	0.08	155	22.6
		10	1	0	0.14	204	16.5
		11	0	0	0.14	195	41.0
		12	1	0	0.06	277	49.9
2021	1981	1	6	0	0.26	195	32.1
		2	1	0	0.30	192	33.1
		3	2	0	0.32	273	30.2
		4	2	0	0.28	202	33.1
		5	2	0	0.12	198	65.3
		6	1	0	2.11	238	32.8
		7	0	0	0.37	224	42.4
		8	2	0	0.08	159	23.2
		9	2	0	0.16	223	58.3
		10	1	0	0.12	193	37.8
		11	3	0	0.12	187	24.8
		12	3	0	0.24	197	31.3

Table A4. ECR Testing Results, Epoxy Coating Evaluation (cont.)

Structure #	Constr. year	Bar	Holidays #	Holes #	Damage % area	Thickness μm mean [b]	std. dev.
1004	1983	1	2	0	0.10	167	28.8
		2	4	0	0.10	154	36.7
		3	2	0	0.12	170	36.0
		4	4	0	0.12	146	35.1
		5	3	0	0.10	204	14.8
		6	2	0	0.20	253	22.8
		7	3	0	0.26	192	43.6
		8	2	0	0.10	206	23.9
		9	0	0	0.08	189	51.4
		10	3	0	0.16	174	41.7
		11	2	0	0.22	163	33.1
		12	0	0	0.08	190	22.4
1020	1983	1	0	0	0.16	192	27.9
		2	4	0	0.10	127	28.4
		3	1	0	0.06	241	53.8
		4	2	0	0.14	163	42.7
		5	6	0	0.14	190	23.2
		6	4	0	0.18	157	67.4
		7	3	0	0.18	180	21.9
		8	2	0	0.26	164	34.5
		9	4	0	0.10	203	43.1

Table A4.   ECR Testing Results, Epoxy Coating Evaluation (cont.)

Structure #	Constr. year	Bar	Holidays #	Holes #	Damage % area	Thickness μm	
						mean [b]	std. dev.
2262	1985	1	0	0	0.12	136	33.3
		2	0	0	0.00	183	28.3
		3	0	0	0.14	165	44.3
		4	1	0	0.08	163	22.1
		5	0	0	0.06	139	36.0
		6	0	0	0.28	184	23.8
		7	2	0	0.08	147	24.3
		8	0	0	0.34	139	12.3
		9	1	0	0.08	149	28.5
		10	1	0	0.12	157	25.7
		11	0	1	0.12	157	33.9
		12	0	0	0.22	163	39.0
1029	1986	1	3	0	0.04	151	31.9
		2	0	0	0.04	167	28.3
		3	1	0	0.06	152	16.7
		4	2	0	0.08	144	30.4
		5	4	0	0.06	142	18.8
		6	0	0	0.00	173	14.8
		7	0	0	0.00	173	35.6
		8	0	0	0.16	177	25.1
		9	0	0	0.14	170	32.6
		10	0	0	0.20	181	53.4
		11	0	0	0.00	232	42.4
		12	2	0	0.16	146	10.4

Table A4.   ECR Testing Results, Epoxy Coating Evaluation (cont.)

Structure #	Constr. year	Bar	Holidays #	Holes #	Damage % area	Thickness μm mean [b]	std. dev.
1015	1987	1	2	0	0.20	339	55.8
		2	0	0	0.22	215	18.2
		3	0	0	0.30	193	61.5
		4	7	0	0.00	159	32.2
		5	3	0	0.12	154	25.4
		6	10	0	0.24	152	71.1
		7	3	0	0.34	257	72.1
		8	3	0	0.00	155	60.6
		9	0	0	0.10	173	54.7
		10	0	0	0.00	227	44.2
6161	1987	1	0	0	0.10	234	61.5
		2	0	0	0.00	165	12.8
		3	0	0	0.24	235	29.9
		4	0	0	0.00	248	26.5
		5	3	0	0.00	211	19.7
		6	1	0	0.00	243	15.9
		7	0	0	0.16	149	15.8
		8	0	0	0.24	138	25.6
		9	0	0	0.32	142	14.2
		10	0	0	0.10	172	13.9
		11	0	0	0.10	164	34.1
		12	0	0	0.12	259	44.1

Table A4.   ECR Testing Results, Epoxy Coating Evaluation (cont.)

Structure #	Constr. year	Bar	Holidays #	Holes #	Damage % area	Thickness μm mean [b]	std. dev.
6005	1989	1	2	0	0.00	149	31.4
		2	0	0	0.04	211	36.0
		3	0	0	0.00	124	39.6
		4B	0	0	0.003	157	84.8
		5	0	0	0.00	162	45.0
		6	1	0	0.02	142	46.5
		7	0	0	0.63	145	56.5
		8	0	0	0.24	151	51.6
		9	0	0	0.00	217	50.1
		10	0	0	0.002	206	58.8
		11	6	0	0.00	109	35.5
		12	0	0	0.08	197	54.3
2022	1989	1	1	0	0.20	184	19.6
		2	0	0	0.16	157	20.7
		3B	0	0	0.16	181	30.0
		4	0	0	0.00	182	19.2
		5	2	0	0.00	187	29.2
		6	1	0	0.00	172	23.7
		7	0	0	0.00	187	29.2
		8	0	0	0.16	190	30.0
		9	0	0	0.32	172	26.1
		10	3	0	0.10	157	15.1

Table A4.   ECR Testing Results, Epoxy Coating Evaluation (cont.)

Structure #	Constr. year	Bar	Holidays #	Holes #	Damage % area	Thickness μm	
						mean [b]	std. dev.
1019	1990	1	4	0	0.14	158	21.4
		2	2	0	0.18	146	20.1
		3	3	0	0.00	138	11.6
		4B	6	0	0.00	137	29.4
		5	1	0	0.00	169	35.5
		6	2	0	0.18	172	36.3
		7	2	0	0.08	152	23.3
		8	3	0	0.00	168	21.8
		9	0	0	0.18	162	32.7
1001	1992	1	1	0	0.00	326	25.9
		2	7	0	0.04	219	26.0
		3	2	0	0.06	304	29.1
		4	2	0	0.00	224	18.1
		5	2	0	0.08	236	22.8
		6	3	0	0.08	209	28.8
		7	1	0	0.04	209	14.4
		8	0	0	0.02	216	30.2
		9	3	0	0.06	191	32.1
		10	3	0	0.02	256	36.8
		11	2	0	0.00	220	22.9
		12	2	0	0.08	233	51.6

Table A4.   ECR Testing Results, Epoxy Coating Evaluation (cont.)

Structure #	Constr. year	Bar	Holidays #	Holes #	Damage % area	Thickness μm mean [b]	std. dev.
1004	1993	1	1	0	0.66	243	15.7
		2	1	0	0.08	212	48.4
		3	0	0	0.08	263	34.7
		4	0	0	0.08	256	32.8
		5	0	0	0.14	303	74.7
		6	0	0	0.22	310	42.0
		7	2	0	0.20	229	34.9
		8	0	0	0.14	278	45.8
		9	2	0	0.24	239	23.4
		10	0	0	0.22	238	22.9
		11	0	0	0.12	286	38.3
		12	0	0	0.16	273	20.7
1006	1993	1	2	0	0.10	220	36.0
		2	3	0	0.20	184	35.9
		3	2	0	0.08	136	20.4
		4	3	2	0.22	148	34.6
		5	3	0	0.30	239	46.8
		6	0	0	0.40	159	50.6
		7	0	0	0.10	285	29.4
		8	4	3	0.08	239	40.8
		9	0	0	0.08	241	35.4
		10	0	0	0.00	185	43.9
		11	3	0	0.04	179	28.9
		12	3	0	0.06	142	21.4

131

Table A4.   ECR Testing Results, Epoxy Coating Evaluation (cont.)

Structure #	Constr. year	Bar	Holidays #	Holes #	Damage % area	Thickness μm mean [b]	std. dev.
6243	1995	1	2	0	0.16	242	43.9
		2	1	0	0.14	215	35.7
		3	0	0	0.08	278	30.3
		4	2	0	0.10	165	16.4
		5	0	0	0.14	182	18.7
		6	0	0	0.06	278	31.6
		7	0	0	0.02	202	57.8
		8	0	0	0.00	265	23.1
		9	2	0	0.04	230	57.2
		10	0	0	0.12	187	11.8
		11	1	0	0.20	190	36.5
		12	0	0	0.18	324	38.5
1136	1995	1	0	0	0.04	278	73.8
		2	2	0	0.08	284	60.8
		3	1	0	0.04	244	40.6
		4	3	0	0.08	159	23.4
		5	1	0	0.06	223	41.1
		6	2	0	0.16	322	63.0
		7	0	0	0.04	301	52.1
		8	2	0	0.14	276	41.6
		9	0	0	0.42	169	47.4
		10	0	0	0.14	172	22.2
		11	0	0	0.18	231	61.9
		12	3	0	0.00	185	57.6

Table A5.   ECR, Adhesion Test Results

Structure #	Constr. year	Adhesion [c] #	Steel Color under Coating [d] #
1056	1977	5,3,4,4,2,1,3,2,3,1,1,1	4,4,4,3,3,0,4,3,4,0,0,0
2068	1978	3,3,5,1,3,1,1,1,1,2,1,5	3,3,3,1,3,0,0,0,1,3,0,4
1032	1980	4,1,4,1,5,5,5,5,5,5,5,5	3,0,3,3,4,3,3,3,3,4,4,3
2021	1981	3,5,1,3,5,1,3,3,5,3,4,4	4,4,0,4,4,1,4,4,4,4,4,4
1004	1983	2,2,1,2,1,1,1,1,1,2,1,2	1,3,0,3,3,0,0,0,1,3,0,3
1020	1983	1,1,1,1,1,1,1,1,1	0,0,0,0,0,1,0,0,0
2262	1985	1,3,1,2,4,1,4,4,4,1,1,1	0,3,0,3,3,0,4,3,3,1,0,1
1029	1986	3,3,2,3,5,4,4,5,2,2,2,4	4,4,1,1,4,4,4,3,4,3,3,3
1015	1987	5,2,5,5,5,5,1,1,1,1	4,3,4,4,4,4,1,0,0,0
6161	1987	1,1,5,1,5,1,4,1,1,1,1,1	0,0,4,0,4,0,4,0,0,0,1,0
6005	1989	1,1,1,1,4,5,1,5,1,1,1,1	0,0,0,0,4,4,0,4,1,0,0,1
2022	1989	1,1,1,1,1,5,1,1,1,1	0,0,0,0,0,4,0,1,1,0
1019	1990	5,5,5,5,4,4,5,5,5	4,4,4,4,4,4,4,4,4
1001	1992	5,5,2,5,5,2,1,1,5,1,2,5	1,4,1,4,4,1,0,0,4,0,1,4
1004	1993	5,2,2,3,5,5,5,4,5,5,1,2	4,1,2,4,4,4,4,4,4,4,0,4
1006	1993	5,5,5,5,5,5,3,5,5,3,3,4	4,4,1,5,4,5,1,4,4,1,4,4
6243	1995	1,1,1,1,1,1,1,1,1,1,1,1	0,0,0,0,0,0,0,0,0,0,0,0
1136	1995	1,1,1,1,1,1,1,1,1,1,1,1	0,0,0,0,0,0,0,0,0,0,0,0

[c] -   description of adhesion rating can be found in Table 6 of Methods and Materials chapter
[d] -   color rating explanation was given in Table 8 of Results section chapter

Appendix B:

ELECTROCHEMICAL IMPEDANCE SPECTROSCOPY (EIS) RESULTS

EIS, Nyquist Plot
SN1056, core #2

EIS, Bode Plot
SN1056, core #2

EIS, Phase Angle Plot
SN1056, core #2

135

EIS, Nyquist Plot

SN1056, core #8

EIS, Bode Plot

SN1056, core #8

EIS, Phase Angle Plot

SN1056, core #8

136

EIS, Nyquist Plot
SN1056, core #12

EIS, Bode Plot
SN1056, core #12

EIS, Phase Angle Plot
SN1056, core #12

EIS, Nyquist Plot
SN2068, core #3

EIS, Bode Plot
SN2068, core #3

EIS, Phase Angle Plot
SN2068, core #3

138

EIS, Nyquist Plot
SN2068, core #8

EIS, Bode Plot
SN2068, core #8

EIS, Phase Angle Plot
SN2068, core #8

139

EIS, Nyquist Plot
SN2068, core #12

EIS, Bode Plot
SN2068, core #12

EIS, Phase Angle Plot
SN2068, core #12

140

EIS, Nyquist Plot
SN1032, core #1

EIS, Bode Plot
SN1032, core #1

EIS, Phase Angle Plot
SN1032, core #1

141

EIS, Nyquist Plot
SN1032, core #8

Nyquist plot with x-axis "Z', ohm" ranging from -500000 to 2500000 and y-axis "-Z'', ohm" ranging from 0 to 500000.

EIS, Bode Plot
SN1032, core #8

Bode plot with x-axis "log f, Hz" ranging from 1E-4 to 1E6 and y-axis "log Z, ohm" ranging from 1E4 to 1E7.

EIS, Phase Angle Plot
SN1032, core #8

Phase angle plot with x-axis "log f, Hz" ranging from 1E-4 to 1E6 and y-axis "Phase Angle, degree" ranging from -100 to 0.

EIS, Nyquist Plot
SN1032, core #10

EIS, Bode Plot
SN1032, core #10

EIS, Phase Angle Plot
SN1032, core #10

EIS, Nyquist Plot
SN2021, core #3

EIS, Bode Plot
SN2021, core #3

EIS, Phase Angle Plot
SN2021, core #3

144

EIS, Nyquist Plot
SN2021, core #8

EIS, Bode Plot
SN2021, core #8

EIS, Phase Angle Plot
SN2021, core #8

145

EIS, Nyquist Plot
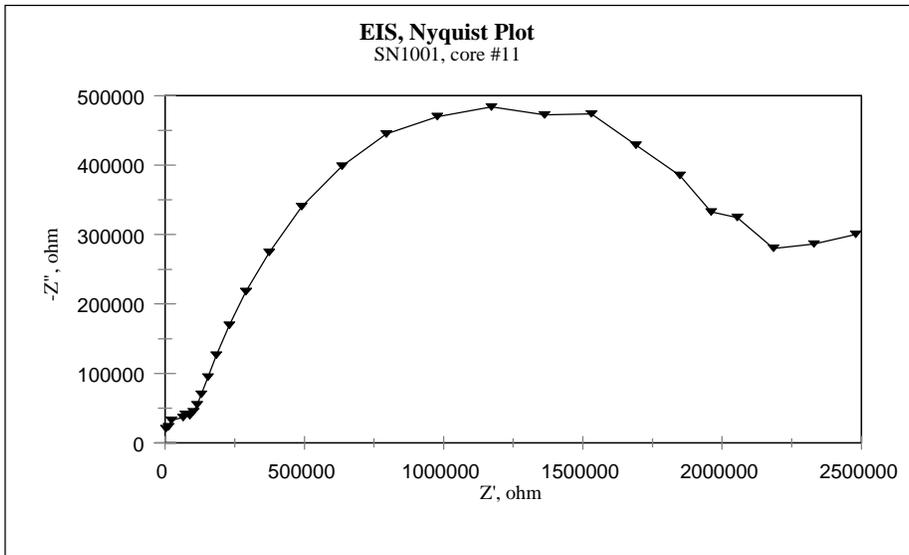SN2021, core #9

EIS, Bode Plot
SN2021, core #9

EIS, Phase Angle Plot
SN2021, core #9

146

EIS, Nyquist Plot

SN1004-3, core #4

EIS, Bode Plot

SN1004-3, core #4

EIS, Phase Angle Plot

SN1004-3, core #4

147
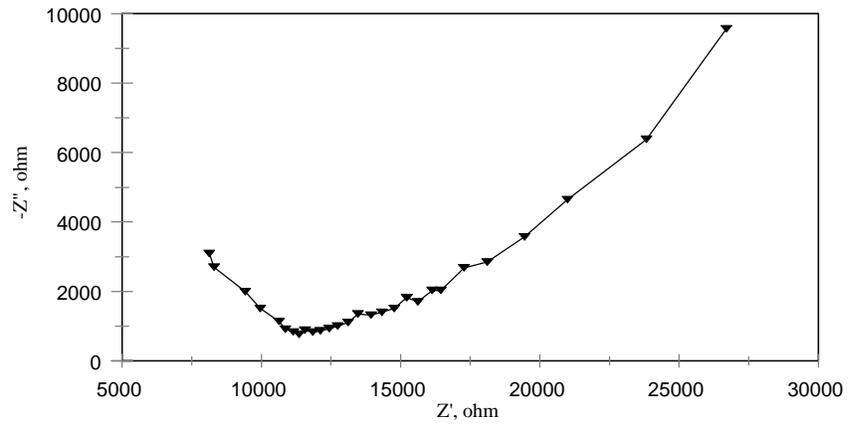
EIS, Nyquist Plot
SN1004-3, core #8

EIS, Bode Plot
SN1004-3, core #8

EIS, Phase Angle Plot
SN1004-3, core #8

148

EIS, Nyquist Plot
SN1004-3, core #10

EIS, Bode Plot
SN1004-3, core #10

EIS, Phase Angle Plot
SN1004-3, core #10

149

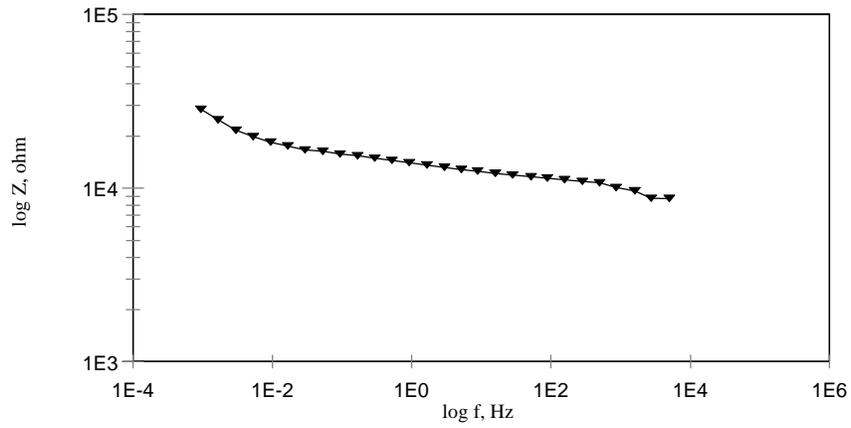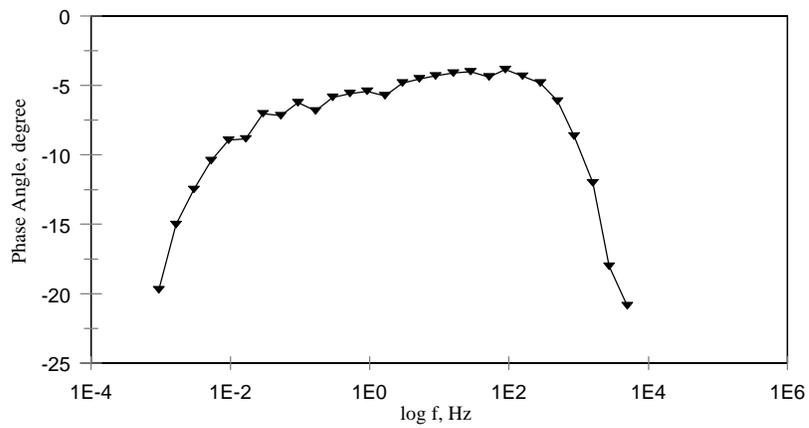**EIS, Nyquist Plot**
SN1020, core #1

EIS, Bode Plot
SN1020, core #1

EIS, Phase Angle Plot
SN1020, core #1

150

EIS, Nyquist Plot
SN1020, core #4

EIS, Bode Plot
SN1020, core #4

EIS, Phase Angle Plot
SN1020, core #4

EIS, Nyquist Plot
SN1020, core #8

EIS, Bode Plot
SN1020, core #8

EIS, Phase Angle Plot
SN1020, core #8

EIS, Nyquist Plot
SN2262, core #3

EIS, Bode Plot
SN2262, core #3

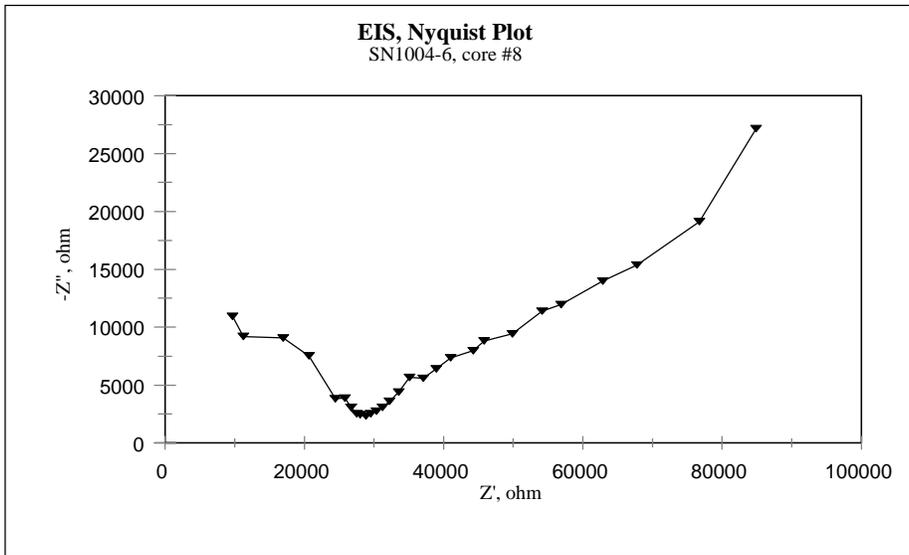**EIS, Phase Angle Plot**
SN2262, core #3

153

EIS, Nyquist Plot

SN2262, core #7

EIS, Bode Plot

SN2262, core #7

EIS, Phase Angle Plot

SN2262, core #7

154

EIS, Nyquist Plot
SN2262, core #9

EIS, Bode Plot
SN2262, core #9

EIS, Phase Angle Plot
SN2262, core #9

155

EIS, Nyquist Plot
SN1029-9, core #4

EIS, Bode Plot
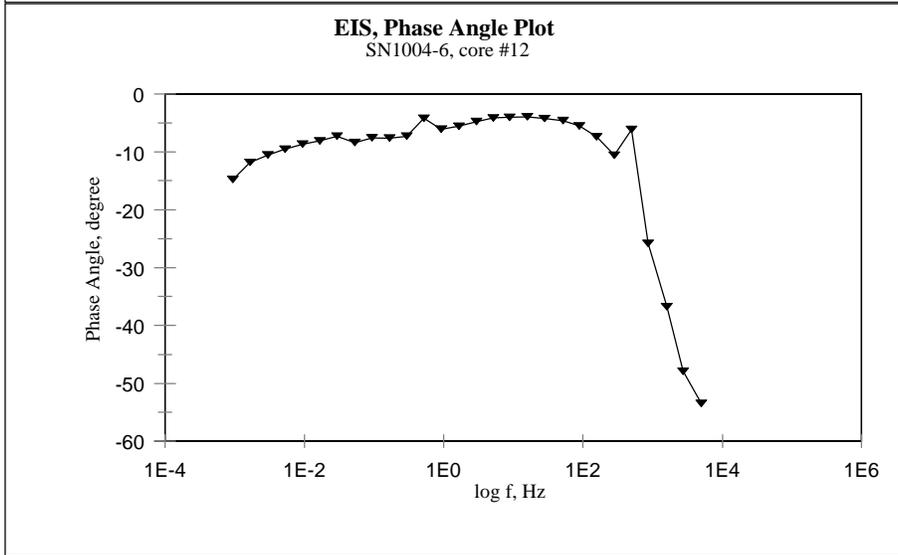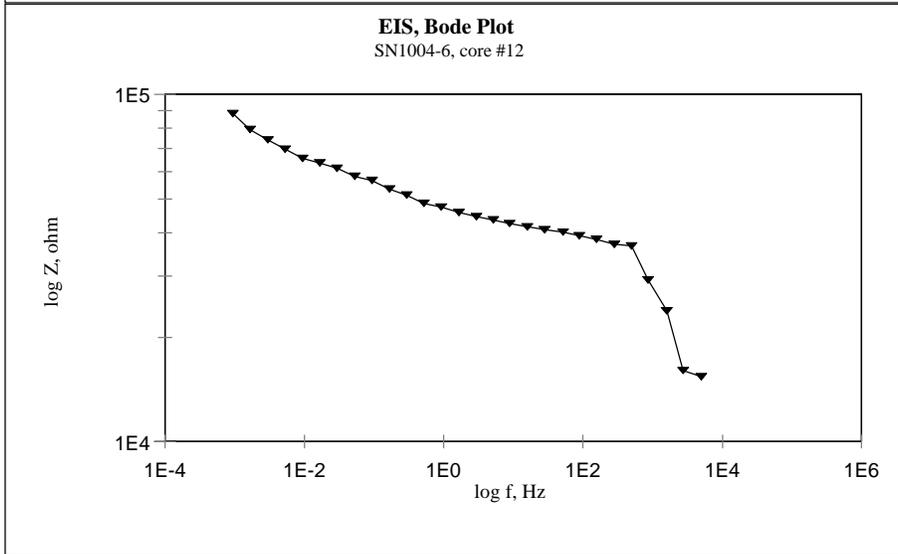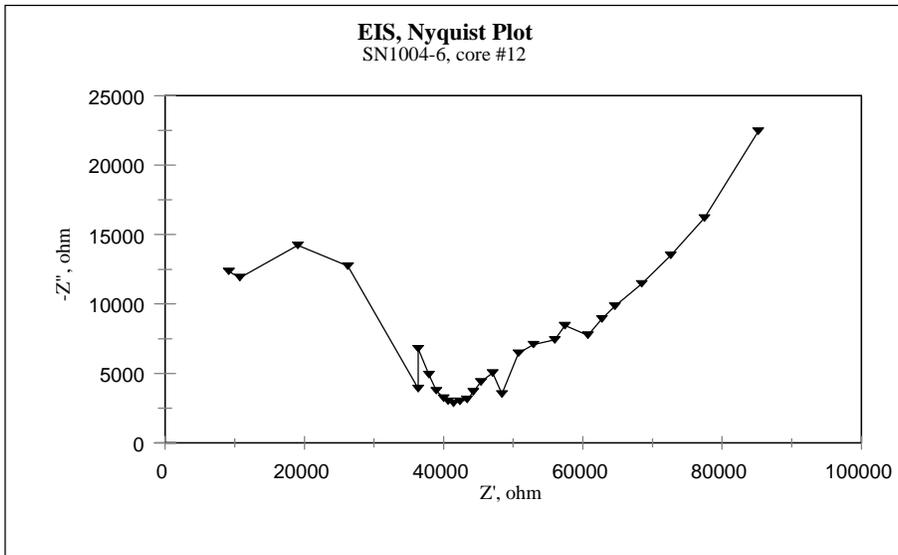SN1029-9, core #4

EIS, Phase Angle Plot
SN1029-9, core #4

EIS, Nyquist Plot
SN1029-9, core #7

EIS, Bode Plot
SN1029-9, core #7

EIS, Phase Angle Plot
SN1029-9, core #7

EIS, Nyquist Plot
SN1029-9, core #9

EIS, Bode Plot
SN1029-9, core #9

EIS, Phase Angle Plot
SN1029-9, core #9

158

EIS, Nyquist Plot
SN1015, core #3

EIS, Bode Plot
SN1015, core #3

EIS, Phase Angle Plot
SN1015, core #3

159

EIS, Nyquist Plot
SN1015, core #5

EIS, Bode Plot
SN1015, core #5

EIS, Phase Angle Plot
SN1015, core #5

160

EIS, Nyquist Plot
SN1015, core #8

EIS, Bode Plot
SN1015, core #8

EIS, Phase Angle Plot
SN1015, core #8

EIS, Nyquist Plot
SN6161, core #3

EIS, Bode Plot
SN6161, core #3

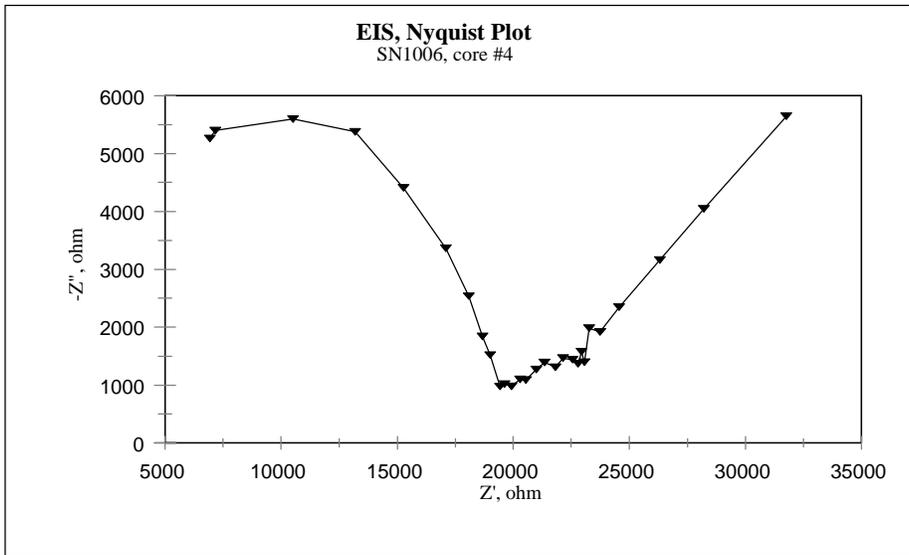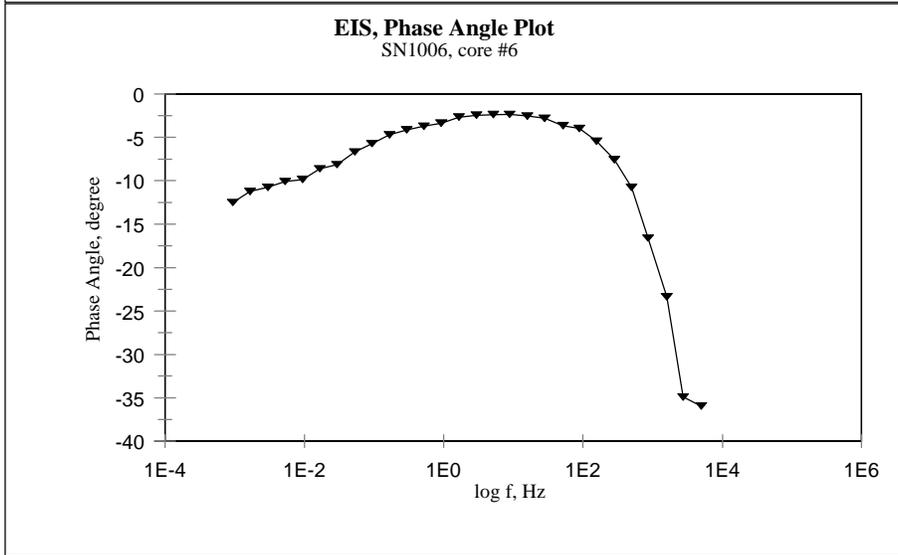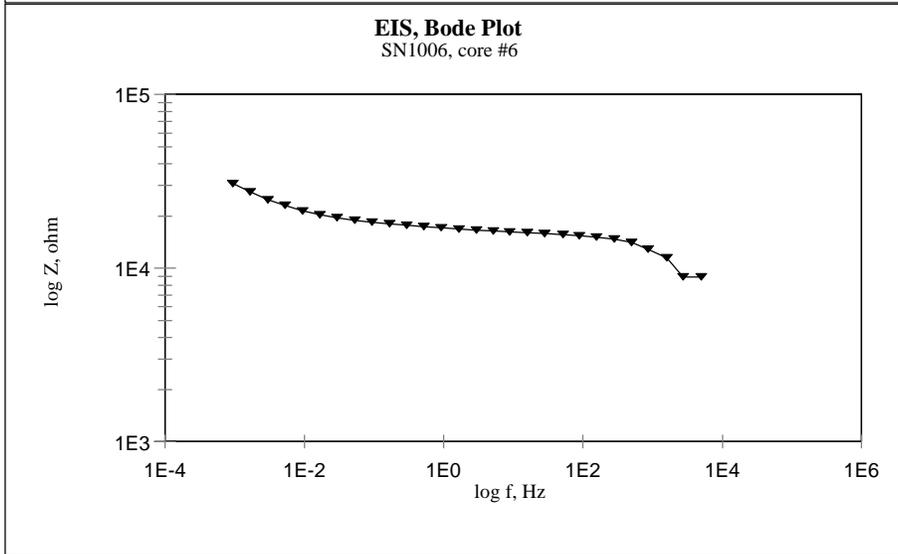**EIS, Phase Angle Plot**
SN6161, core #3

162

EIS, Nyquist Plot
SN6161, core #8

EIS, Bode Plot
SN6161, core #8

EIS, Phase Angle Plot
SN6161, core #8

163

EIS, Nyquist Plot
SN6161, core #10

EIS, Bode Plot
SN6161, core #10

EIS, Phase Angle Plot
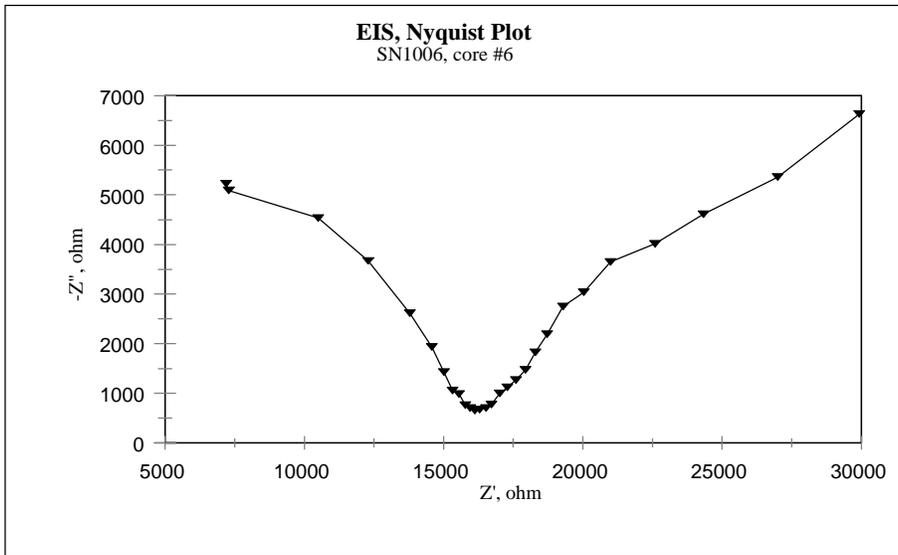SN6161, core #10

164

EIS, Nyquist Plot
SN6005, core #3

EIS, Bode Plot
SN6005, core #3

EIS, Phase Angle Plot
SN6005, core #3

165

EIS, Nyquist Plot
SN6005, core #8

EIS, Bode Plot
SN6005, core #8

EIS, Phase Angle Plot
SN6005, core #8

166

EIS, Nyquist Plot
SN6005, core #12

EIS, Bode Plot
SN6005, core #12

EIS, Phase Angle Plot
SN6005, core #12

EIS, Nyquist Plot
SN2022, core #1

EIS, Bode Plot
SN2022, core #1

EIS, Phase Angle Plot
SN2022, core #1

168

EIS, Nyquist Plot

SN2022, core #4

EIS, Bode Plot

SN2022, core #4

EIS, Phase Angle Plot

SN2022, core #4

EIS, Nyquist Plot
SN2022, core #8

EIS, Bode Plot
SN2022, core #8

EIS, Phase Angle Plot
SN2022, core #8

170

EIS, Nyquist Plot
SN1019, core #3

EIS, Bode Plot
SN1019, core #3

EIS, Phase Angle Plot
SN1019, core #3

EIS, Nyquist Plot
SN1019, core #5

EIS, Bode Plot
SN1019, core #5

EIS, Phase Angle Plot
SN1019, core #5

EIS, Nyquist Plot
SN1019, core #7

EIS, Bode Plot
SN1019, core #7

EIS, Phase Angle Plot
SN1019, core #7

173

EIS, Nyquist Plot
SN1001, core #3

EIS, Bode Plot
SN1001, core #3

EIS, Phase Angle Plot
SN1001, core #3

174

EIS, Nyquist Plot
SN1001, core #5

EIS, Bode Plot
SN1001, core #5

EIS, Phase Angle Plot
SN1001, core #5

175

EIS, Nyquist Plot
SN1001, core #11

EIS, Bode Plot
SN1001, core #11

EIS, Phase Angle Plot
SN1001, core #11

176

EIS, Nyquist Plot
SN1004-6, core #1

EIS, Bode Plot
SN1004-6, core #1

EIS, Phase Angle Plot
SN1004-6, core #1

177

EIS, Nyquist Plot
SN1004-6, core #8

EIS, Bode Plot
SN1004-6, core #8

EIS, Phase Angle Plot
SN1004-6, core #8

178

EIS, Nyquist Plot
SN1004-6, core #12

EIS, Bode Plot
SN1004-6, core #12

EIS, Phase Angle Plot
SN1004-6, core #12

179

EIS, Nyquist Plot
SN1006, core #4

EIS, Bode Plot
SN1006, core #4

EIS, Phase Angle Plot
SN1006, core #4

180

EIS, Nyquist Plot
SN1006, core #6

EIS, Bode Plot
SN1006, core #6

EIS, Phase Angle Plot
SN1006, core #6

181

EIS, Nyquist Plot
SN1006, core #11

EIS, Bode Plot
SN1006, core #11

EIS, Phase Angle Plot
SN1006, core #11

EIS, Nyquist Plot
SN6243, core #4

EIS, Bode Plot
SN6243 core #4

EIS, Phase Angle Plot
SN6243, core #4

EIS, Nyquist Plot
SN6243, core #7

EIS, Bode Plot
SN6243 core #7

EIS, Phase Angle Plot
SN6243, core #7

EIS, Nyquist Plot
SN6243, core #12

EIS, Bode Plot
SN6243 core #12

EIS, Phase Angle Plot
SN6243, core #12

185

EIS, Nyquist Plot
SN1136, core #1

EIS, Bode Plot
SN1136 core #1

EIS, Phase Angle Plot
SN1136, core #1

EIS, Nyquist Plot
SN1136, core #5

EIS, Bode Plot
SN1136 core #5

EIS, Phase Angle Plot
SN1136, core #5

187

EIS, Nyquist Plot
SN1136, core #10

EIS, Bode Plot
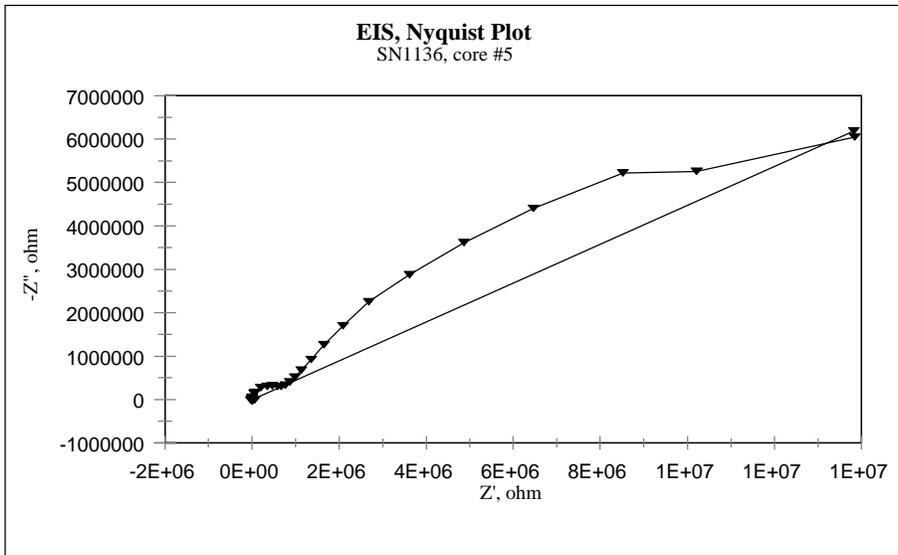SN1136, core #10
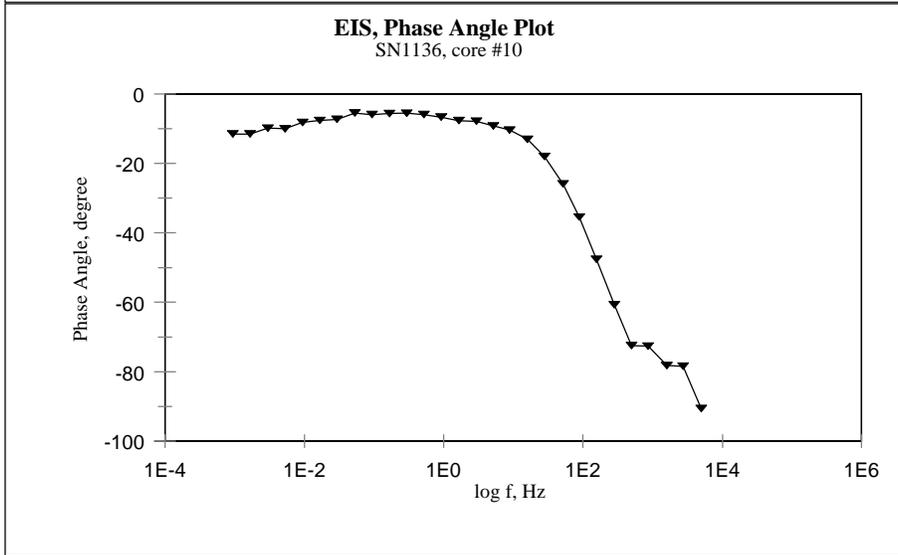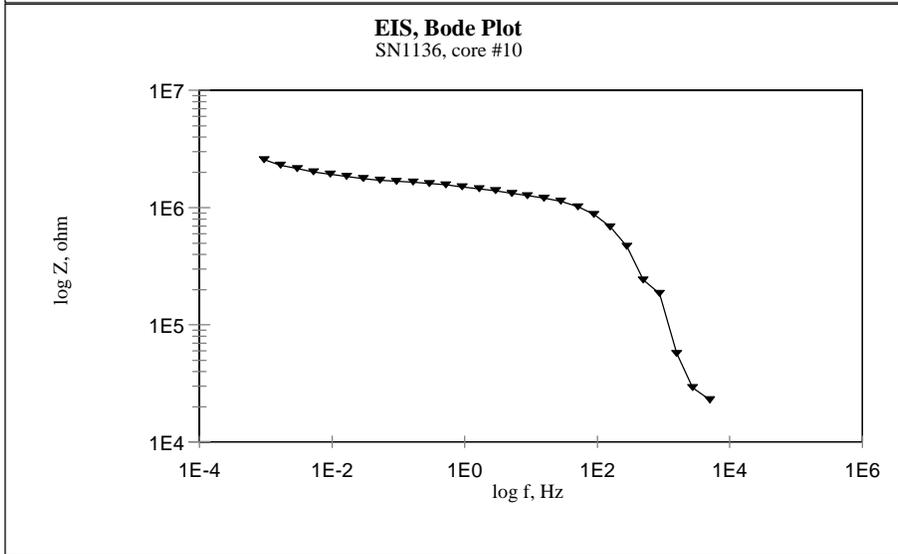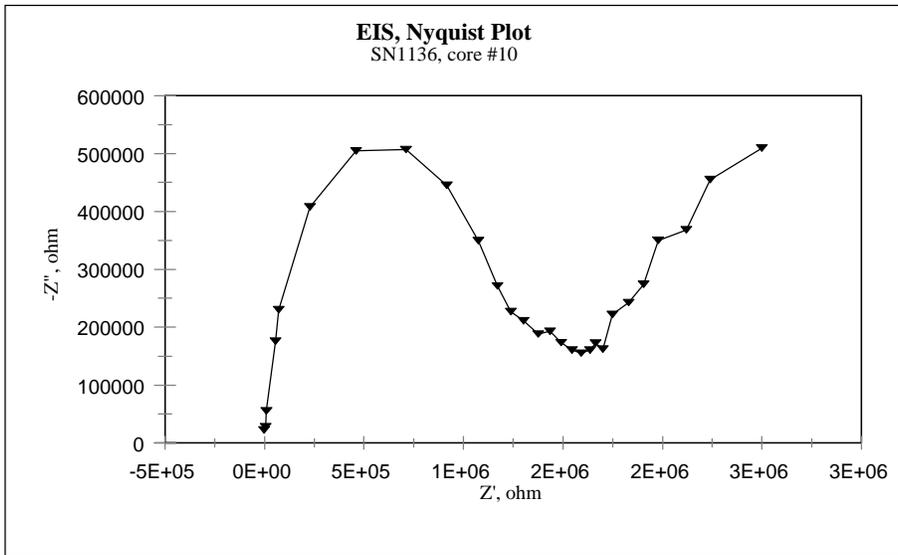

EIS, Phase Angle Plot
SN1136, core #10

188

Vita

Wioleta A. Pyć

Wioleta Agata Pyc was born on August 10, 1965 in Miastko, Poland. She graduated from Adam Mickiewicz High School in Miastko, Poland, in June 1984. In November 1989 she received a B.S./ M.S. degree in Civil Engineering from the Technical University of Gdansk, Poland. After that she worked for a year as an assistant designer in Gdansk Roads and Bridges Design Office.

She entered graduate school in the Materials Division of the Department of Civil Engineering at Virginia Polytechnic Institute and State University in January 1994. While attending graduate school she worked as a graduate teaching assistant and research assistant at the Structures and Materials Laboratory. She received her M.S. degree in Civil Engineering in May 1997. Her Ph.D. in Civil Engineering is expected in December 1998.